

DOTTORATO DI RICERCA IN  
INGEGNERIA CIVILE, AMBIENTALE E DEI MATERIALI

Ciclo XXVIII

Settore Concorsuale di afferenza: 08/B1

Settore Scientifico disciplinare: ICAR/07

**A NUMERICAL INVESTIGATION OF LATERAL SPREADING  
PHENOMENA IN RIVER EMBANKMENTS**

Presentata da: Luca Balbarini

**Coordinatore Dottorato**

**Prof. Luca Vittuari**

**Relatore**

**Prof. Guido Gottardi**

**Correlatore**

**Prof. Laura Tonni**

**Esame finale anno 2017**

---

---

INDEX.....	1
ABSTRACT.....	5
INTRODUCTION.....	6
AKNOWLEDGMENTS.....	6
CHAPTER 1 <b>General features of soil liquefaction</b> .....	9
1.1 Definition of soil liquefaction.....	9
1.2 Historical and geological criteria.....	13
1.3 Cyclic and monotonic loading.....	15
1.4 Remediation techniques.....	18
1.5 Liquefaction aspects of river embankments.....	20
1.5.1. General elements.....	20
1.5.2 Relevant case histories.....	24
1.5.2.1 San Fernando Dam.....	24
1.5.2.2 Kushiro-oki earthquake.....	26
1.5.2.3 Tohoku earthquake.....	31
1.5.2.4 Tottori-Seibu earthquake.....	44
1.5.2.5 Christchurch.....	46
CHAPTER 2 <b>Methods for evaluation of liquefaction triggering</b> .....	53
2.1 Aspects affecting the estimation of liquefaction susceptibility....	53
2.2 Compositional criteria.....	60
2.2 Methods based on in situ tests.....	61
2.2.1 NCEER method.....	62
2.2.2 Boulanger&Idriss (2014) method.....	69
2.2.3 Andrus & Stokoe method.....	69
2.3 Methods based on critical state concept.....	71
2.3.1 Stress-Density method.....	71
CHAPTER 3 <b>Site response analysis</b> .....	76
3.1 Equivalent linear 1D site response analysis.....	76
3.2 Time series method.....	65
3.3 Statistical approach.....	86.
3.4. Signal deconvolution.....	92
CHAPTER 4 <b>The computational platform Opensees</b> .....	95

---

---

4.1 Model commands.....	96
4.2 Elements.....	98
4.3 Materials.....	105
4.3.1 Stress density material.....	107
4.3.2 Pressureindepentmultiyield material.....	108
4.4 Analysis commads.....	111
<b>CHAPTER 5 Emilia earthquake sequence.....</b>	<b>116</b>
5.1 General aspects.....	116.
5.2 Liquefaction.....	122
5.3 Liquefaction of river embankments.....	125
5.3.1 The Scortichino case study.....	128
<b>CAPITOLO 6 The Scortichino case study – in situ and laboratory investigations .....</b>	<b>132</b>
6.1 Geotechnical investigations program.....	132
6.2 In situ tests.....	134
6.2.1 Topographical survey.....	135
6.2.2 Core drilling.....	136
6.2.3 Cone penetration tests (CPTU).....	138
6.2.4 Seismic dilatometer tests (SDMT).....	141
6.3 Laboratory tests.....	142
<b>CHAPTER 7 The Scortichino case study – Liquefaction evaluation based on in situ tests</b>	<b>151</b>
7.1 Preliminary evaluation of liquefaction susceptibility based on historical and geological criterion.....	151
7.1.1 History of Canale Diversivo and of the surrounding areas.....	151
7.1.2 Cracks map.....	153
7.2 Liquefaction potential computation based on in situ tests.....	157
7.2.1 Choice of input parameters.....	158
7.2.1.1 Ground motion.....	162
7.2.1.2 Water table level.....	165
7.2.1.3 Fine content.....	167
7.2.2 NCEER method (2001) .....	172
7.2.3 Boulanger & Idriss method (2014).....	173
7.2.4 Andrus & Stokoe (2000) method.....	175.
7.2.5 Sensitivity analysis for variation of PGA and water table level...	

---

---

7.3 Final remarks on simplified methods.....	
<b>CHAPTER 8 Scortichino case study – numerical analysis.....</b>	<b>178</b>
8.1 General aspects of the model.....	178
8.1.1 Model structure.....	179
8.1.2 Geometrical aspects and boundaries.....	181
8.1.3 Stratigraphy and soil constitutive models.....	183
8.1.4 Ground motion.....	183
8.2 Site response analysis.....	184
8.2.1 Choice of strong motion records.....	
8.2.2 Signal filtering.....	
8.2.3 Soil properties.....	
8.2.4 Signal deconvolution.....	
8.2.5 Definition of motion input parameters for the numerical model	
8.3 Calibration of soil constitutive models.....	
8.3.1 Stratigraphy.....	
8.3.2 Calibration of clayey layers.....	
8.3.3 Calibration of sandy and silty layers.....	
8.3.4 Calibration of deep layers .....	
8.4 Graphical pre and post-processing.....	
8.4.1 model boundaries.....	
8.4.2 mesh.....	
8.5 Analysis.....	
8.6 Discussion.....	
<b>CHAPTER 9 Conclusions.....</b>	<b>186</b>
LIST OF REFERENCES.....	192

---





## ABSTRACT

The 20<sup>th</sup> and 29<sup>th</sup> of May 2012 Emilia region was struck by two main earthquakes having  $M_L=5,9$  and  $5,8$  respectively and epicentres located close the villages of Finale Emilia and Mirandola, in Modena province. The earthquake induced soil liquefaction, concentrated on some areas built on the paleochannel of Reno river and minor areas in Modena province. The left embankment of an irrigation channel called “Canale Diversivo” showed a damage pattern along a section of its path close to the village of Scortichino. The damages appear to be related to lateral movement affecting the embankment body, with formation of longitudinal fissures and seems to be compatible with occurrence of soil liquefaction, especially at the light of a detailed in-situ and laboratory investigation campaign organized by “Gruppo di Lavoro AGI-RER” from which the results from in situ tests and laboratory tests are briefly presented. A detailed survey made with the GNSS (Global Navigation Satellite System) technology has provided the ground surface used to locate the in-situ tests and to perform the preliminary and numerical analysis.

Based on other reconnaissance experiences performed in other case histories a careful evaluation of the damage pattern observed along the embankment has been created. The resulting crack map gives a global spatial overview of the evidences. A further important preliminary research described in chapter 7 is the reconstruction of the history of “Canale Diversivo” and of the surrounding area. Available data allow to define the soil profile through the section: the embankment body is made by a quite mixed material (Unit Ar) mainly silty; underneath Unit Ar a layer classified as sandy silt is located at the base of the embankment (Unit B). Underneath Unit B a clayey layer named Unit C is found. At the base of Unit C and thick sandy layer named Unit A is located. Unit A extends at around 30 m from ground surface and reaches the maximum depth of interest. The surficial water table is located a few meters below the ground surface. Liquefaction susceptibility analysis have been performed using methods based on in-situ tests: 2 methods based on CPT were chosen (NCERR and Boulanger&Idriss 2014); in addition, a method that relies on  $V_s$  values was used (Andrus and Stokoe 2000). A reference  $p_{ga}$  value for the analysis equal to  $0,29g$ . Additional considerations are suggested to evaluate the sensitivity of the liquefaction susceptibility to the variation of acceleration.

---

## INTRODUCTION

The 20<sup>th</sup> and 29<sup>th</sup> of May 2012 Emilia region was struck by two main earthquakes having  $M_L=5,9$  and  $5,8$  respectively and epicentres located close the villages of Finale Emilia and Mirandola, in Modena province; during the following days and weeks many aftershocks occurred, and some of them had magnitude higher than 5. The seismic sequence cause 27 fatalities, hundreds of injuries and billions of euros of damages. Many historical and industrial buildings suffered severe damages, due to the poor resistance of these structures to earthquakes loading.

A peculiar characteristic of the Emilia earthquake, compared to other recent Italian events, is the occurrence of relevant soil liquefaction, concentrated on some areas particularly susceptible to the phenomenon. The villages of San Carlo and Mirabello (FE), built on the paleochannel of Reno river were affected by ground deformations, sand ejecta, lifelines uplifting and significant damages to buildings and structures. Other area in Modena province showed smaller evidences of soil liquefaction.

In particular, the left embankment of an irrigation channel called "Canale Diversivo" showed a damage pattern along a section of its path close to the village of Scortichino. The section interested by the evidences is approximately 2 km long and some groups of houses are located on the embankment crest and showed cracks and deformations. The damages appear to be related to lateral movement affecting the embankment body, with formation of longitudinal fissures. The damage pattern appears compatible with occurrence of soil liquefaction, especially at the light of a detailed in-situ and laboratory investigation campaign organized by "Gruppo di Lavoro AGI-RER".

The aim of this research is to analyse the behaviour under seismic conditions of the embankment and of the soil profile underneath it, and finally to understand if liquefaction occurred and which layer is responsible for it.

A first part, including chapters 1, 2, 3 and 4 is dedicated to the bibliographical background used as reference to the development of the analysis carried on in the second part of the work: the second part, including chapters 5, 6, 7 and 8 is focused on Scortichino case study. Chapter 9 collects the results and conclusion of the study.

---

Chapter 1 is dedicated to the description of the main aspects available in literature related to soil liquefaction with a specific focus on case histories of liquefaction affecting river embankment structures.

Some of the methods available in literature for the evaluation of liquefaction susceptibility are presented in chapter 2. Attention is given to the main elements affecting the soil characterization, the quality of sampling and on the soil properties that play a key role in defining the stress-strain behaviour under cyclic undrained loading. Some methods based on compositional criteria are presented as well as methods based on in-situ tests like CPTU and direct Vs measurements. Finally, some paragraphs are dedicated to the description of advanced constitutive soil models available in literature and based on state concept; these models proved to be able to replicate the behaviour of soils under seismic loading and detect deformations and excess pore pressure build up.

Chapter 3 introduces some general features about site response analysis with attention on those aspects useful to develop a signal deconvolution in order to provide a input velocity time history for the numerical model created in chapter 8.

The computational platform used to perform a finite element numerical analysis of the river embankment is Opensees, described in its general features and main commands in chapter 4.

Chapter 5 introduced the case study, giving a general overview of the Emilia earthquake sequence and consequently a focus on the soil liquefaction evidences. The Scortichino case study, in terms of main features and description of damages is introduced in the last paragraph of the chapter.

The fact that the damage pattern, although not inducing a dramatic collapse of the embankment, has affected some residential buildings, inspired a particular attention from the authorities that created the “Gruppo di Lavoro AGI-RER” and organized a detailed investigation campaign with the aim of understanding the causes of the cracks formation observed on the crest. In chapter 6 all the results obtained from the in-situ and laboratory tests performed along the investigation sections are sintetically presented.

Based on the reconnaissance experiences performed in literature, on the theoretical background introduced in the first part and on the data provided by the investigation campaign a preliminary analysis is arranged in chapter 7. First, an accurate crack map is created, in order to obtain a global understanding of the fissures structure and of other evidences. A detailed reconstruction of the channel history and of the main geological features of the area is presented in the same section. The methods based on in-situ tests and presented in chapter 2 for the determination of liquefaction susceptibility are then used to analyse the main cross sections of interest. Sensitivity analysis for evaluating the

---

influence of the variation of water table level and of the peak ground acceleration on liquefaction are carried on.

Chapter 8 is then dedicated to the numerical analysis with the aim of obtaining detailed information about the deformative pattern of the embankment and of its foundation soil under undrained cyclic loading. The numerical model considers a 2D structure representing a significant cross section of the embankment. The soil profile is defined using the stratigraphy obtained by the investigation campaign. The critical layers in term of liquefaction analysis are studied using advanced constitutive models able to interpretate the deformative behaviour of the soil. The ground motion input at the base of the model is obtained through signal deconvolution from surficial ground motion station. Once the soil profile is defined and the constitutive models are calibrated through the laboratory tests data, the ground motion input is available and the geometry of the model are chosen, the numerical analysis can be run.

## **ACKNOWLEDGMENTS**

---

## CHAPTER 1

# General features of soil liquefaction

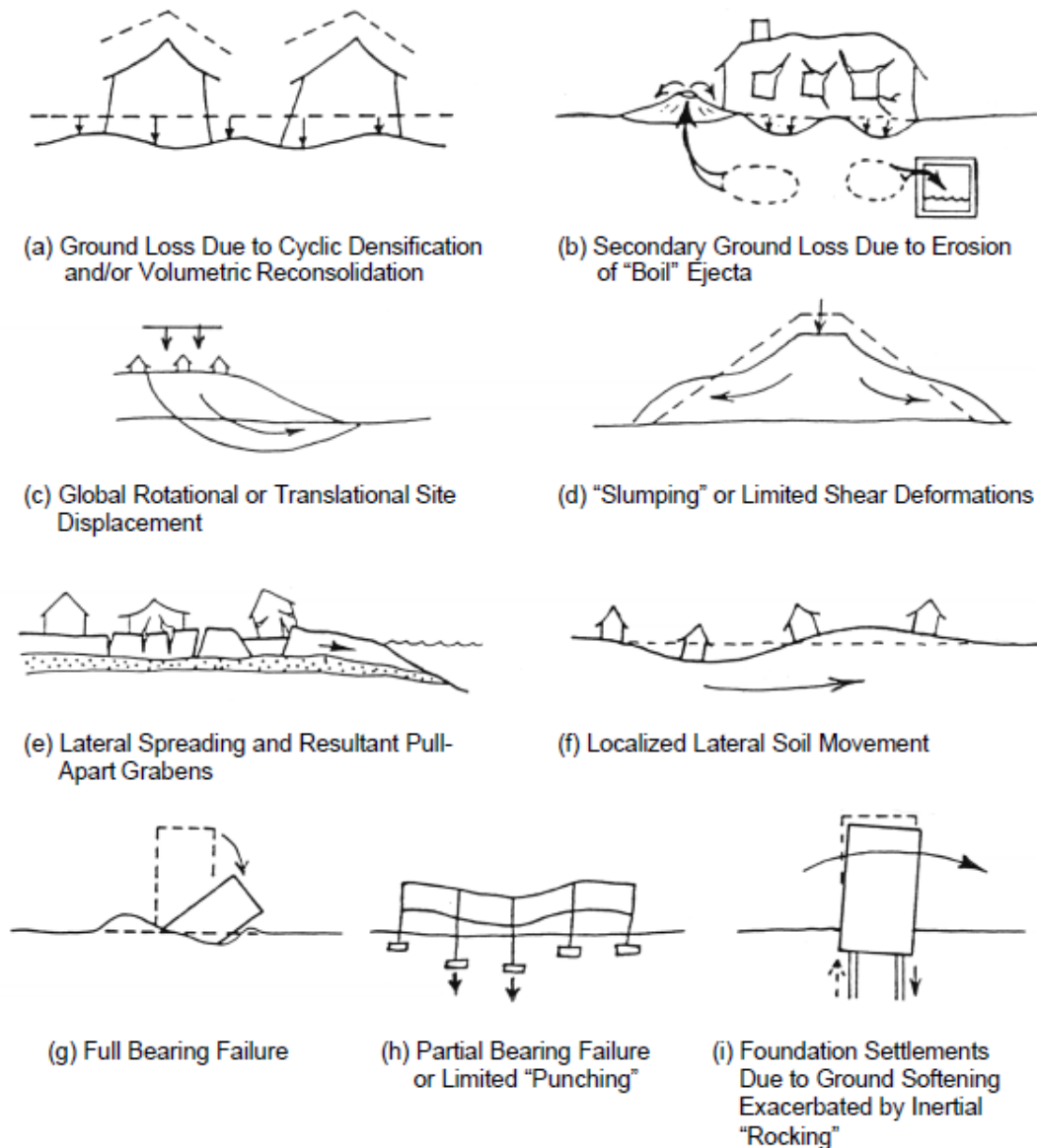
### 1.1 DEFINITION OF SOIL LIQUEFACTION

One of the most dramatic causes of damage to structures during earthquakes is the occurrence of liquefaction in saturated sand deposits. The term soil liquefaction is used to describe the sudden loss of strength of very loose soils that causes settlements, lateral spreading, material ejection, etc.... In figure 1.1 some typical damage patterns due to soil liquefaction are presented (Seed et al. 2003). More details about the horizontal movements will be introduced in paragraph 1.6. The Niigata and Alaska earthquakes in 1964 are certainly the events that focused the attention on the phenomenon of soil liquefaction. Many earthquakes in the last 50 years have illustrated the significance and extent of damage that can be caused by soil liquefaction which and identified it as a major problem in earthquake engineering (Idriss and Boulanger 2008). For example, the loss of shear strength and stiffness in liquefied sands during the 1964 Niigata earthquake resulted in massive bearing failures beneath buildings (Figure 1.3), the uplift of buried structures like tanks and manholes, and the collapse of bridges. Liquefaction was the cause of much of the damage to the port facilities in Kobe in 1995: the earthquake caused extensive liquefaction throughout the reclaimed lands and manmade islands, hosting one of the primary port facilities in the world. Other relevant earthquakes are the 1971 San Fernando and the 1989 Loma Prieta earthquakes in California, the 1995 Kobe earthquake in Japan, the 1999 Kocaeli earthquake in Turkey and more recently the Tohoku earthquake in 2011 in Japan and the Darfield (2010) and Christchurch (2011) earthquakes in New Zealand.

Soil liquefaction is also a major design problem for earth structures such as earth dams and tailing dams. The San Fernando Dam was struck in 1971 by a large earthquake and the earth dam almost totally collapsed causing the evacuation of around 80000 people. This dramatic event, that will be discussed more in detail in paragraph 1.6 has been

---

carefully studied and investigated and marked a major change in embankment design worldwide.



**Figure 1.1** Typical damage pattern related do soil liquefaction (From Seed et al (2003)).



**Figure 1.2** Sand boil from the 1989 Loma Prieta, California earthquake.



**Figure 1.3** Tilting of buildings during the 1964 Niigata earthquake (from Kramer 1996).





**Figure 1.4** Manholes uplifting in Urayasu, Japan, during Tohoku earthquake, 11<sup>th</sup> March 2011 (Koki Nagahama/Getty Images)

Loose sand tends to contract under the cyclic loading imposed by earthquake shaking, which can transfer normal stress from the sand matrix onto the pore water if the soil is saturated and largely unable to drain during shaking. The result is a reduction in the effective confining stress within the soil and an associated loss of strength and stiffness that contributes to deformations of the soil deposit. A common manifestation of liquefaction is the formation of sand boils at the ground surface by water flow through ground cracks. Figure 1.3 shows a typical sand boil profile. The damage from liquefaction is due to different factor: loss of strength and stiffness in the soils that have liquefied, ground deformations, sand boils and deformation induced by the ejected material relocation, deformations and collapses related to lateral movements of slopes.

Figure 1.5 presents a flow chart to clarify the phenomena of soil liquefaction (Robertson 2009).

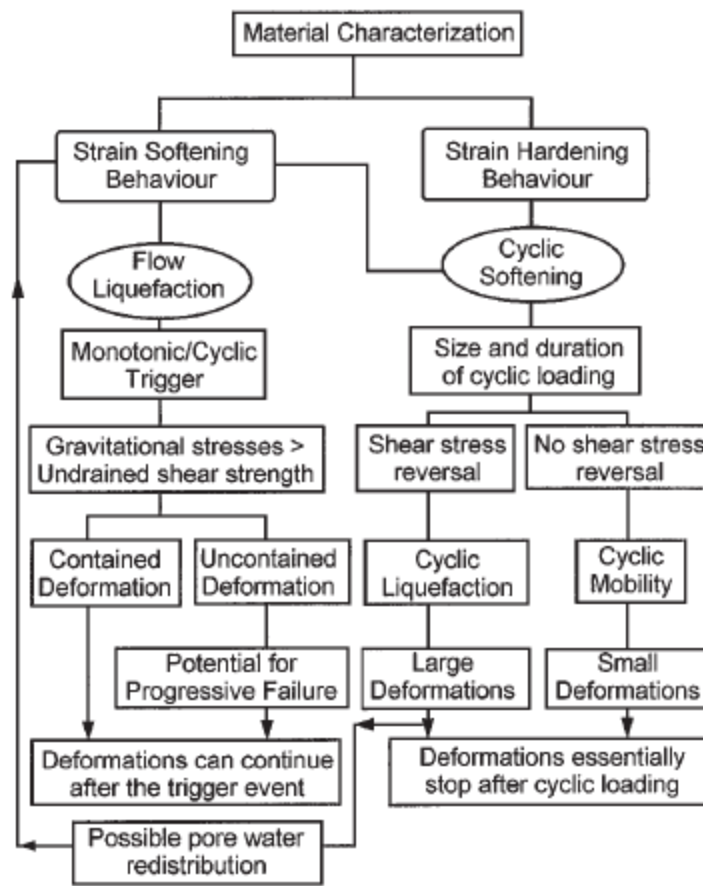


Figure 1.5 Flow chart to introduce liquefaction related phenomena (From Robertson 2009)

## 1.2 HISTORICAL AND GEOLOGICAL CRITERIA

A great amount of information on soil liquefaction is derived from post earthquake field investigations, showing that liquefaction often recurs at the same location when soil and groundwater conditions have remained unchanged. Liquefaction case histories are used to identify specific sites and site conditions where liquefaction may occur again in future earthquakes. Historical evidence of liquefaction is often used to map liquefaction susceptibility. The distance to which liquefaction can be expected strongly increases with increasing magnitude. There are maps based on historical events that report and relate liquefaction evidences to epicentral distance: those maps are helpful for estimation of regional liquefaction hazard scenarios but they offer no guarantee that liquefaction cannot occur at greater distances. Deep earthquakes (focal depths > 50 km) can produce liquefaction at greater distances compared to surficial earthquakes with same magnitude.

Soil deposits that are susceptible to liquefaction are formed within a relatively narrow range of geological environments. The main factors that must be taken into account are

the depositional and hydrological environment, and the age of the soil deposit. Geologic processes that sort soils into uniform grain size distribution and deposit them in loose produce soil deposits with high liquefaction susceptibility. Consequently, fluvial and colluvial deposits when saturated, are likely to be susceptible to liquefaction. Liquefaction has also been observed in alluvial-fan, alluvial-plain, beach, terrace, and estuarine deposits, even though with lower severity which decreases with increasing groundwater depth; the effect of liquefaction are most commonly observed at sites where groundwater is within a few meters of the ground surface. At sites where groundwater levels fluctuate significantly, liquefaction hazards may also fluctuate. Human-made soil deposited also deserve attention. Loose fills, such as those placed without compaction, are very likely to be susceptible to liquefaction. Stability of hydraulic fill dams and mine tailings piles, in which soil particles are loosely deposited by settling through water, remain an important contemporary seismic hazard. Well-compacted fills, on the other hand, are unlikely to satisfy state criteria for liquefaction susceptibility.

Compositional characteristics of soils such as particle size, shape, gradation and all those related to volume change are strongly conditioning liquefaction susceptibility. For many years, liquefaction related phenomena were thought to be limited to sands. Finer-grained soils were considered incapable of generating the high pore pressure and coarser-grained soils were considered too permeable for liquefaction to develop. Some field observations have in the last 20 years proved that the family of liquefiable soils is much wider and in particular includes gravels and low plasticity silts, among sands.

Liquefaction of gravels has been observed in the field and in the laboratory; in real conditions this has happened especially in presence of overlying impermeable layers that induced undrained conditions.

In addition, well-graded soils are generally more susceptible to liquefaction than poorly graded soils because the filling of voids between larger particles with smaller particles in a well-graded soil induces a lower volume change potential and, consequently, lower excess pore pressures. Particle shape can also influence liquefaction susceptibility. Soils with rounded particle shapes densify more easily than soils with angular grains and are for this reason more liquefiable. Typically rounded particles can be found in depositional and fluvial areas, which result proner to liquefaction.

Cohesive sediments are not considered liquefiable but can develop significant strains under seismic conditions, particularly if the sediments are soft and sensitive and the ground motion is strong. The term "liquefaction" is used to describe the behavior of cohesionless soils (gravels, sands, and very-low-plasticity silts) and for cohesive soils (clays and plastic silts) the term "cyclic softening" is preferred.

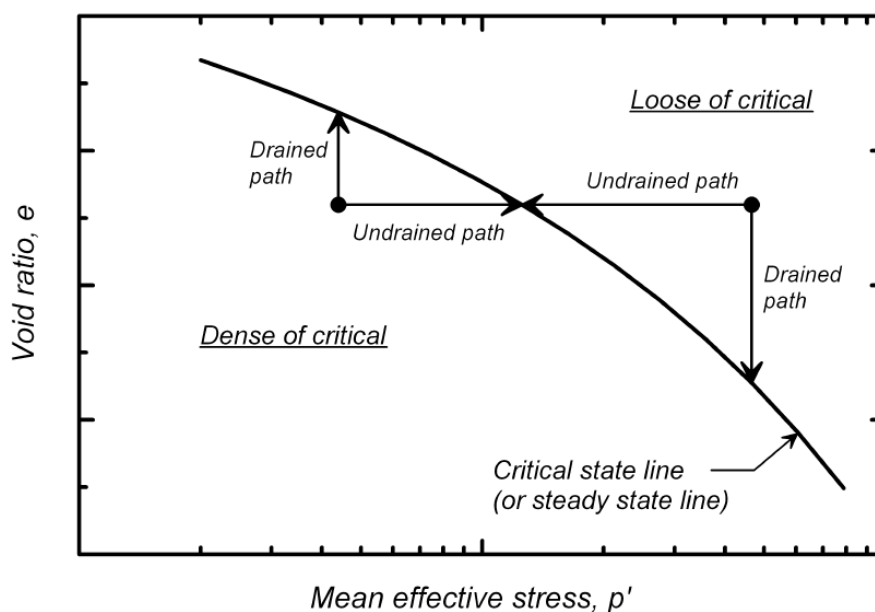
---

## 1.3 CYCLIC AND MONOTONIC LOADING

Before describing methods to evaluate liquefaction potential, it is important to first explain the phenomena of soil liquefaction.

The principal features of the response of saturated sand to drained and undrained monotonic and cyclic loading are described. Most of studies that form the theoretical base of the liquefaction analysis under seismic conditions refer to clean sands. As mentioned before, the phenomenon has been observed not only in sandy soils but also in silty and gravelly soils. The results obtained for sandy soils are used also as reference theory even for different materials, but more studies are required especially for what concerns the models calibration. The methods for the evaluation of liquefaction susceptibility introduced in chapter 2 have been improved in terms of database to include different kinds of soil.

The critical state concept is a key element for the analysis of monotonic and cyclic behaviour under drained and undrained condition. The critical state for a soil is defined as conditions when it is being sheared continuously and no further changes in volume or stress are occurring. All the points where this condition happen form a line called critical state line (CSL), which represents all possible combinations of void ratio and confining stress at the critical state. In case the the critical state line satisfies the requirement of a steady rate of deformation, the line is called “steady state line”. Typically the steady state and critical state lines are can be assumed to be the same line.



**Figure 1.6** Stress paths for monotonic drained loading (From Idriss and Boulanger 2008)

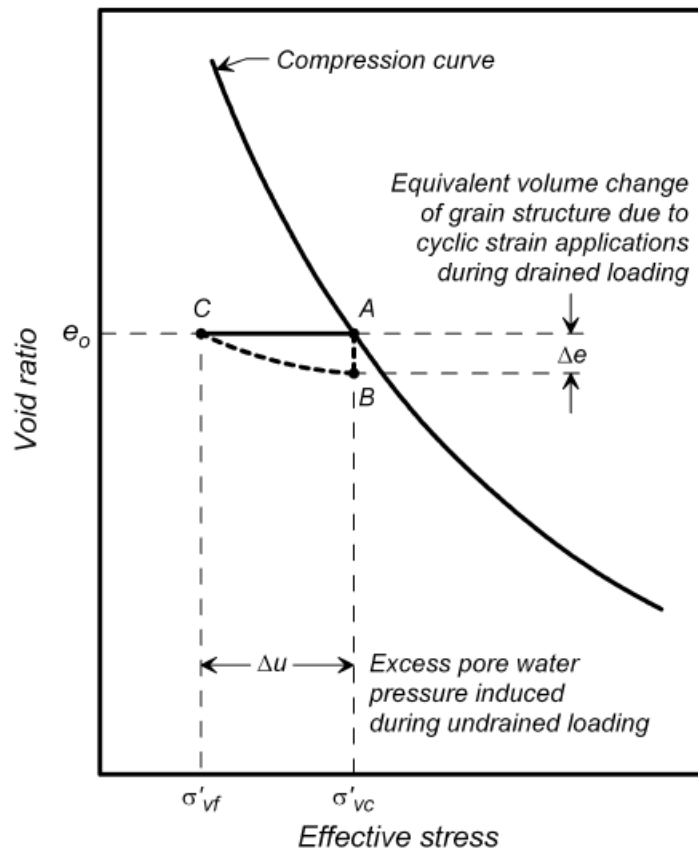
---

Figure 2.1 shows the critical state line for a sand and the loading paths: the critical state line is represented in a graph the void ratio and mean effective stress are on the axis. The critical state line divide all the possible combinations of void ratio values and mean effective stress values into two region called “dense of critical” and “loose of critical”. The loading paths presented in figure 1.6 show the behaviour of the soil under monotonic loading for drained and undrained conditions; the points on the “loose of critical” and “dense of critical regions” tend to reach the critical state line with a contractive behaviour (points in the “loose of critical region”) and dilative behaviour (points in the “dense of critical” region).

It is relevant to note that The stress-strain response of sand to monotonic or cyclic loading is strongly dependent on the sand’s relative density ( $D_R$ ) and the critical state approach is particularly able to capture the effects of volume changes.

In an undrained cyclic loading test (figure 1.7), the sand matrix or skeleton can tend to contract under the cyclic loads, but the resulting rearrangement of sand particles instead transfers normal stresses from the sand matrix to the pore water (i.e.,  $\sigma$  stays constant, while  $\sigma'$  decreases and  $u$  increases) (Idriss and Boulanger 2008). The excess pore water pressure ( $\Delta u$ ) generated during undrained cyclic triaxial loading is normalized by the minor effective consolidation stress ( $\sigma'_{3c}$ ); this ratio is called the excess pore water pressure ratio ( $r_u$ ):

$$r_u = \frac{\Delta u}{\sigma'_{3c}}$$



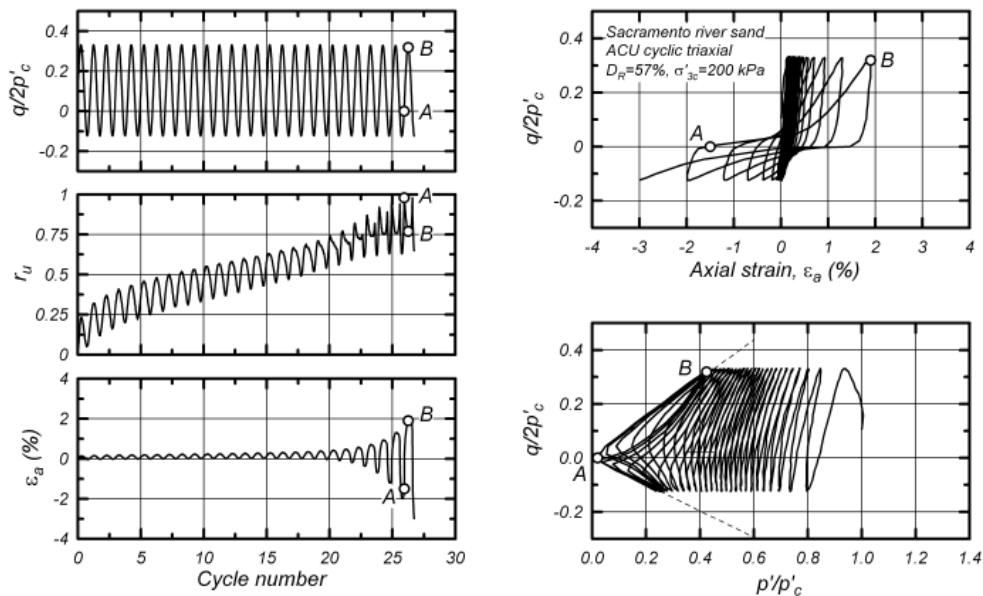
**Figure 1.7** Pore pressure generation during cyclic loading (from Idriss and Boulanger 2008)

For standard cyclic simple shear tests,  $r_u$  is instead computed on the basis of the vertical effective consolidation stress ( $\sigma'_{vc}$ ):

$$r_u = \frac{\Delta u}{\sigma'_{vc}}$$

The maximum possible value for  $r_u$  is again 1.0 when the total vertical stress is held constant, as in a standard cyclic simple shear test. The  $r_u = 1.0$  condition is often called “initial liquefaction”. Several features of the behavior in Figure 1.8 are worth noting. The  $r_u$  increased progressively throughout cyclic loading until  $r_u = 1.0$  was reached after about 27 cycles of loading. The axial strains ( $\epsilon_a$ ) remained relatively small (a fraction of 1%) until  $p'$  approached zero and  $r_u$  approached 100%, after which the axial strains increased to about 2% in less than 2 additional cycles of loading. Axial strains would have increased very rapidly with continued cyclic loading, although this particular test was stopped after

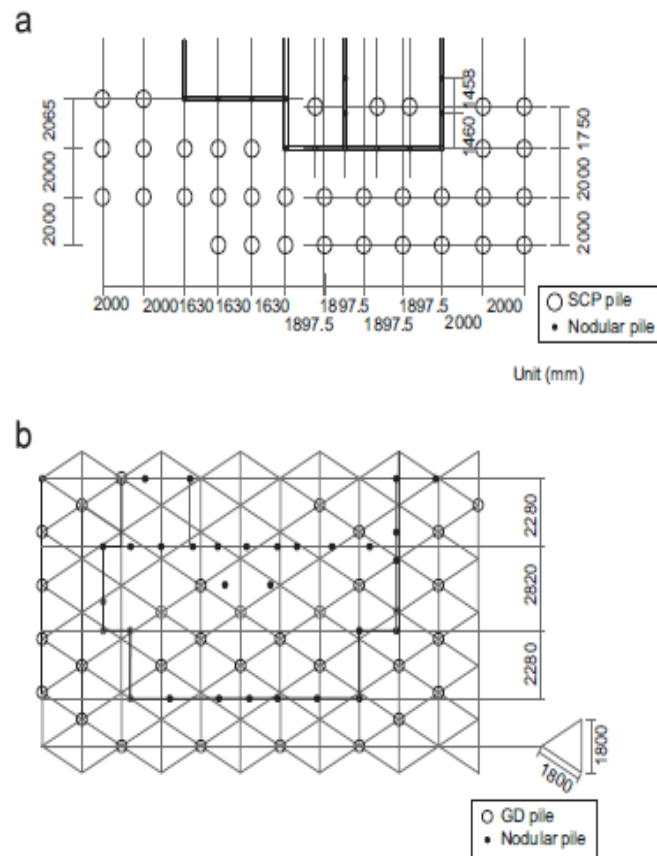
reaching 3% strain. The corresponding stress-strain response shows rapid softening as  $p$  approached zero, with the hysteretic loops taking on an inverted s-shape. The stress path—that is,  $q/(2p'_c)$  versus  $p'/p'_c$ —moved progressively toward the origin during cyclic loading until it stabilized with repeating loops emanating from the origin (Idriss and Boulanger 2008).



**Figure 1.8** Undrained cyclic loading of sands (from Idriss and Boulanger 2008)

## 1.4 REMEDIATION TECHNIQUES

Sand compactions piles and stone columns must follow a regular and uniform distribution on all the area of interest, and must form a net with piles sufficiently close: typical distances vary from 0,5 to 2 m, and strongly depends on the soil characteristics. The geometry of the piles, in terms of diameter, is also another important aspect, together with the properties of the filling material used (figure 1.9)



**Figure 1.9** Typical arrangement for sand compaction piles and stone columns (from Yamaguchi et al. 2012)

Robertson (2009) presented a chart (figure 1.10) with a summary of all the main remediation technologies adopted and available.



General Category	Mitigation Methods	Notes
I. Excavation and/or compaction	(a) Excavation and disposal of liquefiable soils (b) Excavation and recompaction (c) Compaction (for new fill)	
II. In-situ ground densification	(a) Compaction with vibratory probes (e.g.: Vibroflotation, Terraprobe, etc.) (b) Dynamic consolidation (Heavy tamping) (c) Compaction piles (d) Deep densification by blasting (e) Compaction grouting	-Can be coupled with installation of gravel columns  -Can also provide reinforcement
III. Selected other types of ground treatment	(a) Permeation grouting (b) Jet grouting (c) Deep mixing (d) Drains - Gravel drains - Sand drains - Pre-fabricated strip drains (e) Surcharge pre-loading (f) Structural fills	-Many drain installation processes also provide in-situ densification.
IV. Berms, dikes, sea walls, and other edge containment structures/systems	(a) Structures and/or earth structures built to provide edge containment and thus to prevent large lateral spreading	
V. Deep foundations	(a) Piles (installed by driving or vibration) (b) Piers (installed by drilling or excavation)	-Can also provide ground densification
VI. Reinforced shallow foundations	(a) Grade beams (b) Reinforced mat (c) Well-reinforced and/or post-tensioned mat (d) "Rigid" raft	

Figure 1.10 List of the main remediation technology for soil liquefaction (from Robertson 2009)

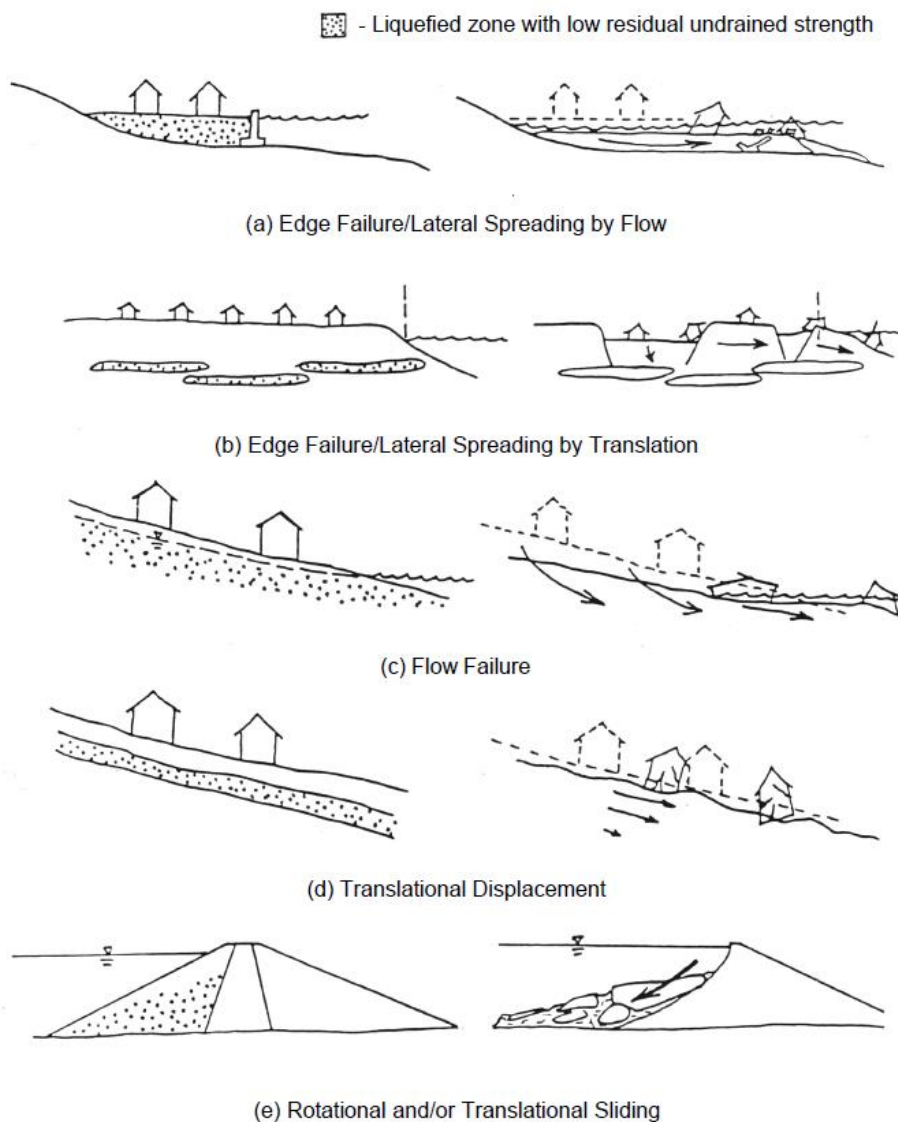
## 1.5 LIQUEFACTION ASPECTS OF RIVER EMBANKMENTS

### 1.5.1 General elements

Earth structures such as dams and embankments are quite vulnerable to liquefaction effects and require a careful analysis. In particular these structures meet the presence of a surficial water table and are formed by materials that can meet the compositional requirements described in paragraph 1.2. Another critical aspect that is in reality quite common, is the presence of liquifiable layers underneath the earth structures. For

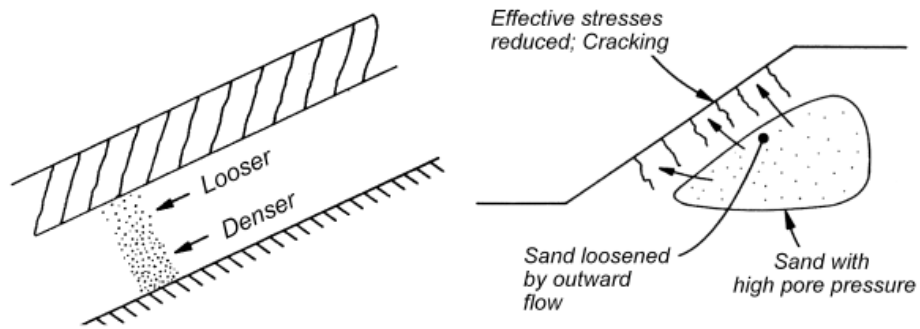
example, the fact that a river embankment is placed on a soil that is made of river deposition sediments, young and saturated, might induce liquefaction at the base and consequent damages on the earth structure. In other cases, liquefaction might occur inside the earth structure itself.

Figure 1.11 shows typical damage patterns of slopes, embankments, dams and other earth structures characterized by the presence of a slope. The common feature of these structures is called lateral spreading.



**Figure 1.11** Typical damage pattern for sloping ground connected to liquefaction (from Seed et al. 2003)

Figure 1.12 shows a typical situation manifestation of damages and material ejecta for an embankment with inclusion of sandy liquefiable layer in its core.



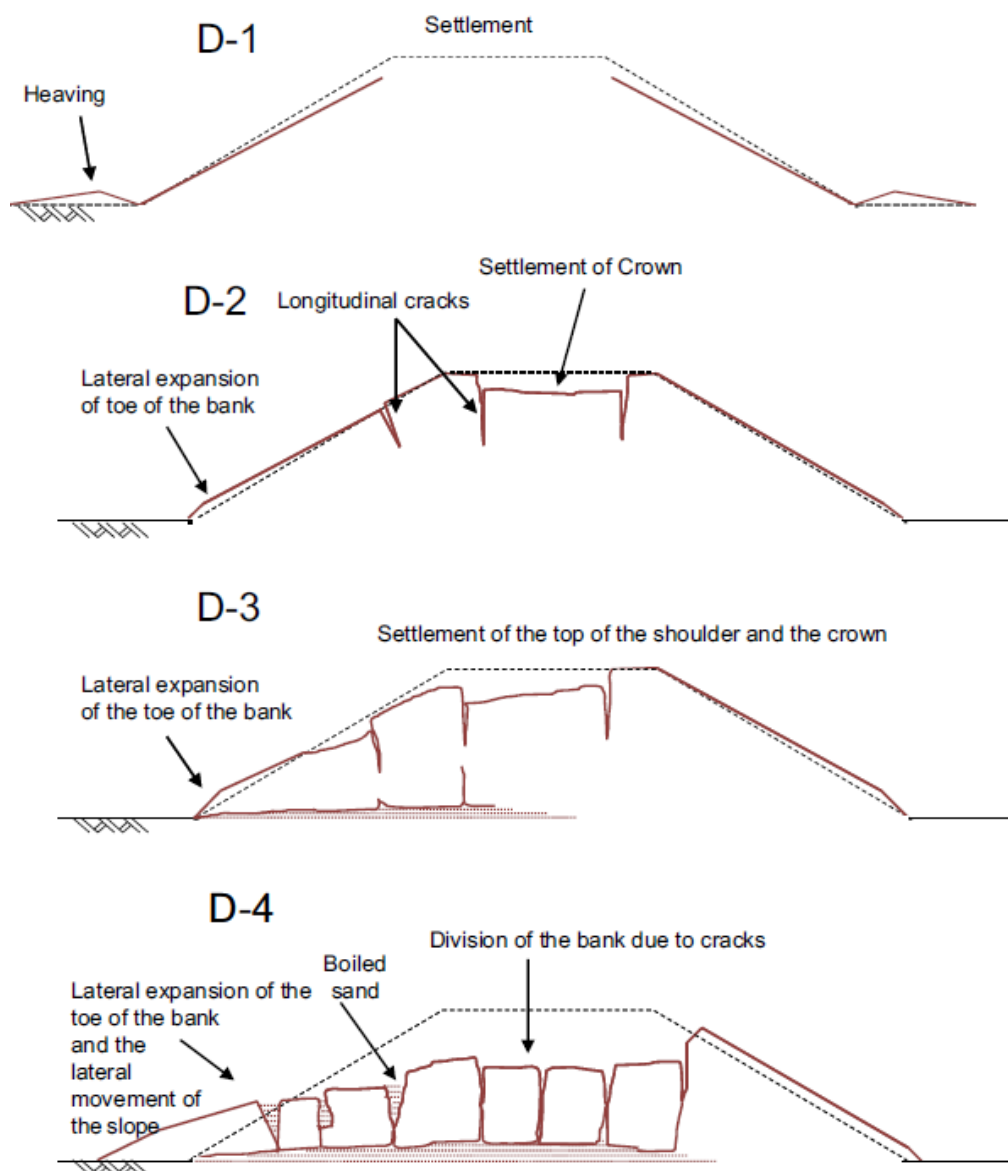
**Figure 1.12** Liquefaction of sandy layers in embankment body (from idriss and Boulanger 2008)



Soil liquefaction can occur in the following situations:

- coastal areas, surficial water basins and river embankments;
- harbours,
- holocene or pleistocene loose sand deposits with high water table level ( $H < 5$  m)


Oka et al. (2012) suggested a classification for the damage pattern due to soil liquefaction for earth river embankments and earth dam in general. Different evidences can appear on the embankment surface. Typically heaving at the embankment toe and, going to more severe events, settlement of the crest, longitudinal cracks, lateral deformations and, in the worse cases, total collapse of the structure. San boils, can occur more easily at the toe, and only for severe events, on the crest and on the slopes because of the higher resistance met by the liquefied soil to go through the embankment body. A settlement of the embankment base, and consequent subduction, can be observed when there is liquefaction of the layers underneath the earth structure.



**Figure 1.14** Classification of river embankment damages (from Oka et al. 2012)

## 1.5.2 Relevant case histories

### 1.5.2.1 San Fenando Dam

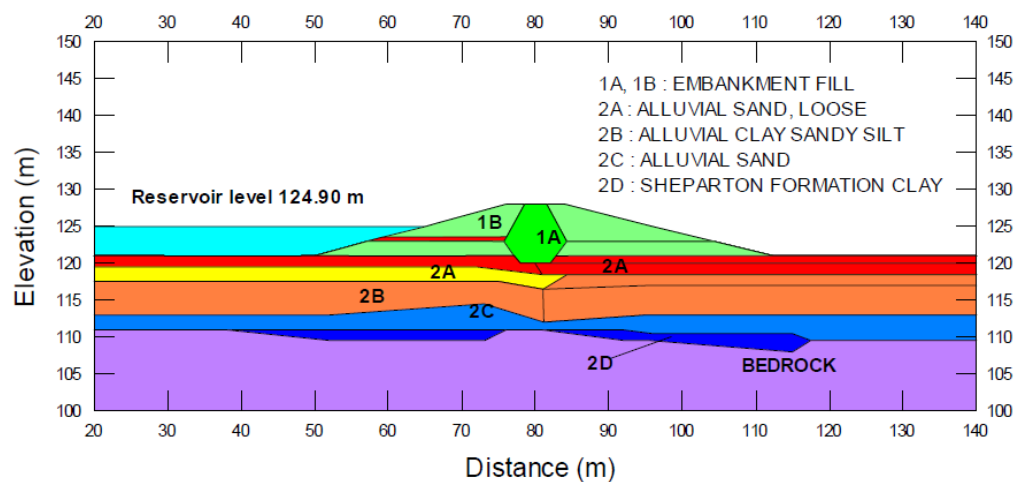
<b>COUNTRY:</b>	<b>U.S.A.</b>	<b>MAGNITUDE:</b>	<b>6.6</b>
<b>LOCATION:</b>	<b>Lower/upper San Fernando dam</b>	<b>DATE:</b>	<b>9/02/1971</b>
			



Da Jitno 2009

San Fernando Dam case history is one of the most famous, resonant and well documented cases of liquefaction of an earth dam under seismic load. During the same event 2 earth dams experienced severe damages: lower San Fernando dam and Upper San Fernando dam.

The slide that formed in the internal side of the Lower San Fernando Dam during the 1971 San Fernando earthquake and caused the evacuation of about 80,000 people who were living close to the dam. The dramatic extent of the slope failure is shown by a photo (Figure ).



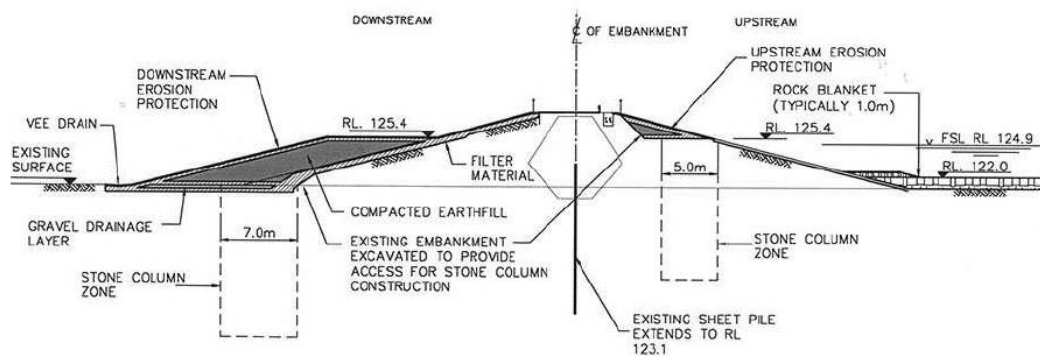
From Jitno 2009

The liquefaction of loose sandy layers at the base of the embankment has caused the complete collapse of the Lower dam. At the end of the seismic event the free surface was only 1,5 m high. The liquefaction of reported sandy soil in the lower part of the internal side of the dam caused the almost total collapse of the structure.






Small damages have instead occurred at the Upper San Fernando dam, with maximum deformations of the embankment body close to 0,8m. Remediation works have been carried on in order to strengthen and stabilize the dam. In particular the embankment body has been widened on the external side, the material has been additionally compacted and the stone columns have been realized.



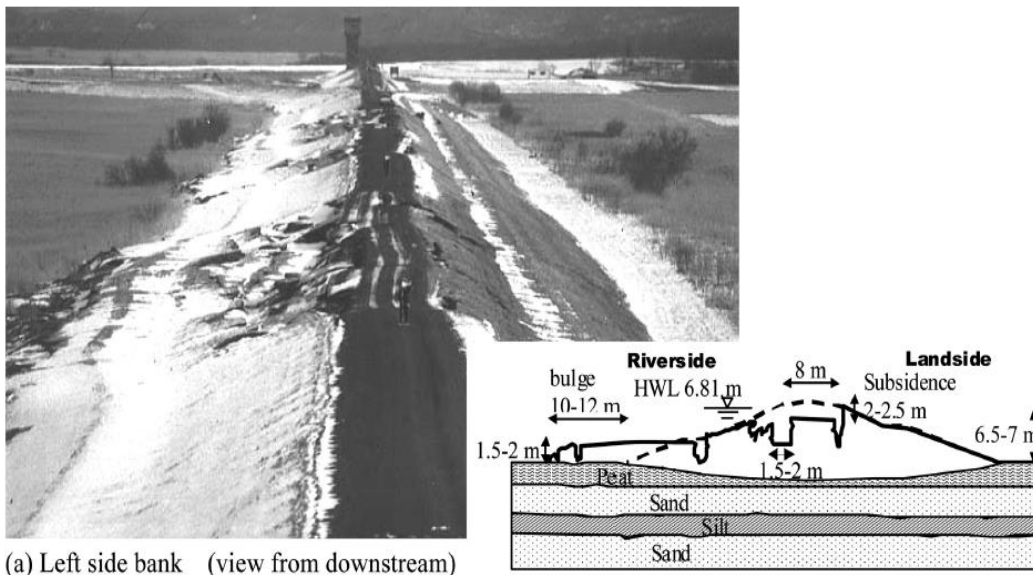
From jitno 2009

### 1.5.2.2 Kushiro-Oki earthquake

<b>COUNTRY:</b>	<b>JAPAN</b>	<b>MAGNITUDE:</b>	<b>7.8</b>
<b>LOCATION:</b>	<b>Kushiro-Oki</b>	<b>DATE:</b>	<b>15/01/1993</b>
			

The Kushiro-oki earthquake has caused extensive liquefaction effects on river embankments. Previously the problem of liquefaction of river embankments was considered marginal, compared to other liquefaction effects on structures. In fact the low probability of having a strong earthquake simultaneously to a river flood was thought to consider not particularly dangerous the damages occurred to river embankment. It was expected to restore the earth structures in a reasonably short time and make it able again to resist to a river flood. The high extension of the damaged section has instead made clear that the reparation time would have been much longer than expected. The probability to face a river flood before the end of the reparation works has been thus considered unacceptable and this had pointed out the need to provide mitigations techniques to apply on earth structures to prevent possible damages connected to seismic soil liquefaction.





Fiume Kushiro - da Sasaki 2009

During the Kushiro-Oki earthquake soil liquefaction has been observed inside embankment bodies realized with sandy material. Subsidence of the embankment crest, widening at the toe and slope rotations have been observed. The embankment is built on a peat layer, not liquefiable. The dense sandy layers underneath have not shown liquefaction effects.

It appears clear that the consolidation settlement of the peat layer due to the weight of the embankment has allowed the water table to reach the base of the embankment. The sand used to realize the embankment was not compacted with the aim to reduce the settlement of the peat underneath it, and this choice has increased the liquefaction susceptibility of the soil.

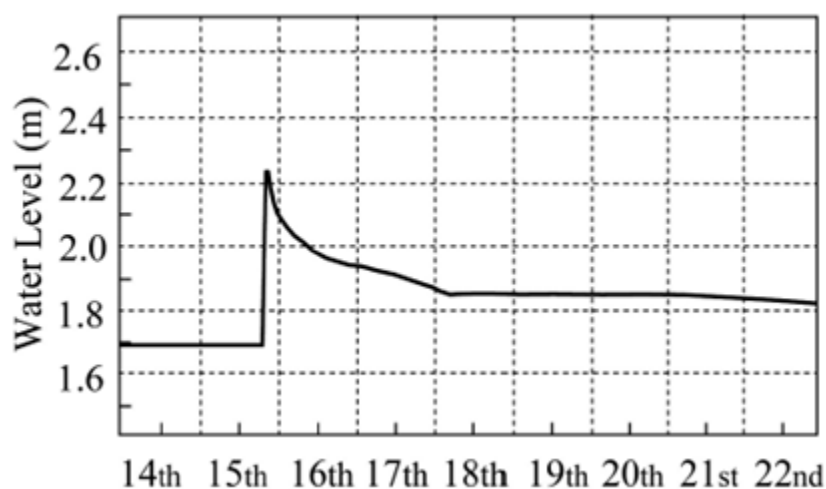


From Sasaki 2009

Longitudinal cracks of important size has appeared along the crest and close the the slopes, as well as lateral spreading and swelling of the toes.

Sections with same characteristics in terms of geometry and materials have reacted differently to the event. The differences were quite relevant and this has been related to a 3D effect in the embankment behaviuor Damages have been observed both on riverside and landside, but were more relevant on riverside.

The excavation of trenches and more detailed internal inspections have proved the presence of internal fissures not visible on the external surface. This kind of damages is considered to be particularly dangerous for the embankment strength during flood event, since it cannot be discovered with surficial inspections.



The monitoring wells realized in the sorroundings and already existing before the earthquake have pointed out that the water table level has increased during the event. This fact, combined with the presence of loose sand at the base of the embankment has created the conditions for soil liquefactions to occur. In figure... it is possible to see the time required for the water table to reduce again to its normal level, that is below the embankment base. To reduce most of the increase the time required is around a couple of days. This makes clear that aftershocks taking place in a short time, even of lower intensity than the main event, can generate further liquefaction. To prevent the presence of the water table and the storage of rain water inside the embankment body it is of particular importance the realization of drainage works.

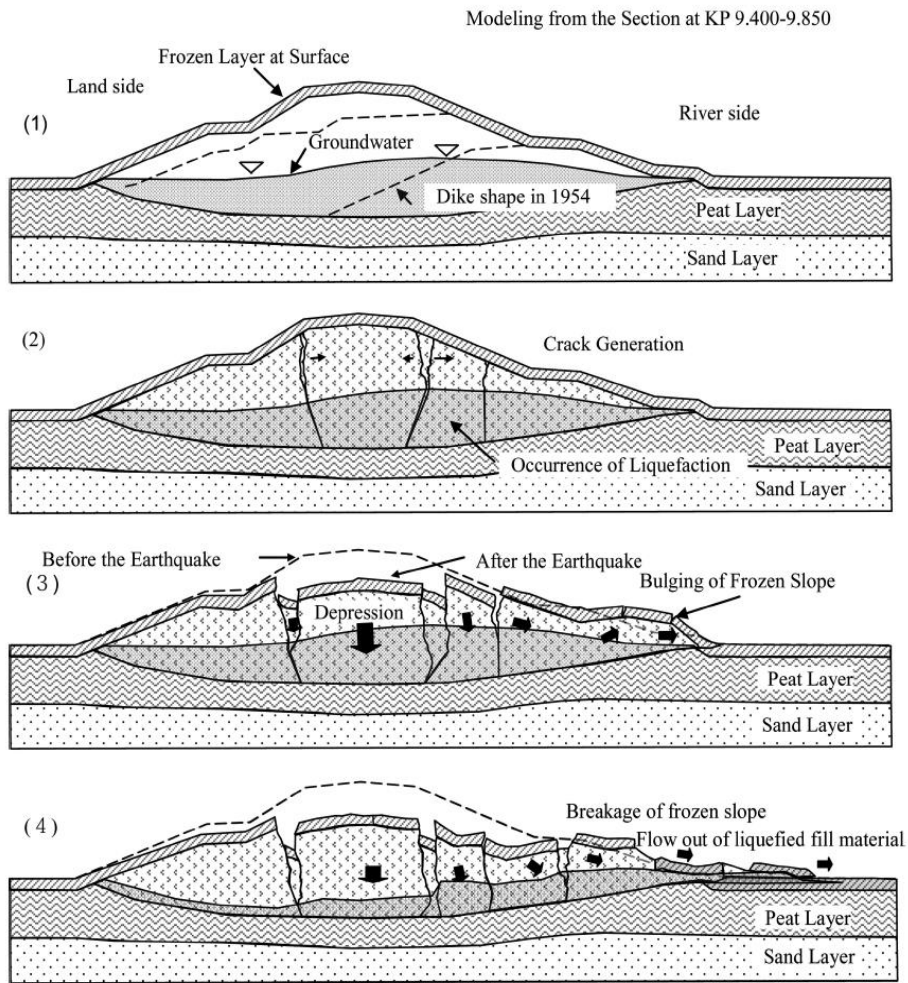
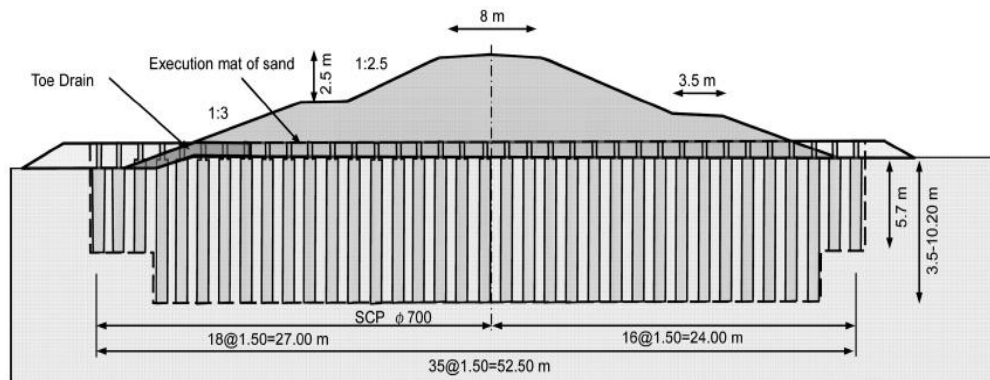



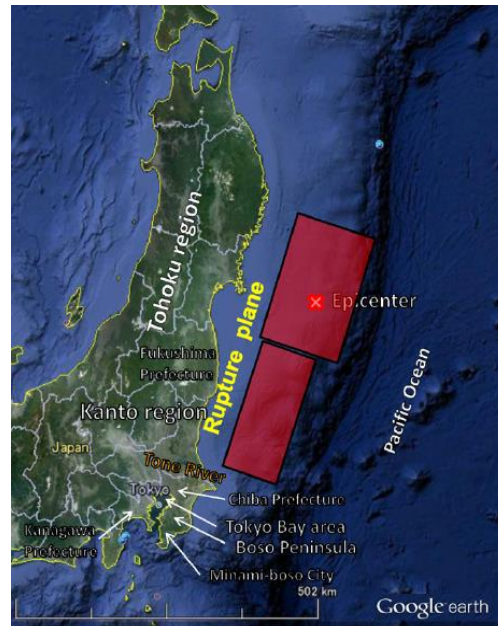
Figure...shows that the subsidence of the embankment placed on a soil with low bearing characteristics has been in some sections higher than 1 m before the earthquake. This has created the conditions for soil liquefaction. From experimental measurements it is possible to establish a correlation between the amount of pre-earthquake subsidence and the embankment crest settlement.



Restoration works have been realised by the use of sand compaction piles (SCP) in order to increase the density and the strength of the embankment itself and of the soil underneath it. On the sides piles with shorter length have been used in order to create a transition zone and reduce differential settlements. A drainage layer at the toe on landside has been installed to prevent the accumulation of rain water.

### 1.5.2.3 Tohoku earthquake

<b>COUNTRY:</b>	<b>JAPAN</b>	<b>MAGNITUDE:</b>	<b>9</b>
<b>LOCATION:</b>	<b>Tohoku</b>	<b>DATE:</b>	<b>11/03/2011</b>
			



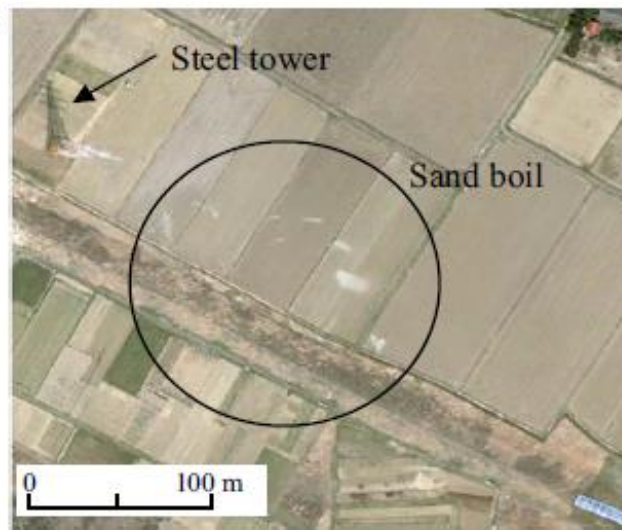
## da Yasuda et al. 2012

Tohoku earthquake has affected a wide area of the eastern coast of Japan, in terms of shaking intensity, of duration and of the size of the rupture plane. Many aftershocks with high magnitude have caused repeated liquefaction phenomena and in most cases with increased severity of damages.

Evidence of soil liquefaction has been detected on:

- Urban areas;
- River embankments;
- Road structures;
- Coastal zones;
- Agricultural fields.

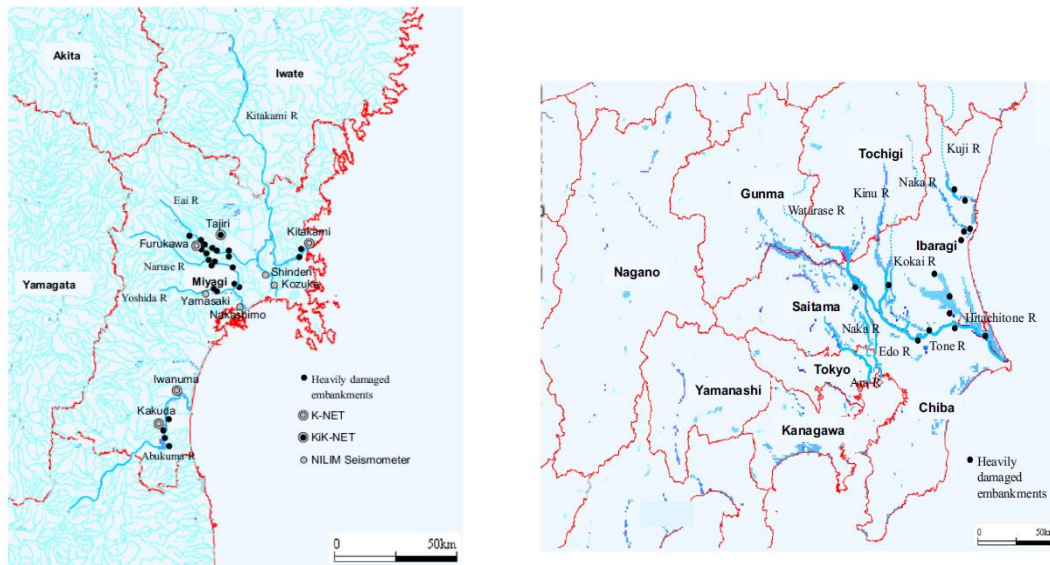
The tsunami that followed the main shock has deleted part of the liquefaction evidence, as it appears from figure....



da Yamaguchi et al. 2012 (a)

Many sand boils have been observed on alluvial planes, especially close to rivers or extinct rivers. Figure.... Shows the situation in 1975, with the presence of a channel that in the picture taken in 2011 appears filled with soil material. It appears clearly that sand boils are located along the the path of the old channel. Extensive fissures are a typical evidence of soil liquefaction. The semicircular shape of the fissures in figure ... follows, like the situation of figure..., the path of an old channel.





da Oka et al. 2012 (a)

River embankments that were affected by soil liquefaction are located on a wide and extended area. Liquefaction has been observed inside the embankment bodies and in the soil underneath it as well. Maps in figure... show river embankments that experienced liquefaction in the north-east area of Hokkaido Island and along the basin of Edo river.



The cracks generated by soil liquefaction on the crest of river embankments have the same direction of the embankment itself. Figure ....shows longitudinal cracks long up to 100 m along Naruse river, together with lateral spreading and crest settlement. In this case liquefaction has occurred in the soil underneath the embankment.



da Sasaki et al. 2012

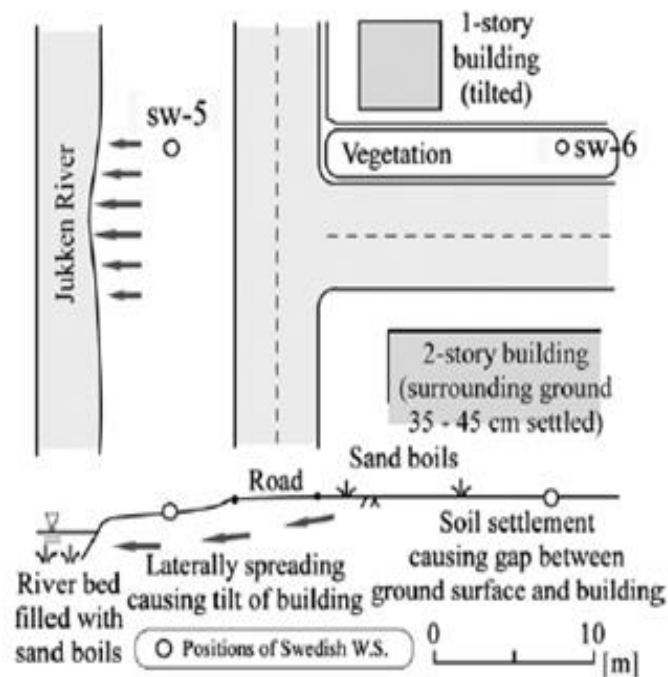
In figure.... damages on a road built on an abandoned river path are reported. Rotation of the body and lateral spreading are clearly visible.

Swelling at the embankment toe is another typical element related to soil liquefaction.



Da Sasaki et al. 2012





Da Tsukamoto et al. 2012

Lateral spreading along Jukken-Gawa river; settlements have caused damages to the road and to the building behind. The great amount of material ejected has partly occluded the bed of Jukken-Gawa river. Effects of liquefaction along abandoned bed of Naka and Tone rivers. There is evidence of sand boils and lateral spreading.

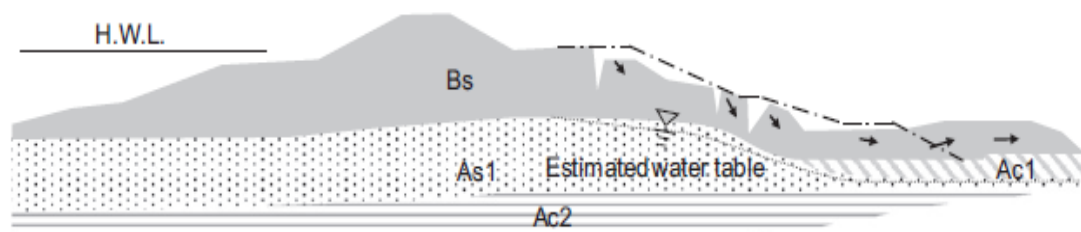


In the extreme cases the total collapse of the embankment can be reached. The embankment along the old path of Naruse river has totally collapsed on a section around 500 m long. The height of the structure at the end of the event has been reduced of 2/3 respect to the original one. Longitudinal fissures with ejected sandy material are clearly visible.

---

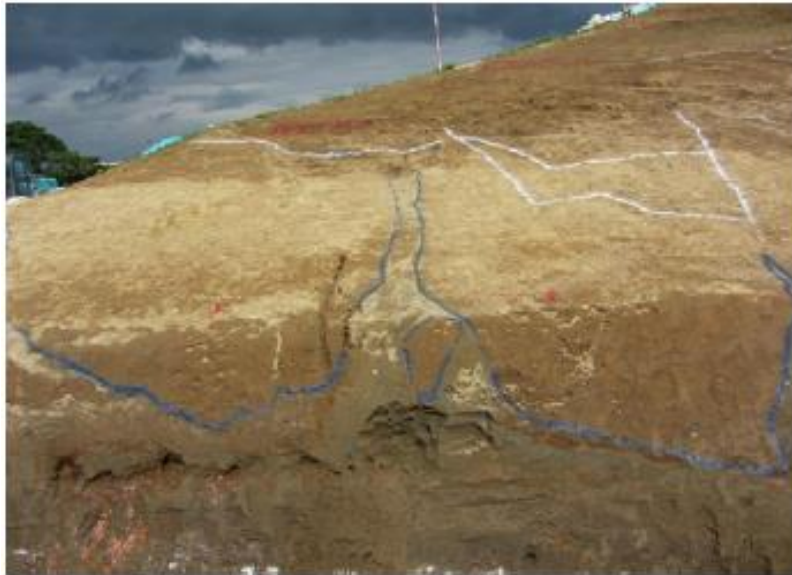


It is evident the almost complete collapse of the earth structure along the Abukuma river. The embankment height has reduced to 2,8 m from the initial 5,7 m, that means a reduction bigger than 50%. Longitudinal cracks around 1 m deep, with extensive sand ejection are present on a wide part of the embankment. The damages have occurred along all the river section, with predominance on the landside.



Da Oka et al. 2012

Damage pattern of the embankment of river Edo, close to Nishisekyado. Liquefaction occurred in the alluvial sandy layer (As1) located immediately under the embankment body. Liquefaction affected mainly the landside, in the direction of a clayey layer (Ac1). The settlement of the crest is close to 1 m. From the cracks that formed on the slopes sandy material was ejected.



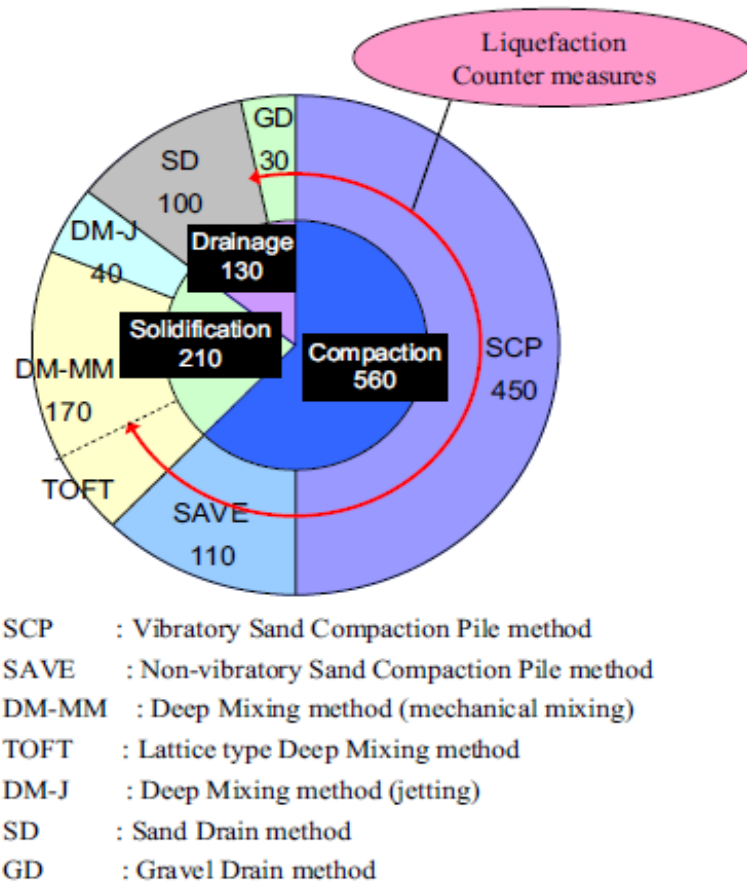
Da Oka et al. 2012

Trenches are a very useful tool to recognize sand boils and flows of material in the embankment body. In this way it is also possible to know with certainty which layer, or part of layer, exactly liquefied. Upwards flow paths are clearly visible. In this specific case liquefaction occurred in the lower layer of the embankment, where sandy material with  $N < 5$  is present. The presence of rain water is considered the possible cause of the liquefaction event. It is important to point out that with a trench it is possible to notice the presence of material flows that don't reach the surface. In some cases it is possible to detect liquefaction phenomena that occurred during past earthquakes. The embankment of figure... has experienced a settlement of around 5,5 m with a total height of around 13 m. The damages caused by soil liquefaction mainly occurred on alluvial depots and along present and past river beds and embankments. Another not negligible situation potentially prone to soil liquefaction is the presence of hydraulic filling. In Japan it is quite typical to have structures on reclaimed areas, where soil material, usually sand, has been placed with hydraulic filling technique. In Onanoma city all liquefaction phenomena occurred on reclaimed areas, where hydraulic filling was used. (fig....). Other parts of the city didn't show any relevant damage.

Dams are susceptible to liquefaction in the same way as river embankment. Many dams, both realized with earth and concrete are present in the area. Damages have affected many dams, both made of concrete and of earth. Concrete dams, despite having shown a strength higher than earth dams, have reported damages that are not negligible.

Repairs consisted of rebuilding and substitution of the part of the dam body realized with material that showed poor performance. In figure... damages occurred to the Ishibuchi dam during the 2008 earthquake are visible.

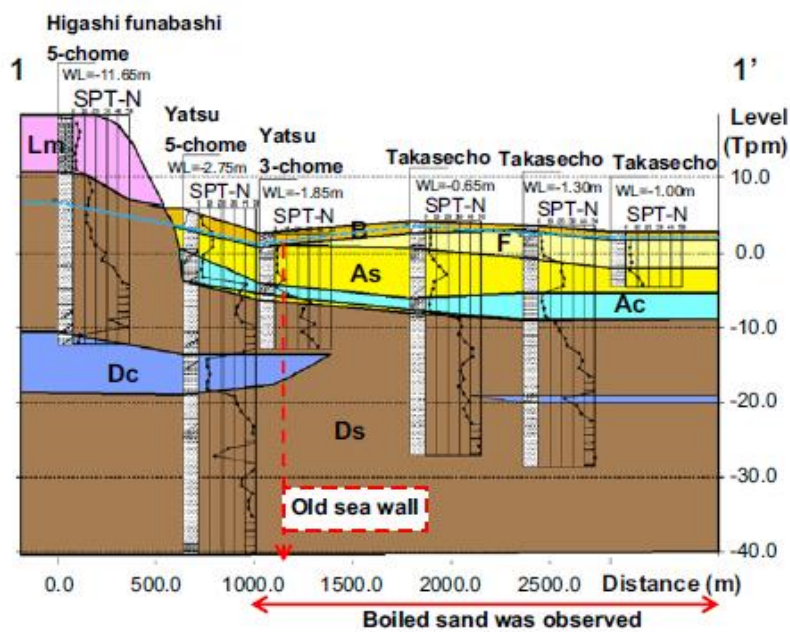
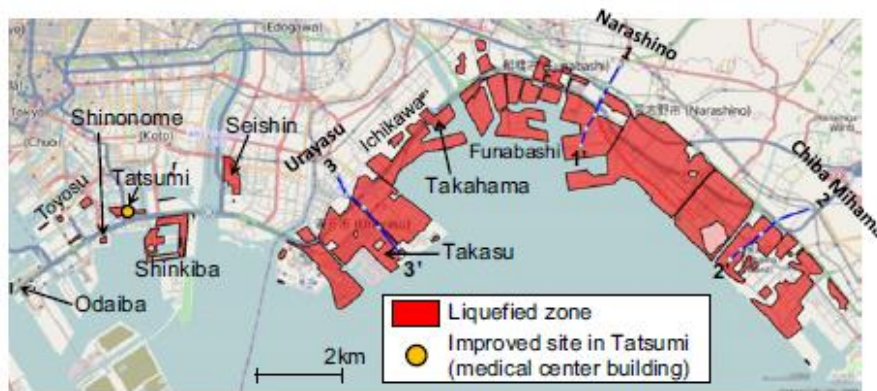
In figure ... the same section is represented after the 2011 earthquake. Apparently no damages were observed, as a proof of the effectiveness of the repairs.



Da Yamaguchi et al. 2012 (a)

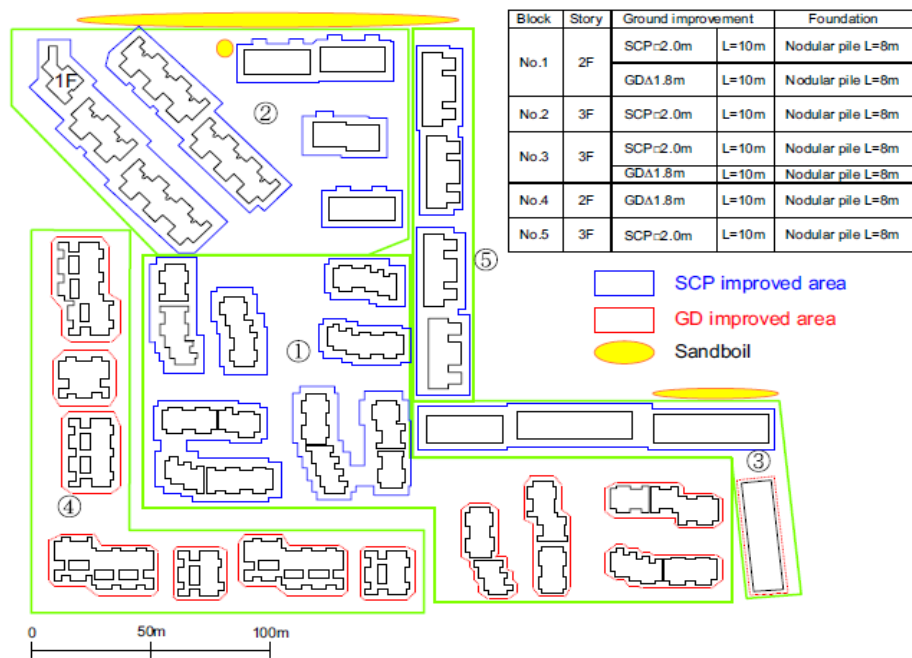
The most used remediation techniques used in Tokyo region are compaction techniques. Most of interventions were performed using sand compaction piles (SCP) and stone columns. Solidification techniques like Lattice type deep mixing soil (TOFT) and drainage techniques (gravel drains, GD) have also proved to be efficient.





Da Yamaguchi et al. 2012 (a)

Tokyo has experienced significant liquefaction effects, mainly in reclaimed areas where hydraulic fill was used. In these areas many work for reducing liquefaction susceptibility have been performed during the years. In figure.... liquefied areas are indicated; they follow precisely the areas where hydraulic fill was used (F layer in the stratigraphy of figure...).



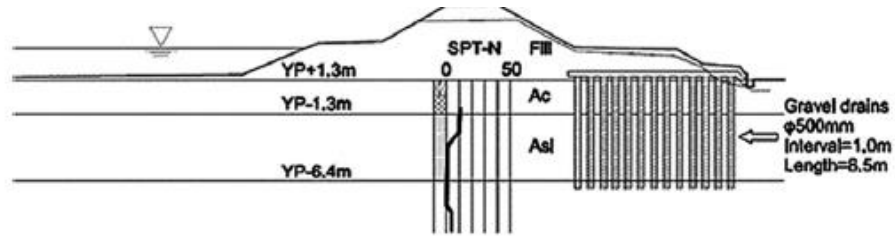
Da Yamaguchi et al. 2012 (a)

Sand Compaction piles (SCP) and gravel drains (GD) intervention have shown good results. Similar techniques have also been used on river embankments with positive results. Along Tone river, on some sections gravel drains have been realized. Earthquakes occurred subsequently to the drain installation have shown a significantly different behavior between the section equipped with gravel drains and the sections with the original embankment structure. The sections with gravel drains have experienced almost no damages, differently from the sections without any remediation work.

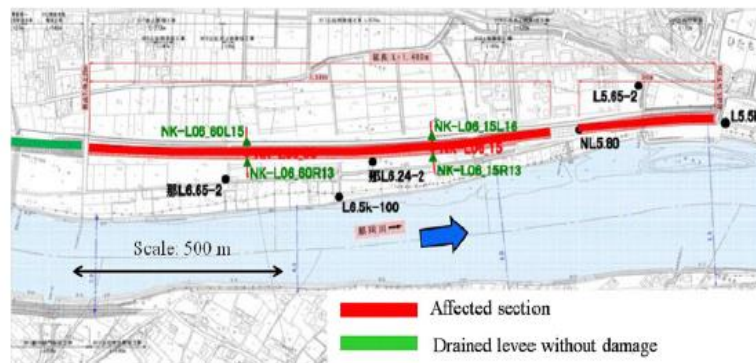


Da Sasaki et al. 2012

Gravel drains can be installed underneath the embankment or inside the embankment body itself, according to the liquefaction susceptibility of the different layers.



Da Sasaki et al. 2012



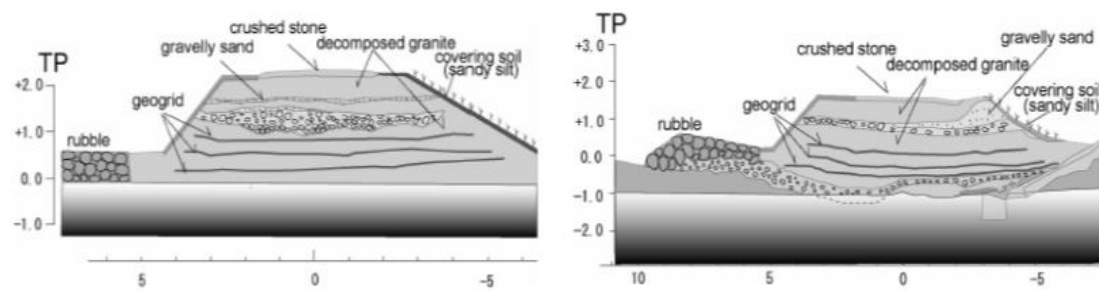
Da Sasaki et al. 2012

Sections treated with gravel drains represented with green line in figure.... didn't show liquefaction evidences. The sections indicated with red line, which were not improved with gravel drains were almost all affected by damages, even if with different levels of severity.



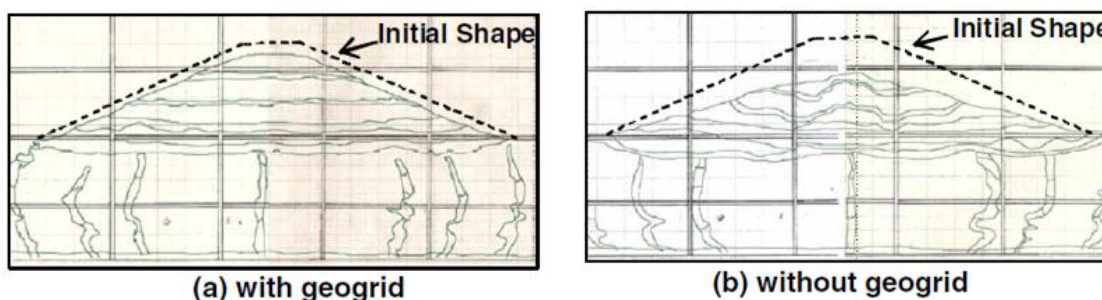







Da Sasaki et al. 2004

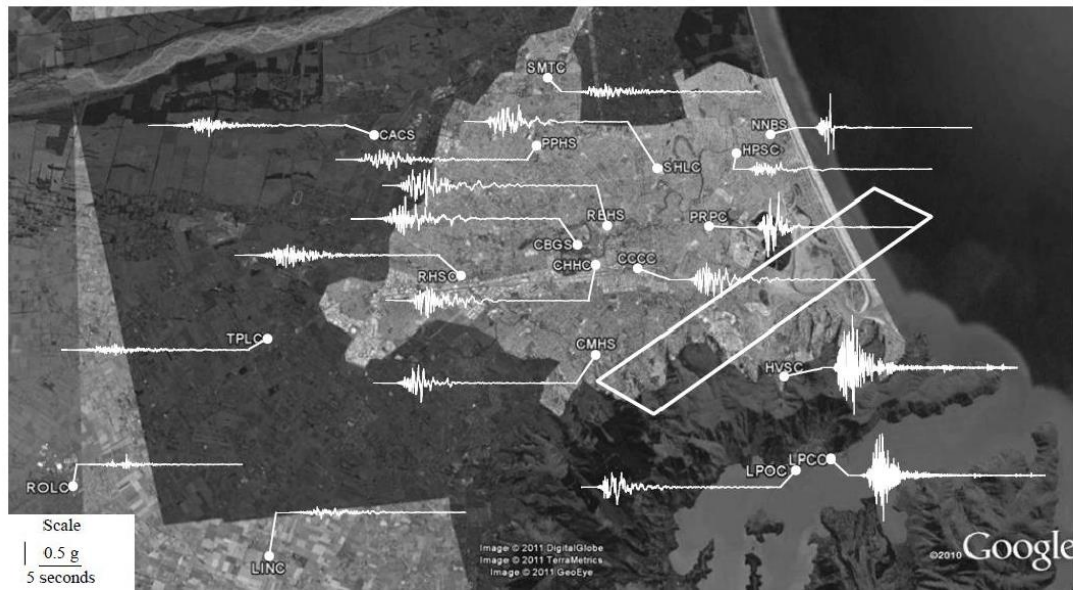
The use of sand compaction piles, stone columns and gravel drains has proved to be very effective for mitigation of liquefaction potential both on buildings and on embankments and earth structures in general. The cost of these remediation techniques is however rather high, especially considering that river embankments have usually remarkable extensions. The use of geogrids can be a valid alternative solution. Figure..... refers to the remediation works performed on earth dam around Naka lake after the 1996 earthquake. The Tottoriken-Seibu earthquake that occurred in 2000 in the same area gave the opportunity to evaluate the effectiveness of this technique. The crest experienced a settlement (figure....) which was anyway quite modest and allowed the dam to maintain its functions without reducing its strength. Figure... shows a section where higher deformations were observed caused by the distortions and rotation of the geogrids and by the reduction of the interspace of the different geogrids layers, probably due to the soil softening. In this case liquefaction is thought to be happened inside the dam body.



Tottoriken earthquake has thus shown that geogrid use can be effective for liquefaction potential reduction on river embankment. The results point out that compaction techniques are a better solution compared to geogrid. On the other hand geogrid have a much lower installation cost and for that reason can be considered a valid solution for river embankment and earth structures, which can tolerate some level of deformations, without losing their operation.

### 1.5.2.5 Christchurch earthquake

<b>COUNTRY:</b>	<b>NEW ZEALAND</b>	<b>MAGNITUDE:</b>	<b>6.3</b>
<b>LOCATION:</b>	<b>Christchurch</b>	<b>DATE:</b>	<b>22/02/2011</b>
 <p>The map displays the outline of New Zealand with regional boundaries indicated by dotted lines. Regions labeled include Northland, Auckland, Waikato, Bay of Plenty, Gisborne, Taranaki, Manawatu, Wanganui, Hawke's Bay, Nelson, Tasman, Marlborough, West Coast, Canterbury, Otago, and Southland. Major cities are marked with dots, and the city of Wellington is specifically labeled. A red star is placed on the east coast of the South Island, near the city of Christchurch, to indicate the location of the earthquake.</p>			



Christchurch earthquake has caused one of the most extensive soil liquefaction events ever observed. The magnitude of the event was not particularly high, but the fact that the epicentre was under the city itself has generated very high accelerations in many neighborhoods (fig.....). These input motion combined with a soil prone to liquefaction and high water table level has caused huge damages to buildings, river embankments and service lines.

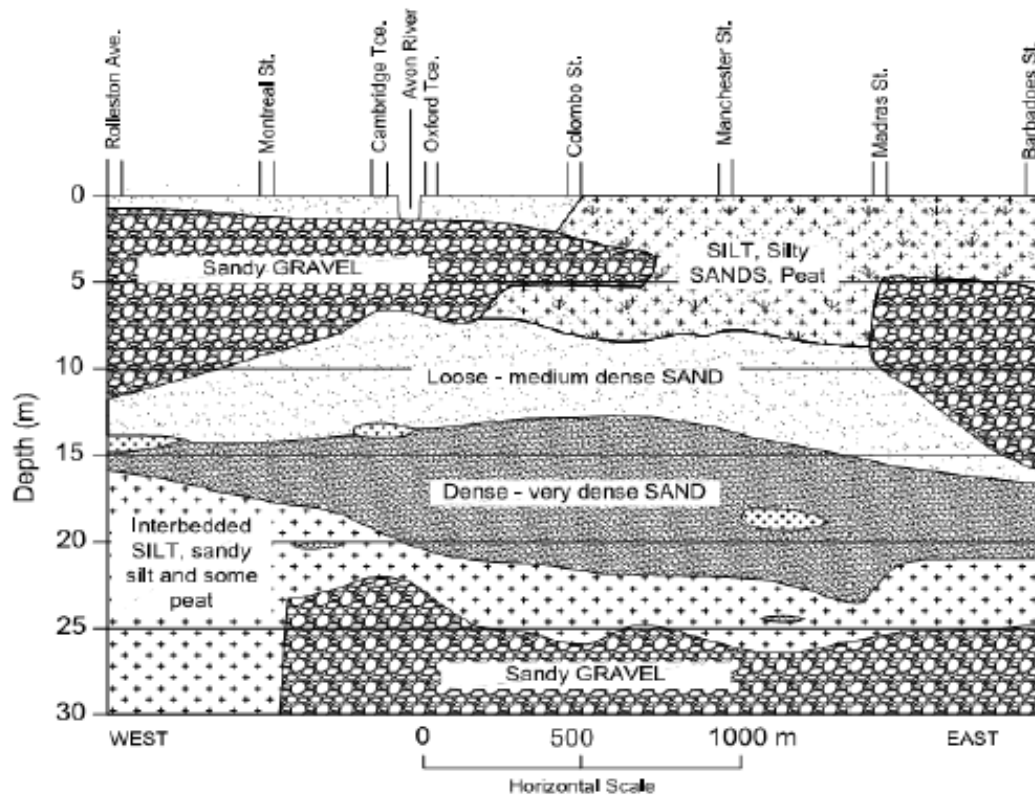




The geological characteristics of Christchurch are quite complex. The western part of the city is based on sediments carried by Waimakariri river, which is now flowing approximately 10 km north from the city. The eastern part of the city is showing a more varied geological structure. For long time it has been occupied by by swamps and coastal deposits. This area has been covered with alluvial deposit carried by the 2 city rivers, the Avon and the Heathcote.



Almost all the eastern area of Christchurch experienced soil liquefaction. Most of the embankment, especially those of Avon river were completely damaged.



From Cubrinovsky 2011

Liquefaction took place in the loose sandy layers located between 3 and 8 m from ground surface. In the liquified area the water table level is rather high, around 1-2 m from the surface.



---

From Cubrinovsky 2011

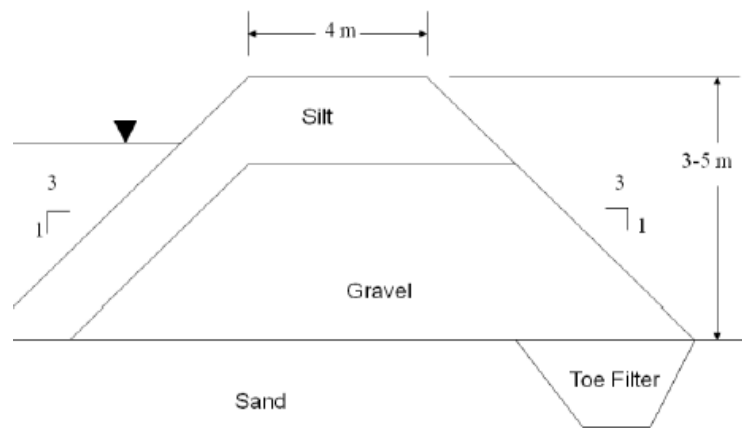
Lateral spreading effects have caused damages not only to the earth structures but also to roads and buildings in the surroundings, considering the level of urbanization of the area. Lateral spreading occurred in fact even in zone with very small inclination of the surface; this means that not only the proper embankment structures faced damages but also the slightly inclined surfaces in the proximity of the river path.



Lateral spreading caused important damages to bridge structures. The horizontal movement of the upper layer of soil that liquefied was following the surface inclination and directed towards the river bed. This caused the back rotation of the abutments, since the deck was blocking the movement of the top of the abutments. Almost all bridges on Avon river were damaged by lateral spreading and the all showed a similar damage pattern, even if with different levels of severity. Fortunately, the characteristics of the bridges along Avon river, which are of short length, limited height and of squat and stiff structure avoided total collapses and catastrophic consequences.

---





Typical longitudinal cracks on the crest of the embankment. Samples taken from sand boils proved that the surficial layer liquefied.





Emergency repairs on the earth structures were realized with geogrids, in order to protect the eastern neighbourhood of the city in a short time from high tides. The earthquake, and the consequent liquefaction, caused in fact the subsidence of many areas close to Avon estuary. The subsidence was quite relevant, many tens of cm and in some zones around 1 m. This made any areas vulnerable to high tides.

---

## **CHAPTER 2**

# **Methods for liquefaction triggering**

The main aspects of sand behaviour and soils in general under seismic conditions have been introduced in chapter 1. A further step is the development of methods able to evaluate the liquefaction susceptibility. This is a difficult task to reach because the soil behaviour is conditioned by several factors, including the number of loading cycles, relative density, confining stress, depositional method, fabric, prior stress-strain history, age, cementation, and other environmental factors. Many methods have been suggested in literature: some of them are quite simplified and base of soil properties that can be easily obtained. Some methods, that will be described in detail in paragraph... are based on in-situ tests such as CPTU, SPT and SDMT; other methods are instead based on laboratory tests. There are, finally more sophisticated methods based on advanced soil constitutive models.

### **2.1 Main aspects affecting the estimation of liquefaction susceptibility**

The liquefaction occurrence of a certain soil can be considered as a dual problem: on one side there is the soil resistance, considered as the soil tendency or non-tendency to develop excess pore water pressure and to loose its strength; on the other side there is the cyclic load applied to the soil in terms of frequency, number of cycles ecc.. Obviously the two aspects are strictly related since a same soil could liquefy or not liquefy is subjected to two different cyclic loads.

Focusing first on defining soil properties in resisting to cyclic loading, apparently they could be determined by obtaining high-quality field samples and then testing them in an appropriate laboratory device. Unfortunately sand sampling is a quite delicate operation: the use of conventional techniques provides quite unreliable results, because of the excessive sample disturbance. More reliable sampling techniques that provide

---

lower sampling disturbance are available even if they are usually associated to a great costs increase and for this reason not always usable. In any case, every kind of sampling provide some disturbance and therefore a good knowledge of how the sampling technique affects the laboratory tests results is required.

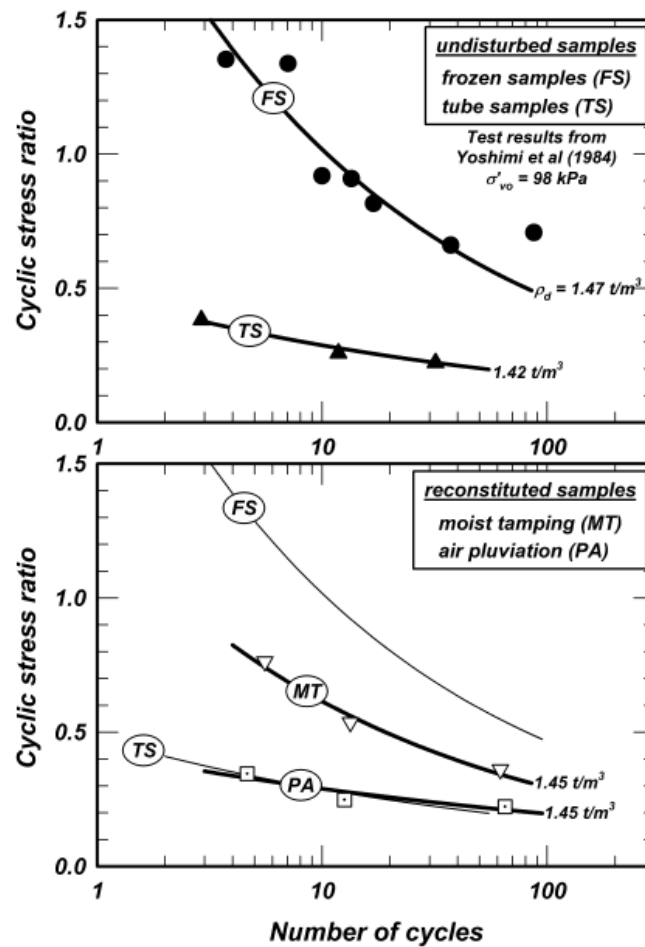
Conventional tube sampling can be performed using more refined high-quality sampler in order to reduce the disturbance. An alternative can be the frozen sampling techniques, which is considered nowadays the best technique to obtain undisturbed samples in sandy soil, because of its ability to preserve the original void distribution and fabric structure: the sand is frozen in situ and then samples are obtained by coring the frozen ground. The frozen samples are transported to the laboratory and tested. A more recent technique known as Gel-Push technique (.....) has proved to be a valid alternative to the frozen sampling: a tube sampler is filled with a special gel before penetrating the soil for sampling. The gel has the function to maintain the in-situ soil structure without altering the soil structure. Experiments have proved that Gel-Push technique provide results similar to the frozen sampling technique with the advantage of lower operational costs.

Reconstituted specimens are an additional option to provide samples for laboratory test. The most traditional moist tamping technique have prove to provide results in terms of soil density and fabric not enough accurate for good quality testing. It is relevant to note that for liquefaction aspects in particular, the volumetric properties of soils are of fundamental importance and it is essential to use samples with the same characteristics of in-situ soils. A secondo option to provide reconstituted specimens is the pluvation technique, which provides good results, especially considering that liquefiable soil are young soils typically coming from fluvial deposition and having layering procedure similar to the in-situ one helps in obtaining good samples. In any case, reconstituted samples of a specific soil should be compared with undisturbed samples of the same soil in order to calibrate the reconstitution procedure and obtain the same relative density. Reconstituted sand specimens must be used with care and with a good calibration and comparison with undisturbed samples since in situ fabric, cementation, aging affect greatly the resistance of soils under cyclic loading and in the reconstitution process those properties can be easily altered (Porcino and Ghionna 2002).

In summary, careful laboratory testing can provide a valuable measure of a soil's cyclic stress-strain behavior, if the samples are truly undisturbed.

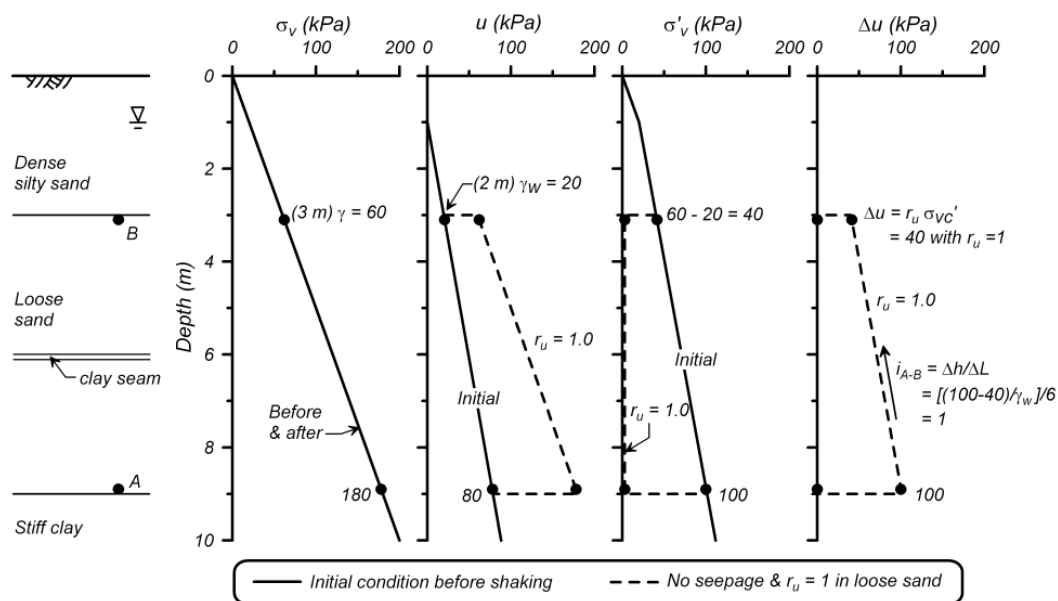
Nonuniformities of strain in laboratory test specimens can alterate experimental results. A tipycal situation that occur on dense sand samples during drained loading is the formation of shear bands: after the formation of the shear band, any additional deformation take place along the band.

---



From Idriss and Boulanger 2008

In addition, there are in situ conditions that cannot be replicated in laboratory tests, even using a high quality sampling technique. The excess pore water pressures generated by a generic perturbation, mainly seismic events, dissipate with time through a water flow from the areas with high water pressure to areas with lower water pressure. The water flow affects the soil behaviour (strength loss and deformation) and is greatly conditioned by the site stratigraphy and can hardly be evaluated through laboratory tests.

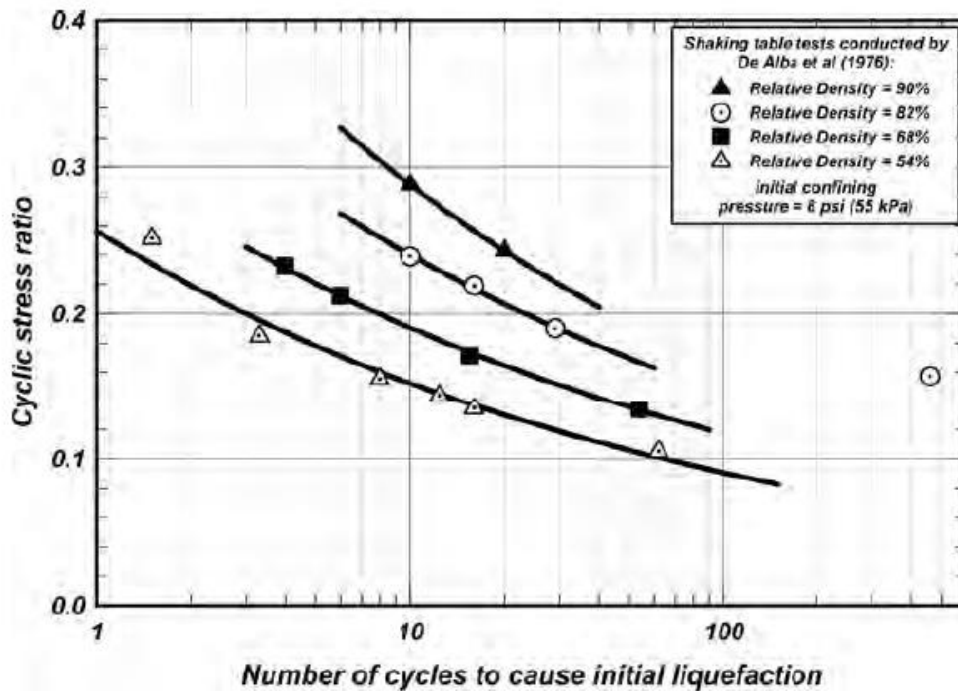


From Idriss and Boulanger 2008

Typically the excess pore pressure generates in the liquefiable soil and the flow goes in the direction of non-liquefiable soils or less liquefiable soils and eventually of the surface, in this case with material ejecta. The flow is often concentrated along cracks and localized channels and producing sand and water boils at the ground surface. In some cases the water flow can increase the water pressure in layers with lower liquefaction susceptibility until inducing liquefaction in those layers as well. Pore water can also accumulate in the interface between a liquefiable layer and an impermeable low liquefiable layer, such as a clayey layer, creating water films.

The development of analytical procedures for assessing liquefaction triggering is based on empirical data to provide the link between liquefaction resistance and in-situ test parameters. Cyclic triaxial tests and cyclic simple shear tests are the two most reliable laboratory test for studying the cyclic behaviour of soils. The two kind of tests provide different results on testing the same specimen, due to the different loading scheme used in the devices. For evaluating liquefaction purposes cyclic shear test is considered more reliable because the loading scheme is more similar to the real loading pattern provided by a seismic event on a soil profile.

Liquefaction of saturated sands can be triggered by different combinations of uniform cyclic shear stress ratio (CSR), which is the uniform cyclic shear stress divided by the initial effective confining stress, and the number of loading cycles (N). A greater CSR will trigger liquefaction in fewer loading cycles, whereas a smaller CSR will require more loading cycles. This aspect of behavior is illustrated by the results of the shaking table tests by De Alba et al. (1976), as shown in Figure ( ).



From Idriss and Boulanger 2008

The CSR that is required to reach liquefaction in a specified number of loading cycles may also be called cyclic resistance ratio (CRR). The relationship between the CRR and  $N$ , can generally be approximated with a power function as

$$CRR = a \cdot N^{-b}$$

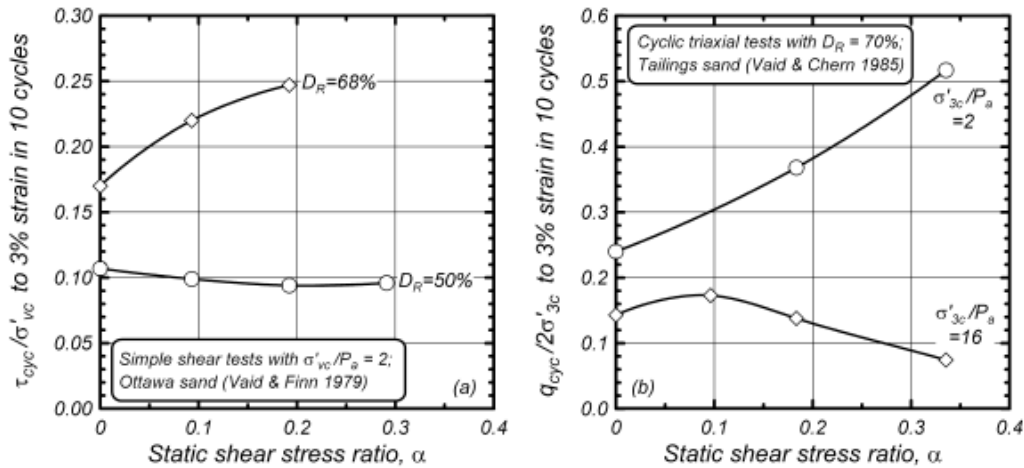
where the parameters  $a$  and  $b$  are experimental parameters.

The CRR of sand increases with increasing relative density. The CRR of sand also depends on the effective confining stress, which reflects the fact that the tendency of sand to dilate or contract depends on confining stress. Seed (1983) introduced the overburden correction factor ( $K_\sigma$ ) as a way to represent the dependence of the CRR on consolidation stress, with  $K_\sigma$  defined as

$$K_\sigma = \frac{CRR_{\sigma'_c}}{CRR_{\sigma'_c=1}}$$

where  $CRR_{\sigma'_c}$  is the CRR of a soil under a specific value of effective consolidation stress  $\sigma'_c$ , and  $CRR_{\sigma'_c=1}$  is the CRR of the same soil when  $\sigma'_c = 1$  atm.

The effect of an initial static shear stress on the undrained cyclic loading behaviour and consequently on pore pressure and shear strain generation of granular soils is not negligible (Idriss and Boulanger 2008). This effect is for example shown on the experiments illustrated on figure .....

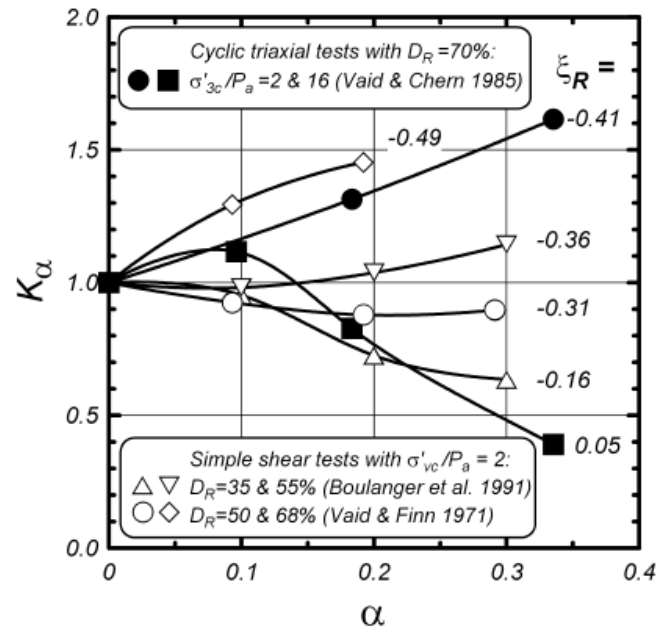


From Idriss and Boulanger 2008

The generation of excess pore pressure and shear strains during undrained cyclic loading of saturated sand is significantly affected by the rotation of principal stress directions, which reverses the shear stress direction on certain planes. Seed (1983) developed the  $K_\alpha$  correction factor to represent the effects of an initial static shear stress ratio ( $\alpha$ ) on the cyclic strength.  $K_\alpha$  is defined as the cyclic strength for some value of  $\alpha$ , divided by the cyclic strength for  $\alpha = 0$ :

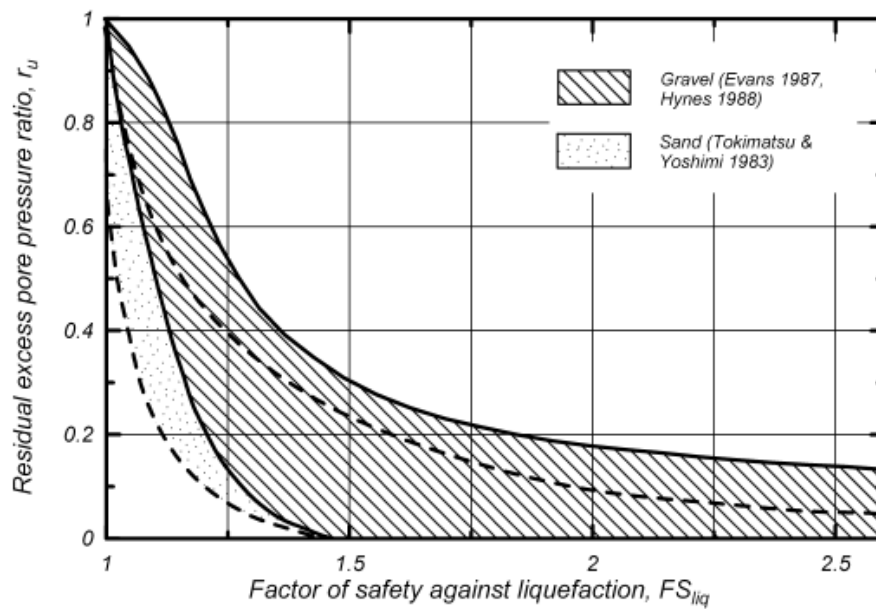
$$K_\alpha = \frac{CRR_\alpha}{CRR_{\alpha=0}}$$

$K_\alpha$  depends on relative density and confining stress, as illustrated in Figure. The  $\xi_R$  index appears to provide a reasonable means of accounting for the combined influence of relative density and confining stress on  $K_\alpha$  relationships for sands.



The factor of safety against liquefaction  $FS_{liq}$  is determined as

$$FS_{liq} = \frac{CRR}{CSR}$$





The CRR is typically taken at about 15 cycles of uniform loading to represent an equivalent earthquake loading of magnitude (M) 7.5, i.e., CRR7.5. The CRR for any other size earthquake can be estimated using the following equation:

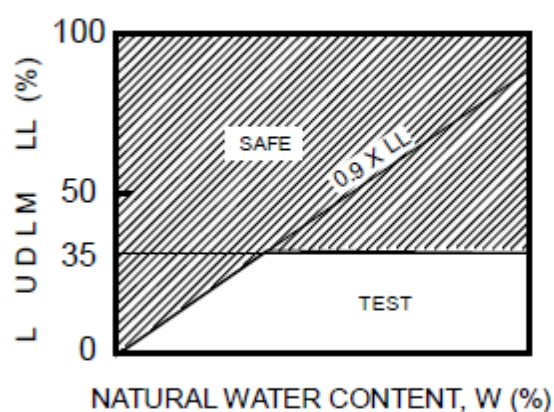
$$\text{CRR} = (\text{CRR}_{7.5}) (\text{MSF})$$

where MSF is the magnitude scaling factor.

## 2.2 COMPOSITIONAL CRITERIA

One of the first and simplest methods for the evaluation of liquefaction susceptibility is the so called Chinese criteria (Wang, 1979) which plots the soils liquefiable and not-liquefiable on a chart based on water content (W) and liquid limit (LL); in addition there are some requirements related to the fine content. The Chinese criteria is based on empirical data from liquefaction case histories and does not consider the ground motion parameters. It does not provide then a Factor of Safety as the Seed and Idriss (1971) does, but simply evaluates the soils that, according to their compositional characteristics might be liquefaction prone.

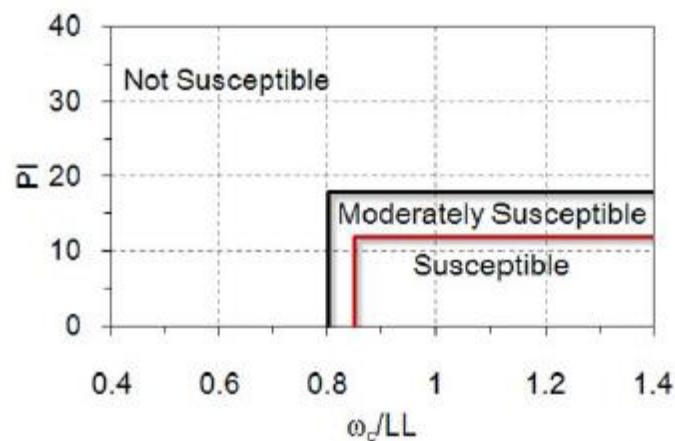
1. Percent Finer than 0.005mm  $\leq 15\%$
2. Liquid Limit (LL)  $\leq 35\%$
3. Water Content (W)  $\geq 0.9 \times \text{LL}$



The soil properties in terms of type and state (void ratio, effective confining stress, stress history, etc.) are the key elements for evaluating the behaviour under cyclic loading: to seismic loading varies with soil type and state. The same concept emerging from the

Chinese criteria has been clarified by Boulanger and Idriss (2004) distinguishing between *sand-like* and *clay-like* behavior. Sand-like soils are susceptible to cyclic liquefaction when their behavior is typically characterized by Plasticity Index (PI) < 10 and Liquid Limit (LL) < 37 and natural water content ( $w_c$ ) > 0.85 (LL) (Robertson.....). Clay-like soils are generally not susceptible to cyclic liquefaction when their behavior is characterized by PI > 15 but they can experience cyclic softening (Robertson....).

Bray and Sancio (2006) provided their own criteria based on soil properties, considering water content (W), liquid limit (LL) and plasticity index (PI) and obtaining a chart for the evaluation of liquefaction susceptibility (fig .....). This latter method considers also a transition zone which must be evaluated with care and with additional tests.



## 2.3 Methods based on in situ tests

The "simplified procedure", introduced by Seed and Idriss (1971), is currently used for evaluating the liquefaction potential. This method requires the calculation of the seismic demand on a soil layer generated by the earthquake, or cyclic stress ratio (CSR) and of the capacity of the soil to resist liquefaction, or cyclic resistance ratio (CRR).

If CSR is greater than CRR, liquefaction can occur (factor of safety against liquefaction).

The cyclic stress ratio CSR is calculated by the equation:

$$CSR = \tau_{av} / \sigma'_{v0} = 0.65 (a_{max} / g) (\sigma_{v0} / \sigma'_{v0}) r_d$$

where  $\tau_{av}$  = average cyclic shear stress,  $a_{max}$  = peak horizontal acceleration at ground surface generated by the earthquake,  $g$  = acceleration of gravity,  $\sigma_{v0}$  and  $\sigma'_{v0}$  = total

and effective overburden stresses and  $r_d$  = stress reduction coefficient dependent on depth, mostly in the range  $\approx 0.8$  to 1.

CRR is instead calculated with different methods based on in-situ or laboratory tests and provide the resistance that the soil is able to provide against a cyclic load.

One reason for the continued use of the SPT has been the need to obtain a soil sample to determine the fines content of the soil. However, this has been offset by the generally poor repeatability of the SPT data.

Currently, the most popular simple method for estimating CRR is the CPT because of its repeatability and the continuous nature of its profile.. A simplified method to estimate CSR was also developed by Seed and Idriss (1971) base on the maximum ground surface acceleration ( $a_{max}$ ) at the site. This simplified approach can be summarized as follows:

$$CSR = \frac{\tau_{av}}{\sigma'_{vo}} = 0.65 \left( \frac{a_{max}}{g} \right) \left( \frac{\sigma'_{vo}}{\sigma_{vo}} \right) r_d$$

where  $\tau_{av}$  is the average cyclic shear stress;  $a_{max}$  is the maximum horizontal acceleration at the ground surface;  $g$  is the acceleration due to gravity;  $\sigma_{vo}$  and  $\sigma'_{vo}$  are the total and effective vertical overburden stresses, respectively; and  $r_d$  is a stress-reduction factor which is dependent on depth which can be calculated with the equation:

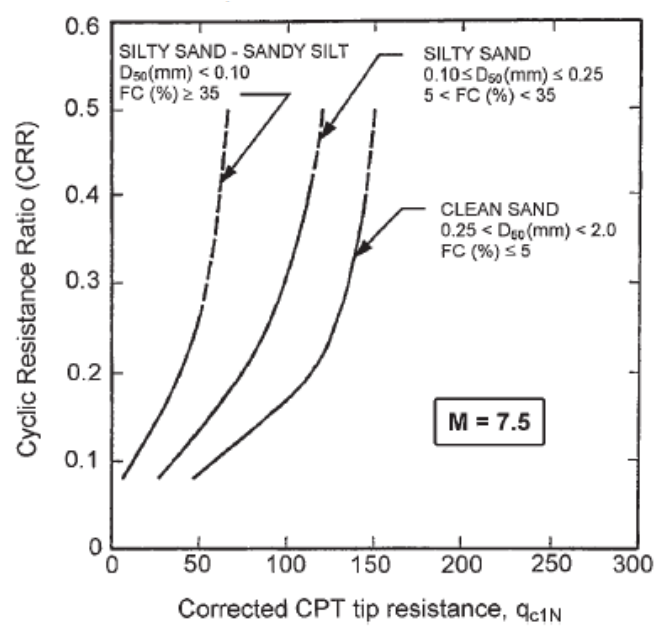
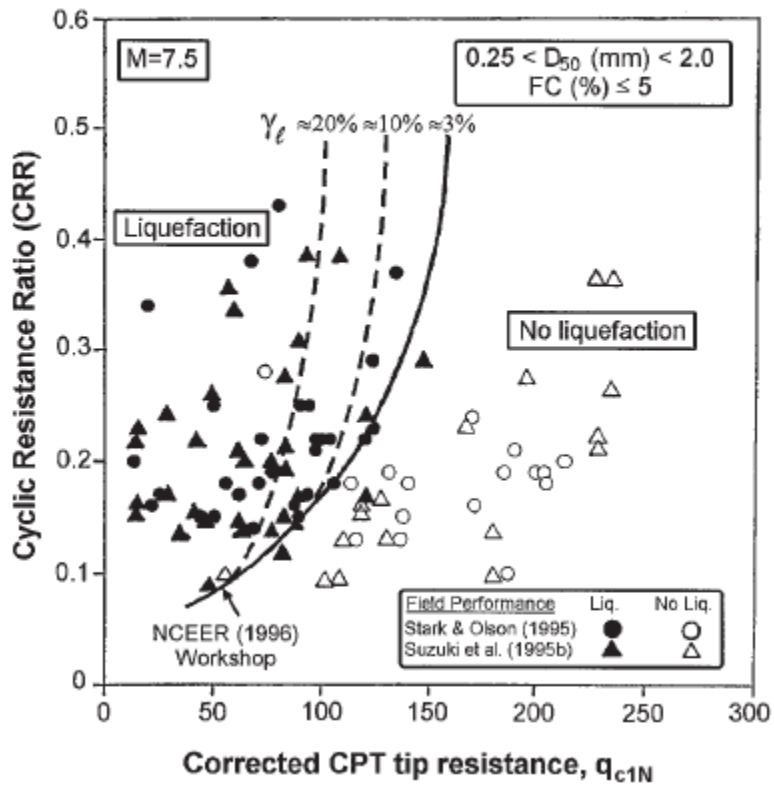
$$\begin{aligned} r_d &= 1.0 - 0.00765z \\ &\quad \text{if } z < 9.15 \text{ m} \\ &= 1.174 - 0.0267z \\ &\quad \text{if } z = 9.15 \text{ to } 23 \text{ m} \\ &= 0.744 - 0.008z \\ &\quad \text{if } z = 23 \text{ to } 30 \text{ m} \\ &= 0.5 \\ &\quad \text{if } z > 30 \text{ m} \end{aligned}$$

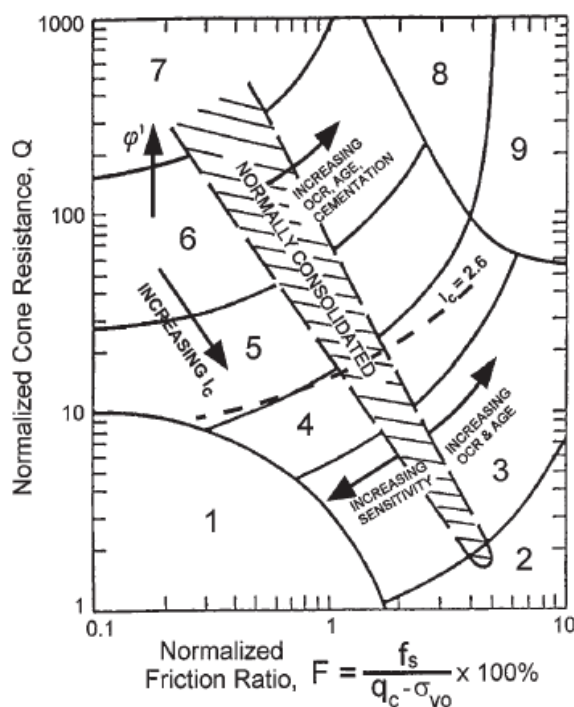
### 2.3.1 NCEER method

In recent years, there has been an increase in available field performance data, especially for the CPT. The recent field performance data have shown that the existing CPT-based correlations to estimate CRR are generally good for clean sands. The proposed equation to obtain the equivalent clean sand normalized CPT penetration resistance,  $(q_{c1N})_{cs}$ , is a function of both the measured penetration resistance,  $q_{c1N}$ , and the grain characteristics of the soil, as follows:

$$(q_{c1N})_{es} = K_c q_{c1N}$$

where  $K_c$  is a correction factor that is a function of the grain characteristics of the soil.





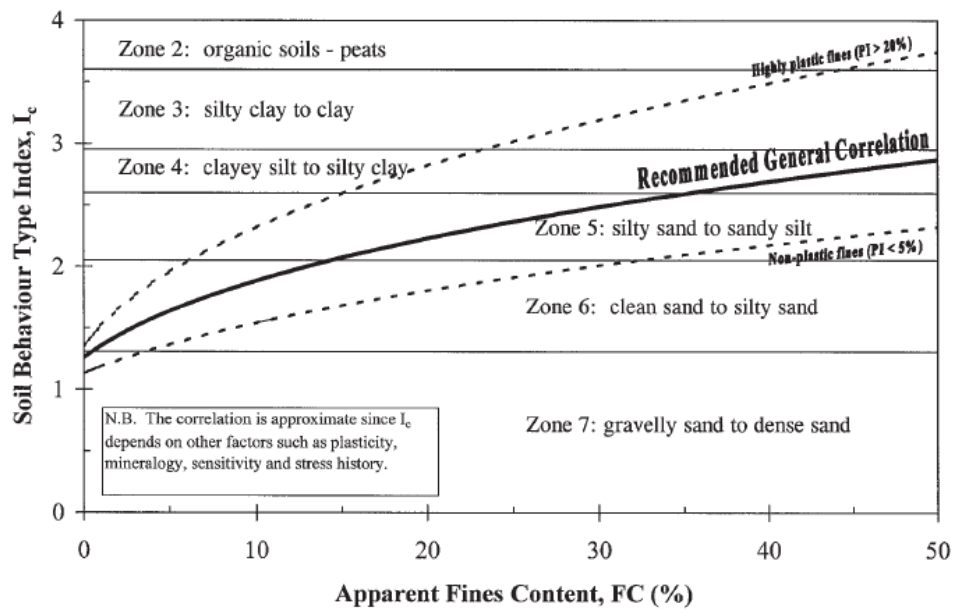
Grain characteristics such as apparent fines content of sandy soils can be estimated directly from CPT data using soil behaviour charts (Robertson....) available in literature, since CPT friction ratio increases with increasing fines content and soil plasticity. The measured penetration resistance can then be corrected to an equivalent clean sand value. Using the CPT chart by Robertson (1990), the soil behaviour type index,  $I_c$ , can be defined as follows:

$$I_c = [(3.47 - Q)^2 + (\log F + 122)^2]^{0.5}$$

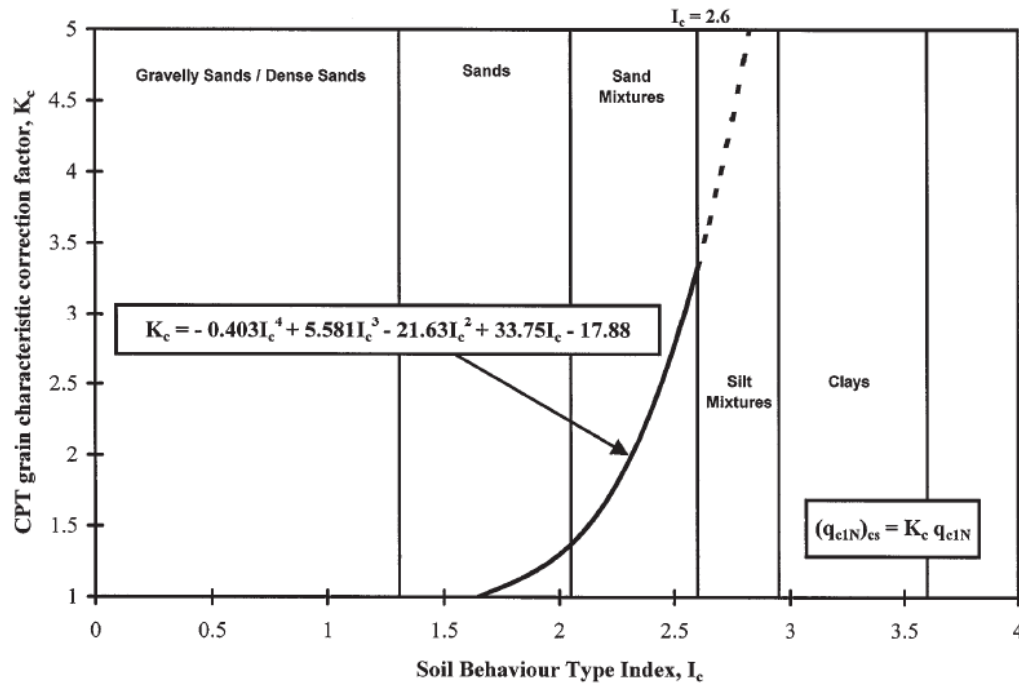
An important reference value, which prove to be a good tool for a preliminary liquefaction susceptibility evaluation, is the  $I_c$  value = 2,6. Typically soils with  $I_c > 2,6$  are not liquefiable, pointing out that  $I_c$  is a soil behaviour type index.

**Table 1.** Boundaries of soil behaviour type (after Robertson 1990).

Soil behaviour type index, $I_c$	Zone	Soil behaviour type (see Fig. 8)
$I_c < 1.31$	7	Gravelly sand to dense sand
$1.31 < I_c < 2.05$	6	Sands: clean sand to silty sand
$2.05 < I_c < 2.60$	5	Sand mixtures: silty sand to sandy silt
$2.60 < I_c < 2.95$	4	Silt mixtures: clayey silt to silty clay
$2.95 < I_c < 3.60$	3	Clays: silty clay to clay
$I_c > 3.60$	2	Organic soils: peats



The chart presented in figure.... (Robertson...) provides a correlation  $I_c$  and the fine content, combined with the plasticity index. The chart is of great importance for the liquefaction related problems, since fine content and plasticity play a key role on it. Relevant to note that the correlation based on the CPT is affected by a level of uncertainties since the CPT measured parameters ( $q_c$ ,  $f_s$ , and  $u$ ) responds to many other factors affecting soil behaviour, such as soil plasticity, mineralogy, sensitivity, and stress history. Figure... shows the chart for obtaining the correction factor  $K_c$  from the  $I_c$  values.



When thin sand layers are embedded in softer deposits, the CPT will not always measure the correct mechanical properties: the difficulty of analysing profile with complex layering has been proved in different situations (Robertson...) and consequently additional tests must be performed and different analysis techniques should be combined. Procedures are proposed with the aim to correct cone data in thin layers; for example a correction factor is given by Robertson and Wride (1998) in the NCEER report and will be used in chapter 7 to perform preliminary analysis.

Using the equivalent clean sand normalized penetration resistance  $(q_{c1N})_{cs}$ , the CRR (for  $M = 7.5$ ) can be estimated using the following simplified equation:

[8a]

$$\text{if } 50 \leq (q_{c1N})_{cs} < 160, \quad \text{CRR} = 93 \left[ \frac{(q_{c1N})_{cs}}{1000} \right]^3 + 0.08$$

[8b]

$$\text{if } (q_{c1N})_{cs} < 50, \quad \text{CRR} = 0.833 \left[ \frac{(q_{c1N})_{cs}}{1000} \right]^3 + 0.05$$

The proposed integrated CPT method is summarized in Fig. () (Robertson ...) in the form of a flow chart.





$$CRR_{7.5} = 93 \left[ \frac{(Q_{m,cs})}{1000} \right]^3 + 0.08$$

if  $50 \leq Q_{m,cs} \leq 160$

$$CRR_{7.5} = 0.833 \left[ \frac{(Q_{m,cs})}{1000} \right] + 0.05$$

if  $Q_{m,cs} < 50$

The correlation to estimate CRR7.5 for silty sands is different than that for clean sands and a correction is needed to determine an *equivalent clean sand penetration resistance* based on grain characteristics. Robertson and Wride (1998) suggest estimating an equivalent clean sand cone penetration resistance with the equation :

$$(Q_{tn})_{cs} = K_c Q_{tn}$$

where  $n \leq 1.0$  (see Figure () for flow chart).

The factor of safety against cyclic liquefaction is defined as:

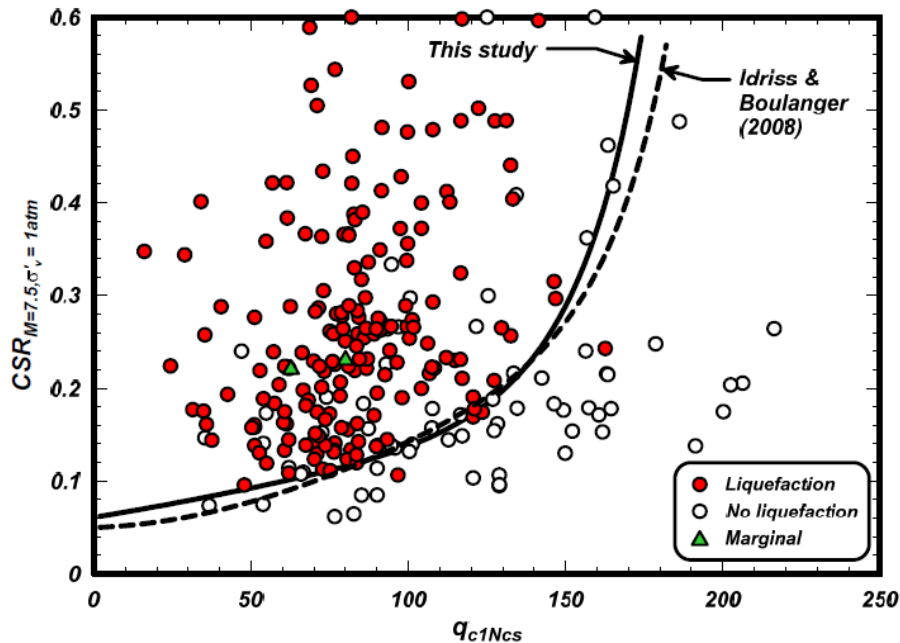
$$\text{Factor of Safety, } FS = \frac{CRR_{7.5}}{CSR} \text{ MSF}$$

Where MSF is the Magnitude Scaling Factor to convert the CRR7.5 for  $M = 7.5$  to the equivalent CRR for the design earthquake. The NCEER recommended MSF is given by:

$$MSF = \frac{174}{M^{2.56}}$$

Clay-like materials tend to develop pore pressures more slowly under undrained cyclic loading than sand-like materials and generally do not reach zero effective stress under cyclic loading. Hence, clay-like materials are not susceptible to complete cyclic liquefaction. However, when the cyclic stress ratio (CSR) is large relative to the undrained shear strength ratio of clay-like materials, deformations and softening can develop. The term 'cyclic softening' is used to define this build-up of deformations under cyclic loading in clay-like soils. The CRR for cyclic softening in clay-like materials is controlled by the undrained shear strength ratio, which is controlled by stress history (OCR).

### 2.3.2 Boulanger & Idriss (2014)



### 2.3.3 Andrus & Stokoe (2000)

The Andrus and Stokoe (2000) is based on the same procedure introduced by Seed and Idriss (1971) described in the previous paragraphs. The seismic demand on a soil layer generated by the earthquake, or cyclic stress ratio (CSR) is obtained with the same formulation used for the other methods based on CPT tests:

$$CSR = \tau_{av} / \sigma'_{v0} = 0.65 (a_{max} / g) (\sigma_{v0} / \sigma'_{v0}) r_d$$

where  $\tau_{av}$  = average cyclic shear stress,  $a_{max}$  = peak horizontal acceleration at ground surface generated by the earthquake,  $g$  = acceleration of gravity,  $\sigma_{v0}$  and  $\sigma'_{v0}$  = total and effective overburden stresses and  $r_d$  = stress reduction coefficient dependent on depth, mostly in the range  $\approx 0.8$  to 1.

The liquefaction resistance CRR, which was derived in the previous paragraphs from CPT tests, is instead based on  $V_s$  measurements. CRR is generally evaluated from in situ measurements (normalized to overburden stress) by use of charts in which the CRR curves define the liquefaction and no-liquefaction areas on the charts, mainly based on

historical earthquakes database. The CPT based methods introduced in the previous paragraphs are more the most common and used methods and can rely on wide database of case histories for the validation of the methods. Nevertheless, considering the importance of using different approaches and combining the results of different analysis, the VS (shear waves velocity) parameter appears a good index for liquefaction resistance analysis. The most popular CRR-VS correlation (Figure ) was proposed by Andrus and Stokoe (2000) for uncemented Holocene-age soils, based on a database including 26 earthquakes and more than 70 test sites. CRR is obtained as a function of an overburden-stress corrected shear wave velocity:

$$VS1 = VS (pa / \sigma'v0)^{0.25},$$

where VS = measured shear wave velocity,

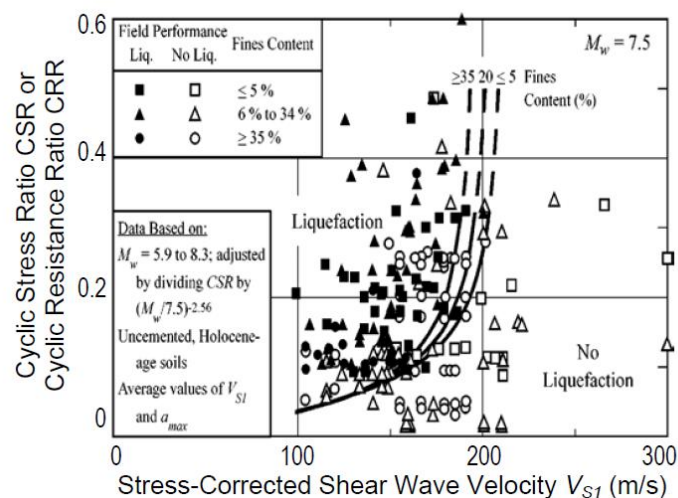
pa = atmospheric pressure ( $\approx 100$  kPa),

$\sigma'v0$  = initial effective vertical stress

Andrus et al. (2004) introduced age correction factors to extend the original correlation by Andrus and Stokoe (2000) to soils older than Holocene. Their CRRVS1 relationship (curves in Figure 3, for various fines contents) is approximated by the equation:

$$CRR = \left[ 0.022 \left( \frac{K_{a1} V_{S1}}{100} \right)^2 + 2.8 \left( \frac{1}{V_{S1}^* - K_{a1} V_{S1}} - \frac{1}{V_{S1}^*} \right) \right] K_{a2}$$

where  $V^* S1$  = limiting upper value of VS1 for liquefaction occurrence,  $K_{a1}$  = factor to correct for high VS1 values caused by aging,  $K_{a2}$  = factor to correct for influence of age on CRR.



Andrus et al. (2004) remarked, however, the high associated uncertainty and the need of additional work to quantify the influence of age on CRR, as well as on VS.

### **2.3.4 Post-earthquake settlements**

Post-earthquake settlements can be estimated using various empirical methods to estimate post-earthquake volumetric strains. The method proposed by Zhang (2007) is based on CPT results and can provide a detailed vertical profile of volumetric strains at each CPT location. Displacement of buildings located above soils that experience liquefaction depend on foundation details and depth, thickness and lateral distribution of liquefied soils. In general, building movements result from a combination of deviatoric and volumetric strains plus possible loss of ground due to ejected soil (sand boils, etc.). Lateral deformation (lateral spreading) can be estimated in an approximated way using various empirical methods (Youd et al, 2002 and Zhang et al, 2004). The method by Zhang et al (2004) is based on CPT results and can provide a detailed vertical profile of strains at each CPT location. The CPT-based approach is generally conservative but particular care is required to evaluate the consequences of the calculated lateral displacements taking into account, soil variability, site geometry, depth of the liquefied layers and project details. In general, assume that any liquefied layer located at a depth more than twice the depth of the free-face will have little influence on the lateral deformations (Robertson 2009).

## **2.4 Methods based on critical state concept**

The state concept approach relies on the use of a state measure (state index or state parameter) for modelling sand behaviour. Both state index and state parameter provide measures for the initial state of the soil (in terms of density and normal stress, e.g.  $e-p'$  state) relative to the steady state line (Cubrinovsky 2011). The state concept is not explicitly related to cyclic behaviour but it provides an accurate way of modelling cyclic behaviour. No postulated failure and deformation modes are required, as these are predicted by the analysis itself. The types and number of laboratory tests required for the parameters of the constitutive model may vary significantly and are model-dependent.

---

### 2.4.1 Stress-density method

Stress-Density Model (SD) was developed by Curinovsky (1998 a, b) with the aim to provide a tool to analyze soil liquefaction under seismic conditions, able to simulate real soil behaviour taking into account significant temporal and spatial variation of in-situ conditions (changes in the effective stress due to rise of pore water pressures), loads (irregular cyclic stresses) and consequent stress-strain behaviour (highly irregular stress paths including continuous, but also large and abrupt variation in soil stiffness, and significant reduction in strength). A relevant attention must also be given to the post-liquefaction behaviour which leads to large ground deformation and permanent displacements, besides a complete change and redistribution in the soil particles structure.

SD Model is based on the state concept approach for modelling the combined effects of density and normal stress on the stress-strain behaviour of sand. The model is based on the State Index ( $I_s$ ), a parameter proposed by Ishihara (1993) and Verdugo (1992) and defined as:

$$I_s = \frac{e_U - e}{e_U - e_Q}$$

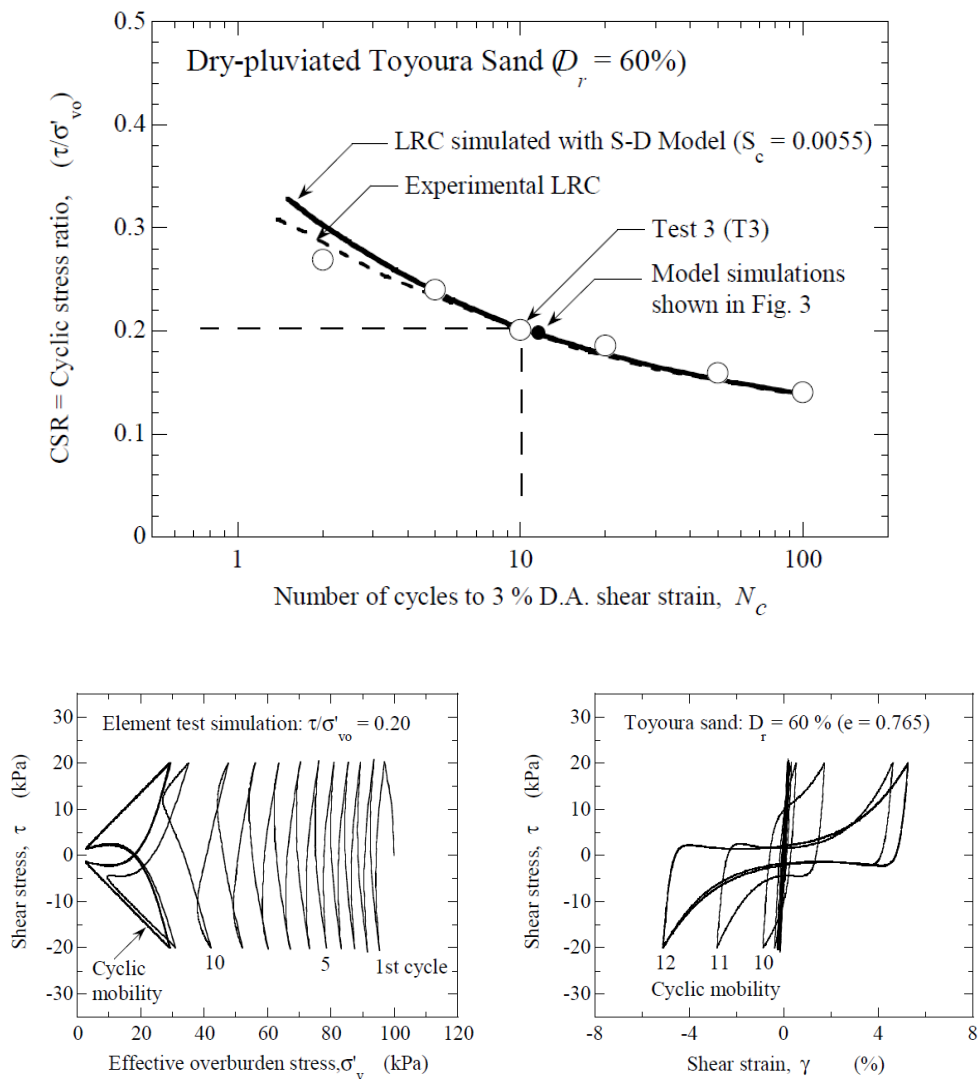
The State Index is used as variable in the model controlling the effects of density and normal stress on the deformative behaviour of sand. It is relevant to note that the state index is employed in the model as a current variable rather than an initial state parameter, that means that the stiffness and peak strength of the sand are dependent on the current value of the state index (Cubrinovski, 1993; Cubrinovski and Ishihara, 1998a). Hence, the stress-strain curve of the soil will change with variation of the current state index (or relative state of the soil).

The key assumptions of the elastic-plastic formulation of the S-D Model are (Cubrinovsky 2011):

- continuous yielding or vanishing elastic region;
- combined isotropic and kinematic hardening plasticity,
- dependence of the plastic strain increment direction on the stress increment direction, or hypoplasticity,
- modified hyperbolic stress-strain relationship,
- an energy-based stress-dilatancy relationship.

The formentioned elements imply the capability of the model to accurately simulate highly nonlinear stress-strain behaviour both under monotonic loading and cyclic loading. In particular the model has to accurately simulate the development of excess pore water pressures under irregular seismic cyclic loading.

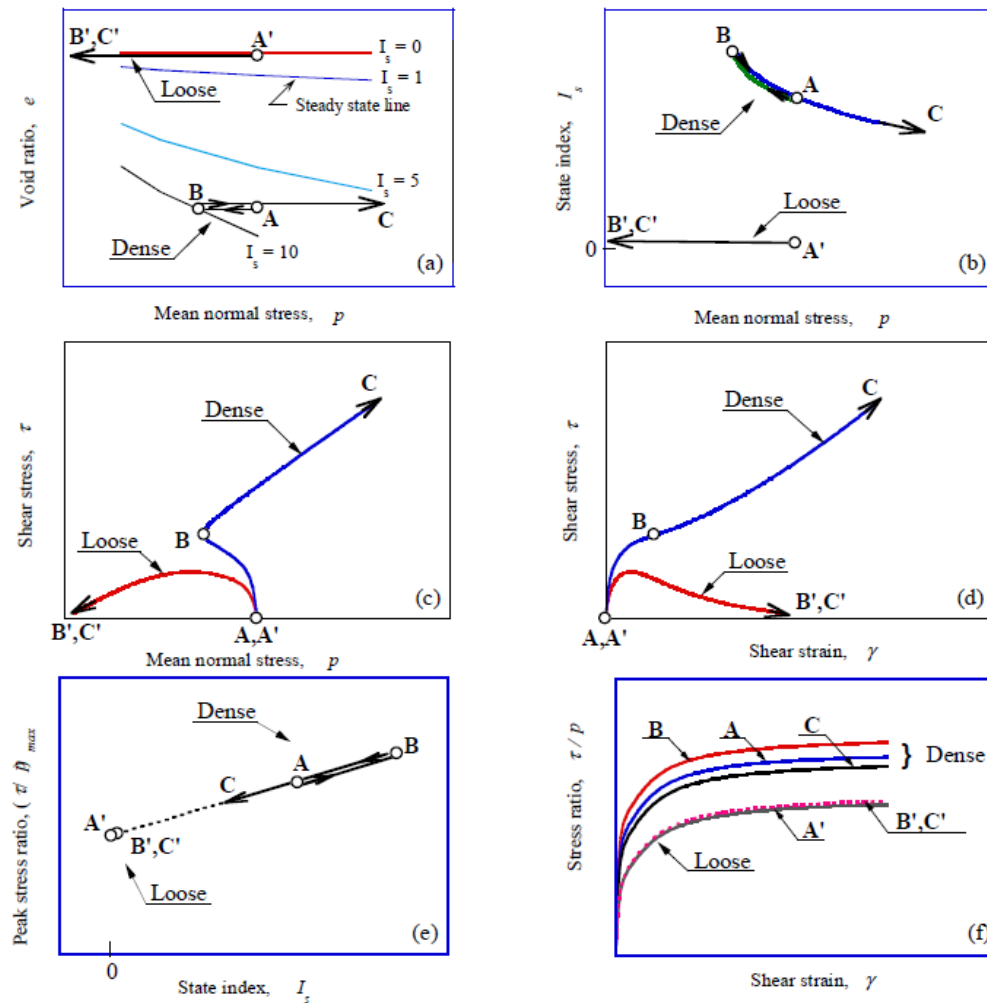
The SD Model has been developed using Toyoura sand samples (Fig. ....). In the figure the results from 6 cyclic torsional shear tests on samples of Toyoura sand with a relative density of  $D_r \approx 60\%$  are reported.



The constitutive model must be able to simulate the experimental curve. Some parameters in the model are iteratively varied to to maximize the correspondence between the experimental and the simulated curve. For the S-D Model, the dilatancy

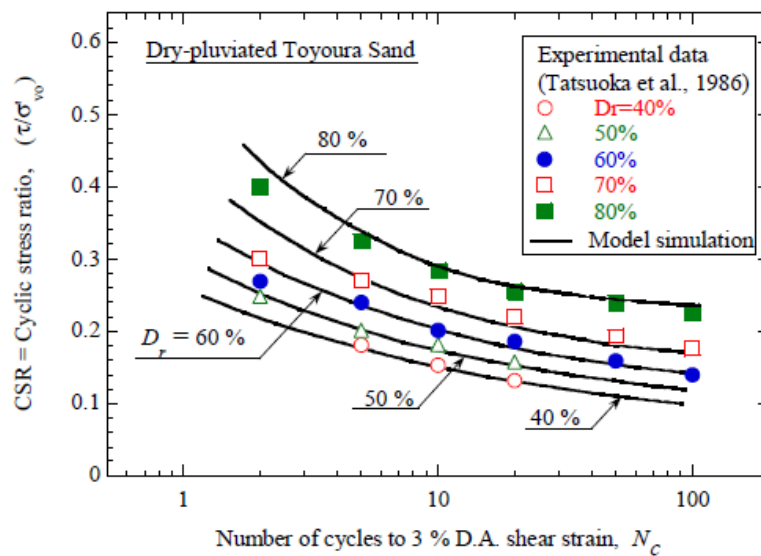
parameter ( $I_s$ ) is the fitting parameter. Figure ... shows the relationships used for incorporating the state index in the S-D model: the initial shear modulus and peak strength of the sand are defined as functions of  $I_s$ . The state concept provides a method for constitutive modelling of the combined effects of density and normal stress on stress-strain behaviour of sand.

The fact that the state index is employed in the model as a current variable rather than an initial state parameter is schematically illustrated in Figure .... Figure 5a shows that for the loose sand  $I_s$  remains nearly constant at  $\sim 0$  during the undrained loading, while for the dense sand  $I_s$  initially increases reaching a value of 10 at phase transformation, and then decreases with the dilation towards the steady state line and an ultimate value of  $I_s = 1.0$ . The  $e-p'$  paths and variations of  $I_s$  for both tests are shown in Figures 5a and 5b, respectively. Figures 5c and 5d show the respective effective stress paths and stress-strain curves, and finally Figures 5e and 5f indicate the variation of the peak strength and change in the stress-strain curve along the undrained paths of these tests (Cubrinovsky 2011).



In addition the use of state index provides a mechanism for modelling of complex post-liquefaction phenomena involving significant change in density/volume such as voids ratio re-distribution.

When sheared cyclically under undrained conditions, the soil will develop positive pore water pressure (due to contractive tendency) and eventually liquefy (if loose enough). Hence, the end state will be at the initial void ratio (because of the undrained condition) and  $p' = 0$  (because of liquefaction). Nevertheless, there appears to be a close link between the monotonic and cyclic behaviour as far as the tendency for contraction or dilation is concerned. Even though the state concept is not explicitly related to cyclic behaviour, it still provides an accurate way of modelling cyclic behaviour. This is illustrated in Figure () where simulations of liquefaction resistance curves obtained by the S-D Model are compared to experimental LRCs for five relative densities of Toyoura sand in the range between 40 % and 80 %. Very good accuracy in the simulation of all liquefaction resistance curves is seen. This clearly demonstrates the capacity of the state concept to capture combined effects of density and normal stress on liquefaction resistance and cyclic stress-strain behaviour.





## CHAPTER 3

# Site response analysis

The following chapter describes the theoretical basis of site response analysis in order to deconvolute the ground motion signal and obtain an input series (velocity time series in this case) for the OpenSees model.

The numerical analysis performed in this study requires a ground motion input at the base of the model; the details of the model and the peculiar aspects of the input motion will be discussed in detail in chapter 8. Anyway, the input motion at the model base is obtained using the data recorded during the Emilia earthquake sequence, specifically data from the Mirandola record station, which is by far the closest to the epicentre and to the study site. The deconvolution of surface acceleration time series is performed to provide representative soil input motion for seismic site response analyses.

Strain dependent soil properties, linear-elastic wave propagation through a layered medium, and the equivalent linear approach to site response analysis are considered.

### 3.1 EQUIVALENT LINEAR 1D SITE RESPONSE ANALYSIS

For linear elastic, one-dimensional wave propagation, the soil is assumed to behave as a Kelvin-Voigt solid, in which the dynamic response is described using a purely elastic spring and a purely viscous dashpot. The solution to the one-dimensional wave equation for a single wave frequency ( $\omega$ ) provides displacement ( $u$ ) as a function of depth ( $z$ ) and time ( $t$ ) (Kramer, 1996):

$$u(z, t) = A \exp[i(\omega t + k^*z)] + B \exp[i(\omega t - k^*z)]$$

---

$$k^* = \frac{\omega}{v_s^*}$$

$$v_s^* = \sqrt{\frac{G^*}{\rho}}$$

$$G^* = G \left( 1 - 2D^2 + i2D\sqrt{1 - D^2} \right) \cong G(1 + i2D)$$

Where  $A$  and  $B$  represent the amplitudes of the upward ( $-z$ ) and downward ( $+z$ ) waves, ( $k^*$ ) is the complex wave number

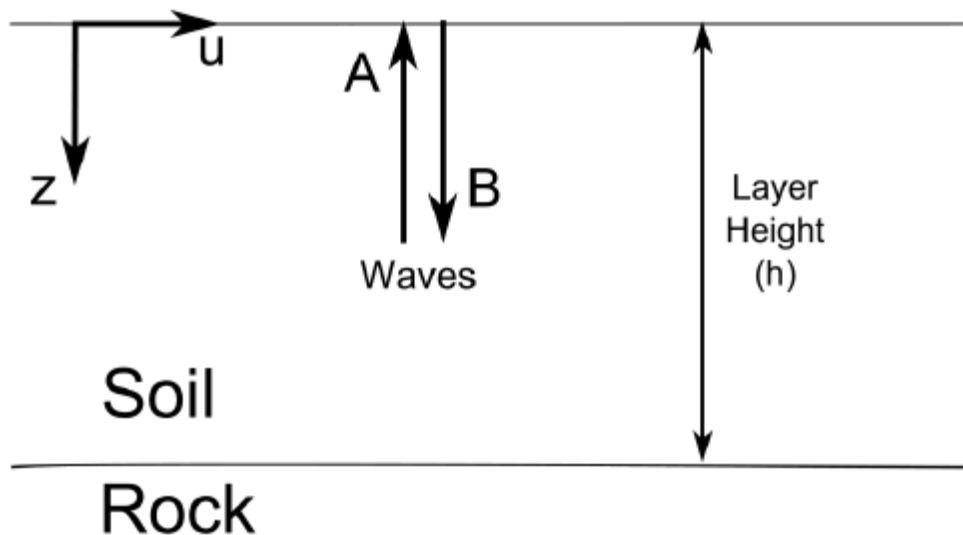
( $G$ ) is the shear modulus,

( $D$ ) is the damping ratio

( $\rho$ ) is the mass density of the soil

$G^*$  and  $v_s^*$  are called the complex shear modulus and complex shear-wave velocity, respectively.

The formula for the complex shear modulus in equation ( ) is appropriate if the damping ratio ( $D$ ) is small (<10-20%). The wave equation ( ) applies only to a single layer with uniform soil properties and the wave amplitudes ( $A$  and  $B$ ) can be computed from the layer boundary conditions.



From Kottke et al. 2013

For a layered system, shown in Figure ( ), the wave amplitudes are calculated using recursive formulas considering compatibility of displacement and shear stress at the layer boundaries. The following recursive formulas are developed (Kramer, 1996):

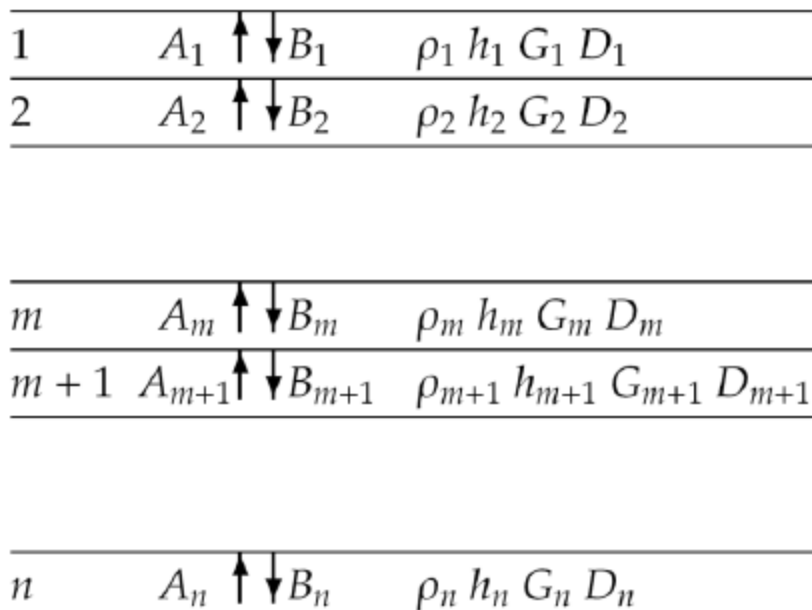
$$A_{m+1} = \frac{1}{2} A_m (1 + \alpha_m^*) \exp\left(\frac{ik_m^* h_m}{2}\right) + \frac{1}{2} B_m (1 - \alpha_m^*) \exp\left(-\frac{ik_m^* h_m}{2}\right)$$

$$B_{m+1} = \frac{1}{2} A_m (1 - \alpha_m^*) \exp\left(\frac{ik_m^* h_m}{2}\right) + \frac{1}{2} B_m (1 + \alpha_m^*) \exp\left(-\frac{ik_m^* h_m}{2}\right)$$

$$\alpha_m^* = \frac{k_m^* G_m^*}{k_{m+1}^* G_{m+1}^*} = \frac{\rho_m v_{s,m}^*}{\rho_{m+1} v_{s,m+1}^*}$$

where  $m$  is the layer number,  $h_m$  is the layer height and  $\alpha_m^*$  is the complex impedance ratio.

At the surface of the soil column in figure .... ( $m=1$ ), the shear stress must equal zero and the amplitudes of the upward and downward waves must be equal ( $A_1=B_1$ ).



From Kottke et al. 2013

The wave amplitudes ( $A$  and  $B$ ) within the soil profile are calculated at each frequency (assuming known stiffness and damping within each layer) and used to compute the response at the surface of a site. This calculation is performed by setting  $A_1=B_1=1.0$  at the surface and recursively calculating the wave amplitudes ( $A_{m+1}, B_{m+1}$ ) in successive layers until the input (base) layer is reached. The transfer function between the motion in the layer of interest ( $m$ ) and in the rock layer ( $n$ ) at the base of the deposit is defined as:

$$TF_{(m,n)}(\omega) = \frac{u_m(\omega)}{u_n(\omega)} = \frac{A_m + B_m}{A_n + B_n}$$

where  $\omega$  is the frequency of the harmonic wave.

The transfer function is the ratio of the amplitude of harmonic motion (displacement, velocity, or acceleration) between two layers of interest and varies with frequency. The locations of the peaks in the transfer function are controlled by the modes of vibration of the soil deposit. The peak at the lowest frequency represents the fundamental (i.e. first) mode of vibration and results in the largest amplification. The peaks at higher frequencies are the higher vibrational modes of the site.

The amplitudes of the peaks are controlled by the damping ratio of the soil. As the damping of the system increases, the amplitudes of the peaks decrease which results in less amplification.

The response at the layer of interest is computed by multiplying the Fourier amplitudespectrum of the input rock motion by the transfer function:

$$Y_m(\omega) = TF_{m,n}(\omega)Y_n(\omega)$$

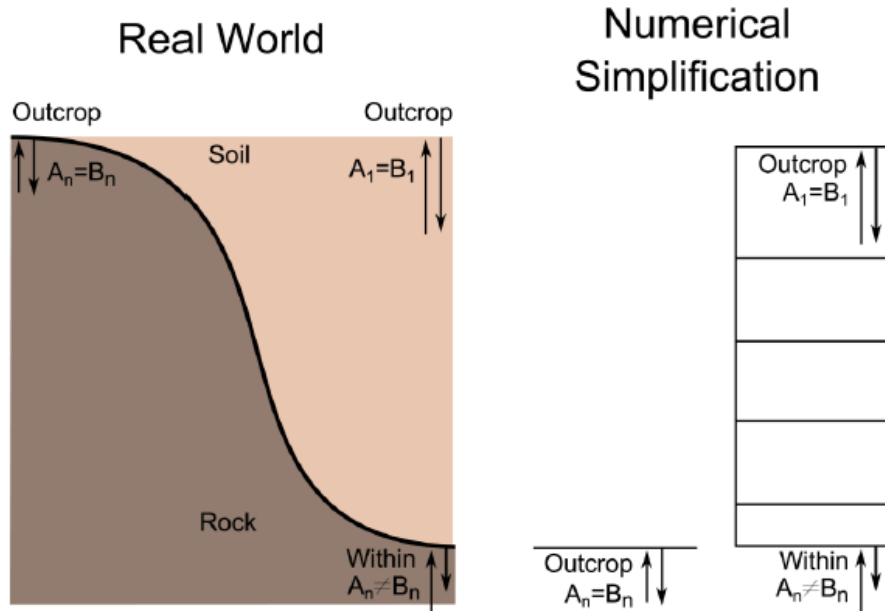
where  $Y_n$  is the input Fourier amplitude spectrum at layer  $n$  and  $Y_m$  is the Fourier amplitude spectrum at the top of the layer of interest.

The Fourier amplitude spectrum of the input motion can be defined using a variety of methods. One issue that must be considered is that the input Fourier spectrum typically represents a motion recorded on rock at a free surface (i.e., the ground surface), where the upgoing and downgoing wave amplitudes are equal ( $A_1=B_1$ ), rather than on rock at the base of a soil deposit, where the wave amplitudes are not equal (Figure ). The change in boundary conditions ( $A_n=B_n$  for a free surface,  $A_n$  is different from  $B_n$  at the base of a soil deposit) must be taken into account. The motions at any free surface are referred to as outcrop motions and their amplitudes are described by twice the amplitude of the upward wave ( $2A$ ). A transfer function can be defined that converts an outcrop motion into a within motion.

$$TF_{m,n}(\omega) = \frac{A_n + B_n}{2A_n} \cdot \frac{A_m + B_m}{A_n + B_n}$$

*outcrop*
*within*  
*to within*
*to layer<sub>n</sub>*

Motions recorded at depth are referred to as within motions. Figure shows the transfer function (surface motion / outcrop motion) for the a site profile. In comparison with the surface / within transfer function, the surface / outcrop transfer function displays less amplification for all modes (Kottke et al. 2013).

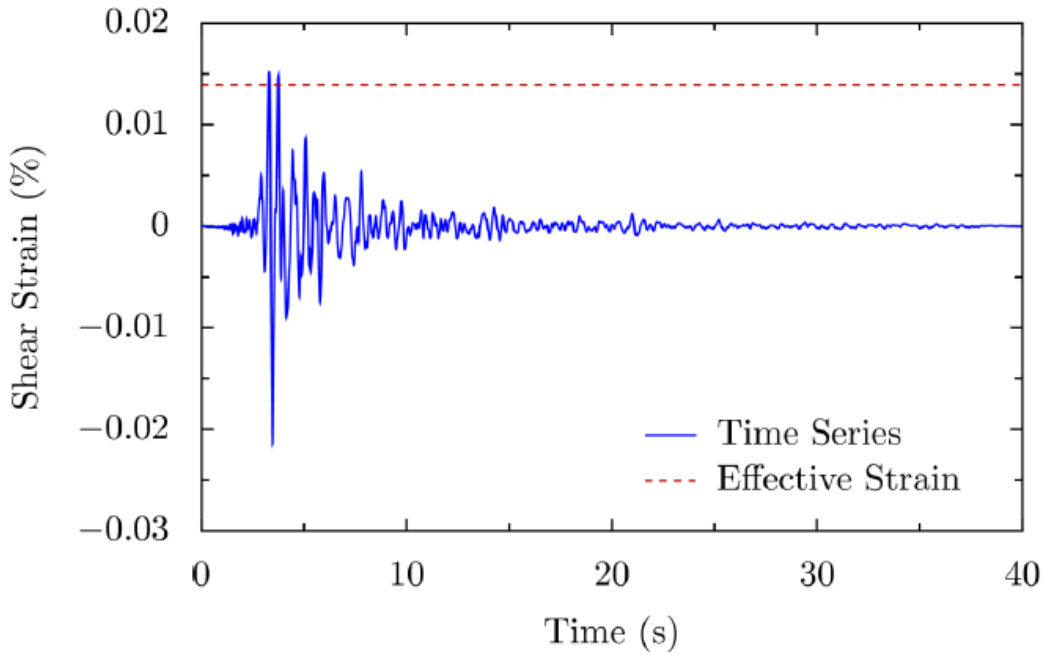


In reality, soil is nonlinear, such that the dynamic properties of soil (shear modulus,  $G$ , and damping ratio,  $D$ ) vary with shear strain and with the intensity of shaking. In equivalent-linear site response analysis, the nonlinear response of the soil is approximated by modifying the linear elastic properties of the soil based on the induced strain level. Because the induced strains depend on the soil properties, the strain compatible shear modulus and damping ratio values are iteratively calculated based on the computed strain.

A transfer function is used to compute the shear strain in the layer based on the outcropping input motion. In the calculation of the strain transfer function, the shear strain is computed at the middle of the layer ( $z=h_m/2$ ) and used to select the strain compatible soil properties. Unlike the previous transfer functions that merely amplified the Fourier amplitude spectrum, the strain transfer function amplifies the motion and converts acceleration into strain. The strain transfer function based on an outcropping input motion is defined by:

$$TF_{m,n}^{strain}(\omega) = \frac{\gamma\left(\omega, z = \frac{h_m}{2}\right)}{\ddot{u}_{n,outcrop}(\omega)} = \frac{i k_m^* \left( A_m \exp\left(\frac{i k_m^* h_m}{2}\right) - B_m \exp\left(-\frac{i k_m^* h_m}{2}\right) \right)}{-\omega^2(2A_n)}$$

The strain Fourier amplitude spectrum within a layer is calculated by applying the strain transfer function to the Fourier amplitude spectrum of the input motion. The maximum strain within the layer is derived from this Fourier amplitude spectrum either through conversion to the time domain or through RVT (random vibration theory) methods; the latter are not taken into account in this research.



Equivalent-linear site response analysis requires that the strain dependent nonlinear properties (i.e.  $G$  and  $D$ ) be defined. The initial (small strain) shear modulus ( $G_{max}$ ) is calculated by:

$$G_{max} = \rho v_s^2$$

where  $\rho$  is the mass density of the site, and  $v_s$  is the measured shear-wave velocity. Characterizing the nonlinear behavior of  $G$  and  $D$  is achieved through modulus reduction and damping curves that describe the variation of  $G/G_{max}$  and  $D$  with shear

---

strain (discussed in the next section). Using the initial dynamic properties of the soil, equivalent-linear site response analysis involves the following steps:

1. The wave amplitudes ( $A$  and  $B$ ) are computed for each of the layers.
2. The strain transfer function is calculated for each of the layers.
3. The maximum strain within each layer is computed by applying the strain transfer function to the input Fourier amplitude spectrum and finding the maximum response.
4. The effective strain ( $\gamma_{\text{eff}}$ ) is calculated from the maximum strain within each layer.
5. The strain compatible shear modulus and damping ratio are recalculated based on the new estimate of the effective strain within each layer.
6. The new nonlinear properties ( $G$  and  $D$ ) are compared to the previous iteration and an error is calculated. If the error for all layers is below a defined threshold the calculation stops.

After the iterative portion of the program finishes, the dynamic response of the soil deposit is computed using the strain-compatible properties.

In a dynamic system, the properties that govern the response are the mass, stiffness, and damping. In soil under seismic shear loading, the mass of the system is characterized by the mass density ( $\rho$ ) and the layer height ( $h$ ), the stiffness is characterized by the shear modulus ( $G$ ), and the damping is characterized by the viscous damping ratio ( $D$ ). The dynamic behavior of soil is challenging to model because it is nonlinear, such that both the stiffness and damping of the system change with shear strain.

The mass density of the system can be well estimated considering the soil type of each layer. Characterization of the stiffness and damping properties of soil is more complicated, and it should be done with field and laboratory tests.

The shear modulus and material damping of the soil are characterized using the small strain shear modulus ( $G_{\text{max}}$ ), modulus reduction curves that relate  $G/G_{\text{max}}$  to shear strain, and damping ratio curves that relate  $D$  to shear strain.

Modulus reduction and damping curves may be obtained from laboratory measurements on soil samples or derived from empirical models based on soil type and other variables. One of the most comprehensive empirical models was developed by Darendeli (2001). The model expands on the hyperbolic model presented by Hardin and Drnevich (1972) and accounts for the effects of confining pressure ( $\sigma'_v$ ), plasticity index (PI), over-consolidation ratio (OCR), frequency ( $f$ ), and number of cycles of loading ( $N$ ) on the modulus reduction and damping curves.

---

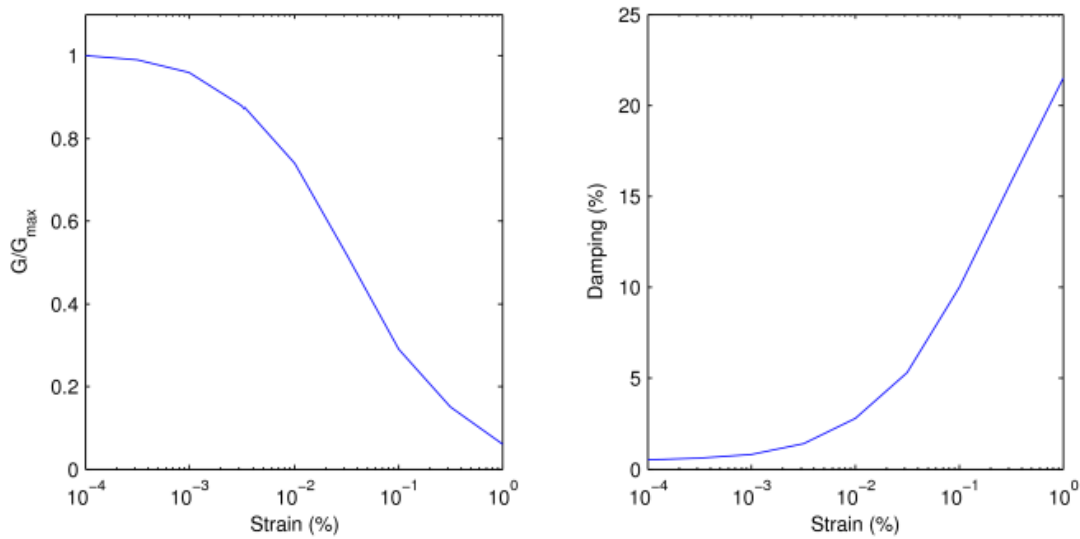


Figure 2.7: Examples of shear modulus reduction and material damping curves for soil.

In the Darendeli (2001) model, the shear modulus reduction curve is a hyperbola defined by:

$$\frac{G}{G_{max}} = \frac{1}{1 + \left(\frac{\gamma}{\gamma_r}\right)^a}$$

where  $a$  is 0.9190,  $\gamma$  is the shear strain and  $\gamma_{ref}$  is the reference shear strain. The reference shear strain (not in percent) is computed from:

$$\gamma_r = \left(\frac{\sigma'_0}{p_a}\right)^{0.3483} (0.0352 + 0.0010 PI OCR^{0.3246})$$

where  $\sigma'_0$  is the mean effective stress

$p_a$  is the atmospheric pressure in the same units as  $\sigma'_0$ .

In the model, the damping ratio is calculated from the minimum damping ratio at small strains ( $D_{min}$ ) and from the damping ratio associated with hysteretic Masing behavior ( $D_{Masing}$ ). The computation of the Masing damping requires the calculation of the area within the stress-strain curve predicted by the shear modulus reduction curve.

The minimum damping is calculated from equation .... and the integration of the Masing damping can be approximated by equation .....



$$D_{min}(\%) = (\sigma'_0)^{-0.2889} (0.8005 + 0.0129 PI OCR^{-0.1069}) (1 + 0.2919 \ln f)$$

$$D_{Masing}(\%) = c_1 D_{Masing,a=1} + c_2 D_{Masing,a=1}^2 + c_3 D_{Masing,a=1}^3$$

where  $f$  is the excitation frequency (Hz).

$$D_{Masing,a=1}(\%) = \frac{100}{\pi} \left\{ 4 \left[ \frac{\gamma - \gamma_r \ln \left( \frac{\gamma + \gamma_r}{\gamma_r} \right)}{\frac{\gamma^2}{\gamma + \gamma_r}} \right] - 2 \right\}$$

$$c_1 = -1.1143a^2 + 1.8618a + 0.2533$$

$$c_2 = 0.0805a^2 - 0.0710a - 0.0095$$

$$c_3 = -0.0005a^2 + 0.0002a + 0.0003$$

The minimum damping ratio in equation ( ) and the Masing damping in equation ( ) are combined to compute the total damping ratio ( $D$ ) using:

$$D = b \left( \frac{G}{G_{max}} \right)^{0.1} D_{Masing} + D_{min}$$

where  $b$  is defined as:

$$b = 0.6329 - 0.0057 \ln N$$

where  $N$  is the number of cycles of loading.

In most site response applications, the number of cycles ( $N$ ) and the excitation frequency ( $f$ ) in the model are defined as 10 and 1, respectively. Figure 2.8 shows the predicted nonlinear curves for a sand ( $PI=0$ ,  $OCR=1$ ) at an effective confining pressure of 1 atm.

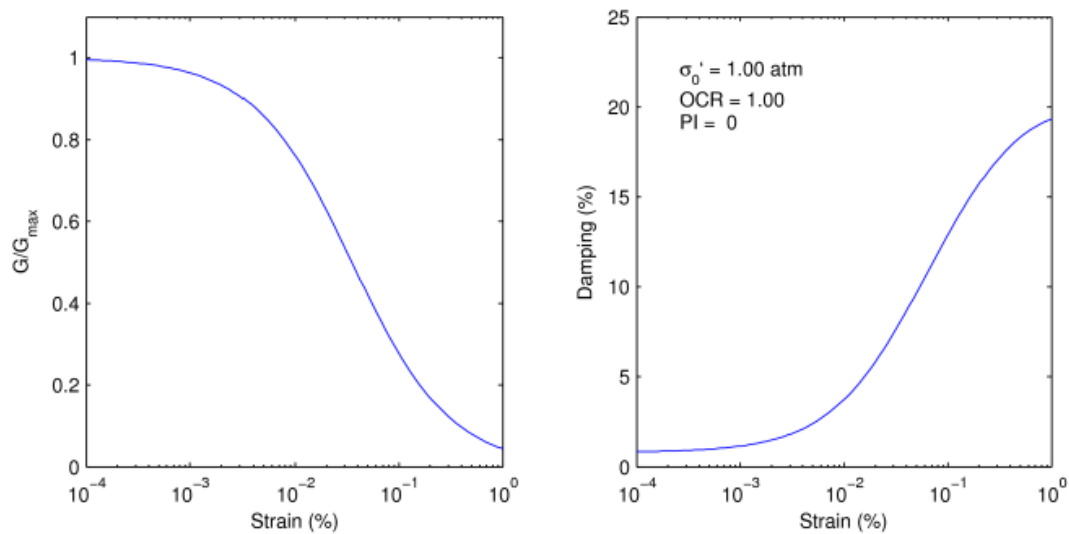


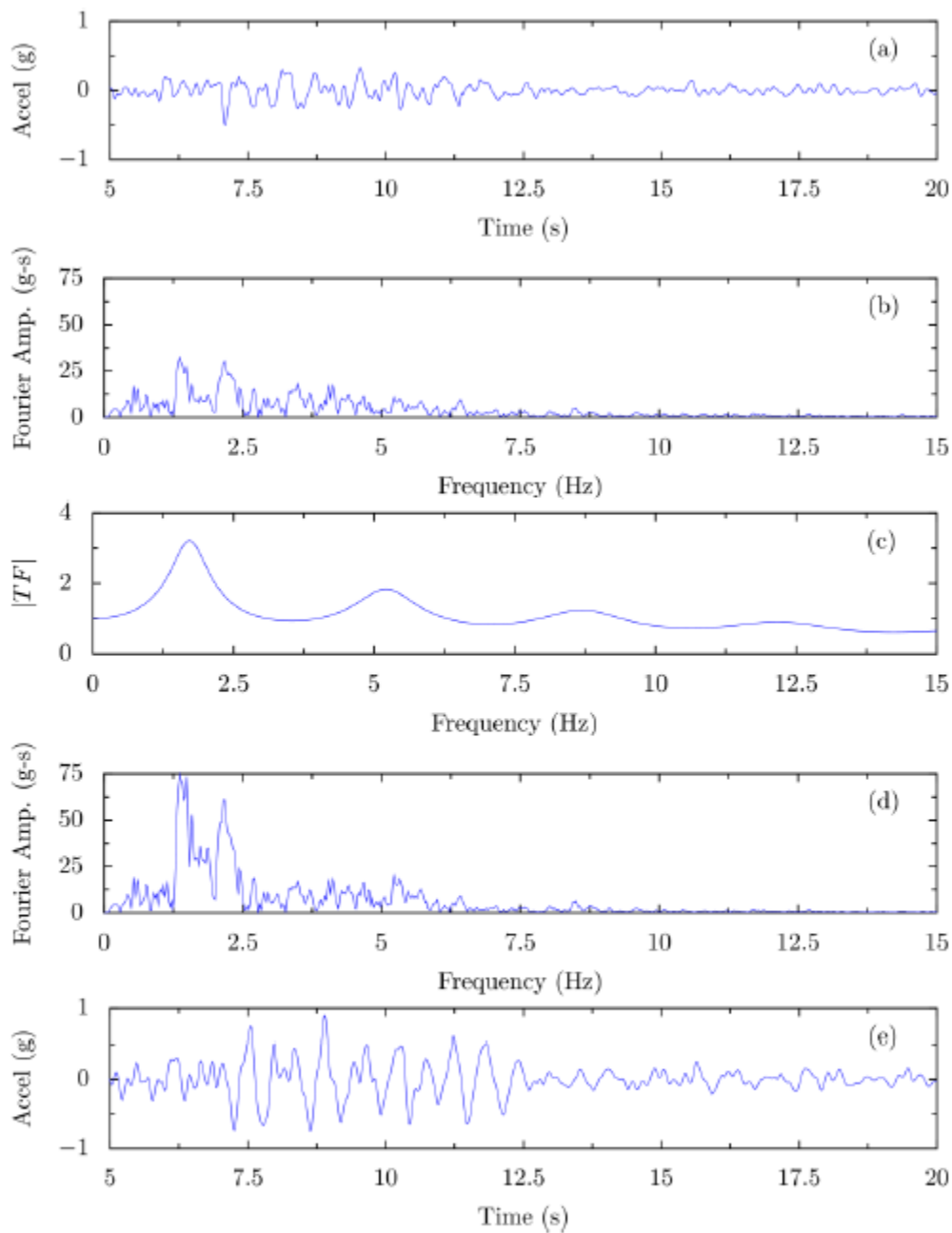
Figure 2.8: The nonlinear soil properties predicted by the Darendeli (2001) model.

### 3.2 TIME SERIES METHOD

In the time series method, an input acceleration-time history is provided and the input Fourier amplitude spectrum (FAS) is computed from that time series using the fast Fourier transform to compute the discrete Fourier transformation on the provided time series. After the FAS of the motion has been computed it is possible to perform site response analysis with the motion.

The following is a summary of the steps to compute the surface acceleration time-series for the a certain site as suggested by Kottke et al. 2013 (figure ....) (after Kramer 1996):

1. Read the acceleration-time series file.
2. Compute the input FAS with the Fast Fourier transformation.
3. Compute the transfer function for the site properties.
4. Compute the surface FAS by applying the transfer function to the input FAS.
5. Compute the surface acceleration-time series through the inverse FFT of the surface FAS.



### 3.3 STATISTICAL APPROACH

A soil profile consists of discrete layers that vary in thickness based on the properties of the soil. The layers are typically discretized based on the soil type, recorded from borehole samples or inferred from a shear-wave velocity profile. In seismic site response analysis, each layer is characterized by a thickness, mass density, shear-wave velocity,

---

and nonlinear properties ( $G/G_{max}$ , and  $D$ ). One of the challenges in defining values for these properties is the natural variability across a site and the uncertainty in their measurement. Because the dynamic response of a site is dependent on the soil properties, any variation in the soil properties will change both the expected surface motion and its standard deviation.

In seismic site response analysis, the nonlinear response of the system does not allow an exact analytic quantification of the variability of the site response. Instead, an estimate of the expected surface response and its standard deviation due to variations in the soil properties can be made through Monte Carlo simulations. Monte Carlo simulations estimate the response of a system by generating parameters of the system based on defined statistical distributions and computing the response for each set of input parameters.

The goal of a Monte Carlo simulation is to estimate the statistical properties of the response of a complex system. To achieve this goal, each of the properties of the system is selected from defined statistical distributions and the response of the system is computed. The response is computed for many realizations and the calculated response from each realization is then used to estimate statistical properties of the system's response. A major disadvantage of Monte Carlo simulation is that a large number of simulations is required to achieve stable results.

Monte Carlo simulations require that each of the components in the system has a complete statistical description. The description can be performed using many different statistical distributions even if the normal and log-normal distributions are mainly used because they can be easily described using a mean ( $\mu$ ) and standard deviation ( $\sigma$ ). For normally distributed variables, a random value ( $x$ ) can be generated by:

$$x = \mu_x + \sigma_x \varepsilon$$

Where ( $\mu_x$ ) is the mean value, ( $\sigma_x$ ) is the standard deviation, and  $\varepsilon$  is a random variable with zero mean and unit standard deviation.

For the properties of the soil to be randomized and incorporated into Monte Carlo simulations, the statistical distribution and properties of the soil need to be characterized. In Strata, which is the reference software for this study, two separate models are used. The first model, developed by Toro (1995), describes the statistical distribution and correlation between layering and shear-wave velocity. The second model by Darendeli (2001) was previously introduced in paragraph .... and is used to describe the statistical distribution of the nonlinear properties ( $G/G_{max}$  and  $D$ ).

---

The Toro (1995) models provide a framework for generating layering and then to vary the shear-wave velocity of these layers. The layering is modeled as a Poisson process, which is a stochastic process with events occurring at a given rate ( $\lambda$ ). In the Toro (1995) model, the layering thickness is modeled as a non-homogeneous Poisson process where the rate changes with depth ( $\lambda(d)$ , where  $d$  is depth from the ground surface). For a non-homogeneous Poisson process with rate  $\lambda(d)$  the cumulative rate ( $\Lambda(d)$ ) is defined as (Kao, 1997):

$$\Lambda(d) = \int_0^d \lambda(s) ds$$

$\Lambda(d)$  represents the expected number of layers up to a depth  $d$ .

Toro (1995) proposed the following generic depth dependent rate model:

$$\lambda(d) = a \cdot (d + b)^c$$

The coefficients  $a$ ,  $b$ , and  $c$  were estimated by Toro (1995) using the method of maximum likelihood applied to the layering measured at 557 sites, mostly from California. The resulting values of  $a$ ,  $b$ , and  $c$  are 1.98, 10.86, and -0.89, respectively. The occurrence rate ( $\lambda(d)$ ) quickly decreases as the depth increases (FIGURE 3.5a). Using equations (3.7) and (3.8), the cumulative rate for the Toro (1995) modeled is defined as:

$$\Lambda(d) = \int_0^d a \cdot (s + b)^c ds = a \cdot \left[ \frac{(d + b)^{c+1}}{c + 1} - \frac{b^{c+1}}{c + 1} \right]$$

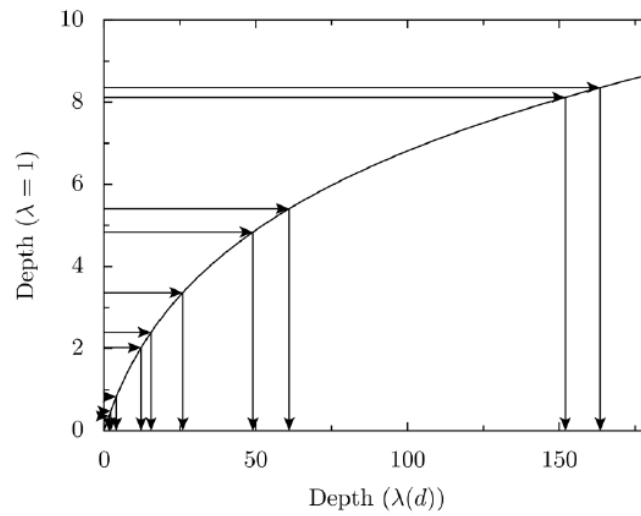


Figure 3.6: Transformation between a homogeneous Poisson process with rate 1 to the Toro (1995) non-homogeneous Poisson process.

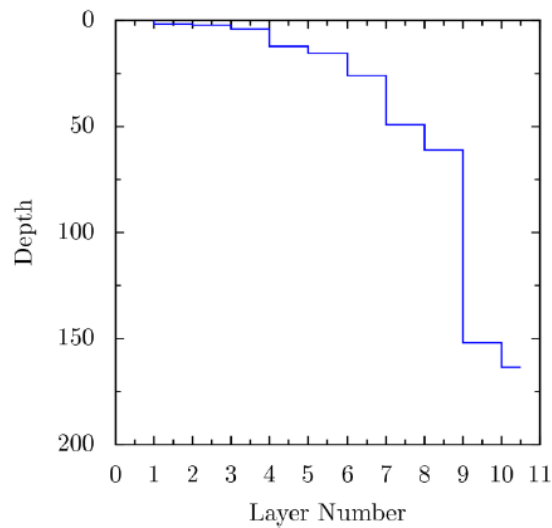


Figure 3.7: A layering simulated with the non-homogeneous Poisson process defined by Toro (1995).

After the layering of the profile has been established, the shear-wave velocity profile can be generated by assigning velocities to each layer. In the Toro (1995) model, the shear-wave velocity at mid-depth of the layer is described by a log-normal distribution. The standard normal variable ( $Z$ ) of the  $i$ th layer is calculated by:

$$Z_i = \frac{\ln V_i - \ln[V_{\text{median}}(d_i)]}{\sigma_{\ln V_s}}$$

where  $V_i$  is the shear-wave velocity in the  $i^{\text{th}}$  layer,  
 $V_{\text{median}}(d_i)$  is the median shear-wave velocity at mid-depth of the layer  
 $\sigma_{\ln V_s}$  is the standard deviation of the natural logarithm of the shear-wave velocity.

Equation (3.11) is then solved for the shear-wave velocity of the  $i^{\text{th}}$  layer ( $V_i$ ):

$$V_i = \exp\{\sigma_{\ln V_s} \cdot Z_i + \ln[V_{\text{median}}(d_i)]\}$$

Equation (3.12) allows for the calculation of the velocity within a layer for a given median velocity at the mid-depth of the layer, standard deviation, and standard normal variable. As the depth of the layer increases, the depth-dependent correlation increases. The final layer in a site response model is assumed to be infinitely thick, therefore the correlation between the last soil layer and the infinite half-space is only dependent on rod.



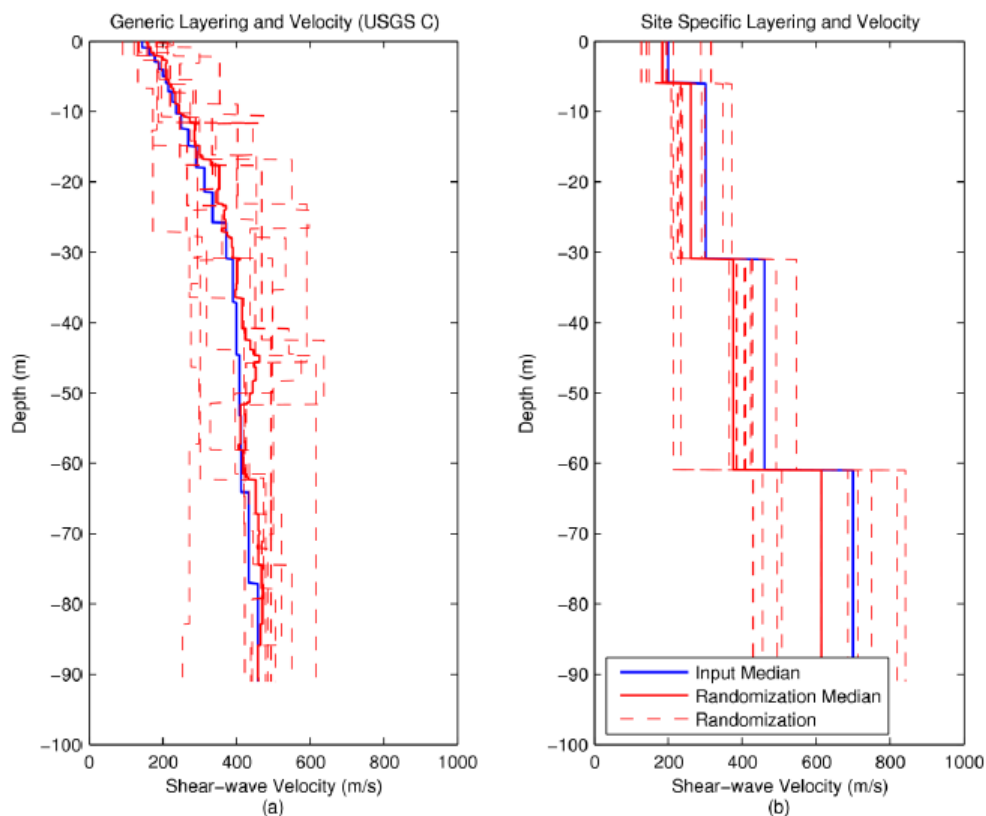


Figure 3.8: Ten generated shear-wave velocity ( $v_s$ ) profiles for a USGS C site class. (a) Using generic layering and median  $v_s$ , (b) using user defined layering and median  $v_s$ .

The Darendeli (2001) empirical model for nonlinear soil properties ( $G/G_{max}$  and  $D$ ) was previously discussed in paragraph ..... The Darendeli (2001) empirical model assumes the variation of the properties follows a normal distribution. The standard deviation of  $G/G_{max}$  and  $D$  varies with the magnitude of the property and is calculated with equations () and (), respectively. Because the variation of the properties is modeled with a normal distribution that is continuous from (-infinity) to (+infinity), the generated values of  $G/G_{max}$  or  $D$  may fall below zero, that may occur at large strains for  $G/G_{max}$  and at low strains for  $D$ . Negative values for either  $G/G_{max}$  or  $D$  are not physically possible, therefore the normal distributions need to be truncated. To correct for this problem, minimum values for  $G/G_{max}$  and  $D$  are specified. The default values in Strata are  $G/G_{max} = 0.05$  and  $D = 0.1\%$ . Strata also includes the ability to specify maximum values of  $G/G_{max}$  and  $D$ .

### 3.4 SIGNAL DECONVOLUTION

Strata computes the dynamic site response of a one-dimensional soil column using linear wave propagation with strain dependent dynamic soil properties. This is commonly referred to as the equivalent linear analysis method, which was first used in the computer program SHAKE (Schnabel et al. 1972; Idriss & Sun 1992). Similar to SHAKE, Strata only computes the response for vertically propagating, horizontally polarized shear waves propagated through a site with horizontal layers.

Considering that the all river Po plain doesn't show any rock outcrop, and that there are not available tools and informations for accurately characterizing the stratigraphy beneath the studied sites to a depth of engineering bedrock, deconvolving recorded surface motions is a valid alternative to compute ground motion input. Deconvolution consists of inputting an outcropping motion at the surface of a 1D soil column and using an equivalent-linear analysis to calculate the acceleration-time history at a point beneath the ground surface. This "within" base motion can be converted to an outcropping motion and used as an input motion for subsequent convolution analyses. Signal deconvolution is a pretty delicate procedure and requires particular care to avoid unrealistic motions being calculated at depth due to the propagation of the total surface motion via an equivalent-linear analysis during the deconvolution process. These steps were adhered to and are as follows (Markham et al. 2015):

1. A low pass (LP) filter was applied to the recorded surface motion to be used for the deconvolution analysis at 15 Hz and scaled by 0.87; SeismoSignal™ was used to perform a 4th order, LP Butterworth filter.
  2. The filtered and scaled motion from step 1 was input at the surface of a 1D soil column.
  3. The motion from a layer of interest at some depth below the surface is obtained via an equivalent linear solution.
  4. The final iteration values of shear modulus reduction ( $G/G_{max}$ ) and material damping ( $\lambda$ ) for each layer during the deconvolution process is obtained.
  5. The deconvolution process was performed again by using a linear analysis with the final values of  $G/G_{max}$  and  $\lambda$  from step 4 for each layer of the 1D soil column and inputting the LP filtered (15 Hz) full surface motion (i.e., not scaled by 0.87) at the top of the column to obtain the "final", outcropping, deconvolved motion.
-

STRATA was utilized to perform all deconvolution analyses. The empirically based normalized shear modulus reduction and material damping relationships proposed by Darendeli (2001) were used.

SeismoSignal constitutes an efficient way to process strong-motion data, featuring a visual interface and being capable of deriving a number of strong-motion parameters.

SeismoSignal calculates:

- Elastic and constant-ductility inelastic response spectra
- Fourier and Power spectra
- Arias ( $I_a$ ) and characteristic ( $I_c$ ) intensities
- Cumulative Absolute Velocity (CAV) and Specific Energy Density (SED)
- Root-mean-square (RMS) of acceleration, velocity and displacement
- Sustained maximum acceleration (SMA) and velocity (SMV)
- Effective design acceleration (EDA) Acceleration (ASI) and velocity (VSI) spectrum intensity
- Predominant ( $T_p$ ) and mean ( $T_m$ ) periods
- Husid and energy flux plots
- Bracketed, uniform, significant and effective durations

SeismoSignal also enables the filtering of unwanted frequency content of the given signal. Three different digital filter types are available, all of which capable of carrying out highpass, lowpass, bandpass and bandstop filtering. The program is able to read accelerograms defined in both single- and multiple-values per line formats (the two most popular formats used by strong-motion databases), and can apply baseline correction and filtering prior to time-integration of the signal (to obtain velocity and displacement time-histories).

Filtering, is employed to remove unwanted frequency components from a given signal:

- Lowpass filtering suppresses frequencies that are higher than a user-defined cut-off frequency (Freq1)
  - Highpass filtering allows frequencies that are higher than the cut-off frequency (Freq1) to pass through
  - Bandpass filtering allows signals within a given frequency range (Freq1 to Freq2) bandwidth to pass through
-

- Bandstop filtering suppresses signals within the given frequency range (Freq1 to Freq2)

To create any of the above filtering configurations, three classical infinite-impulse-response (IIR) filter types are available. Evidently, these digital IIR filters are initially designed in analogue form and then transformed into their digital version through a bilinear transformation, so as to overcome the current impossibility of directly designing digital IIR filters. It is also noted that filtering is carried out in the time-domain and that the employed filters described above are of casual type. In addition to choosing the type of filter to be used and its configuration, users can also define the order and frequency range to be adopted. It is also highlighted that the pre-defined filtering range corresponds, with some approximation, to the filtering configuration usually employed by strong-motion databases to obtain corrected accelerogram records.

---

## CHAPTER 4

# Opensees

In this chapter the main characteristics of Opensees, which is the framework choosed to perform the numerical analysis are described. It is not meant in this section to make a full description and explanation of the functioning and capabilities of Opensees because it would be too wide topic to cover and would be not useful for the purposes of this work. After a general introduction, attention will be focused on the aspects the are of main interest for the analysis described later in chapter 8.

Opensees (OPEN System for Earthquake Engineering Simulation) is a finite element analysis framework for structural and geotechnical earthquake engineering simulation. Opensees is developed at the University of California Berkeley with support of the Pacific Earthquake Engineering Research Center (PEER). Opensees is an open source tool that can be downloaded and used by anyone. It is also possible to modify and implement the code, acting on specific aspects and having thus the possibility to work on different problems.

Opensees has not a graphical user interface (GUI) and this makes its use less immediate and intuitive. To handle complex problems and structures it is necessary to combine Opensees with a graphic pre and post-processor.

Opensees can then be considered an interpreter based on tcl language with additional command able to perform finite element analysis. Tcl is a dynamic programming language. Many commands have been implemented in Opensees and this allow the possibility to solve many different kind of problems.

This interpreter has been choosed to perform numerical analysis for the present thesis because it is an extremely powerful tool, which allows to use advanced constitutive soil models, able to evaluate liquefaction problems under seismic conditions. It is also possible to perform 2D and 3D analysis, fact of great importance when considering river embankments. Another important aspect is the possibility to control in detail every single part of the analysis, unlike many finite element softwares that fgive less possibilities to modify the parameters. The lackness of a graphical user interface creates a difficulty in the use of the tool, but on the other side makes it much faster in performing computations. Being opensource has helped Opensees to spread worldwide through different research groups, companies, professionals and the use and the

---

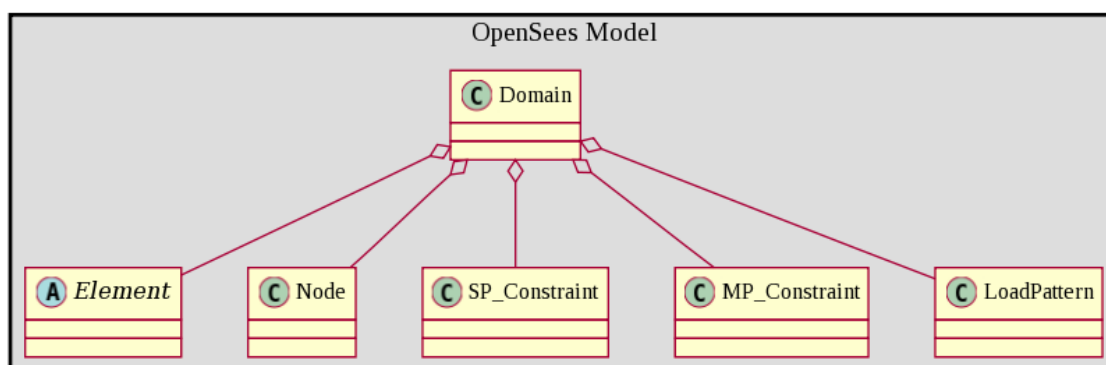
contribution of many subjects has made the program more stable and widened its capabilities.

Tcl is a dynamic programming language for advanced application with interpreted structure. It is considered a powerful tool which allows to construct procedures with a rather simple syntax. It is commonly used embedded into C++ applications. The OpenSees interpreters add commands to Tcl for finite element analysis. Each of these commands is associated with a C++ procedure that is provided. It is this procedure that is called upon by the interpreter. All existing commands that exist in the Tcl language are available to the OpenSees interpreters. OpenSees commands that have been added to Tcl to perform finite element analysis can be grouped into four sections:

1. Modelling commands, added to the interpreter to create the finite element model;
2. Analysis commands added to Tcl to create the analysis procedure.
3. Output commands added to Tcl to monitor what is happening in the model during the analysis.
4. Misc commands added to Tcl to help monitor and modify the model and analysis during the run-time.
5. DataBase commands added to Tcl to construct a FE\_Datastore object.

## 4.1 MODELING COMMANDS

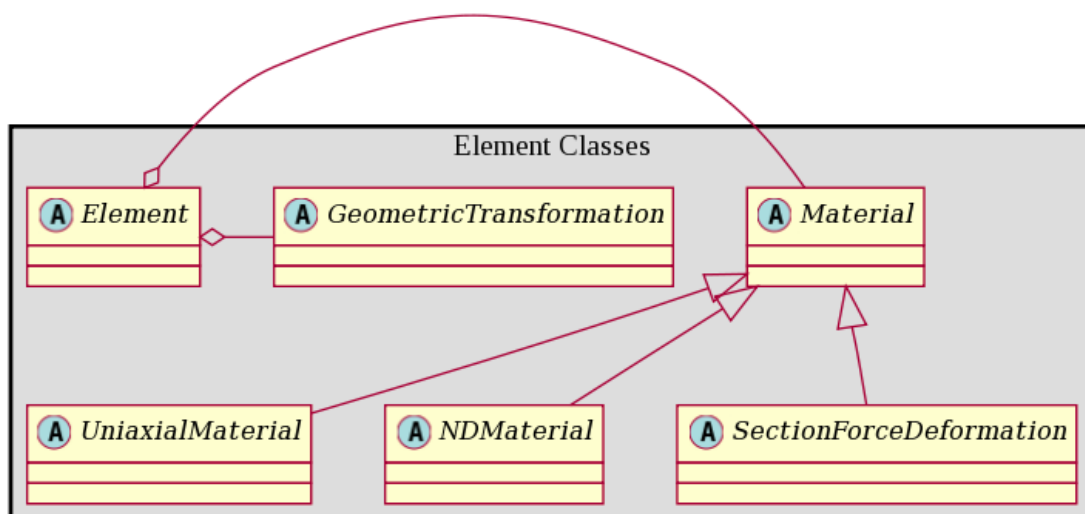
The model or domain in OpenSees is a collection (an aggregation in object-oriented terms) of elements, nodes, single- and multi-point constraints and load patterns. It is the aggregation of these components which define the type of model that is being analyzed. The component classes, are as shown in the figure below:



The following are the modeling commands that have been added to OpenSees interpreter to create these components of the finite element model:

- model
- element
- node
- **SP\_Constraint** (single-point constraint), which prescribe the movement (typically 0) of a single dof at a node. There are a number of commands for creating single-point constraints:
- **MP\_Constraint** (multi-point constraint), which prescribe that the movement of certain dof at one node are defined by the movement of certain dof at another node. There again are a number of commands for defining multi-point constraints.
- timeSeries
- pattern

The typical element in OpenSees has the material nonlinearity and sometimes geometric nonlinearities contained in other objects, materials and geometric transformations. Commands have been added to the interpreter to create these objects as well:



1. uniaxial Material
2. ND Material
3. Section



4. friction Model
5. geometricTransf

### **Model command**

This command is used to define spatial dimension of model and number of degrees-of-freedom at nodes. Once issued additional commands are added to interpreter.

\$ndm                      spatial dimension of problem (1,2, or 3)  
\$ndf                      number of degrees of freedom at node (optional)  
                            default value depends on value of ndm:  
                            ndm=1 -> ndf=1  
                            ndm=2 -> ndf=3  
                            ndm=3 -> ndf=6

## **4.2 ELEMENT COMMAND**

### **Element command**

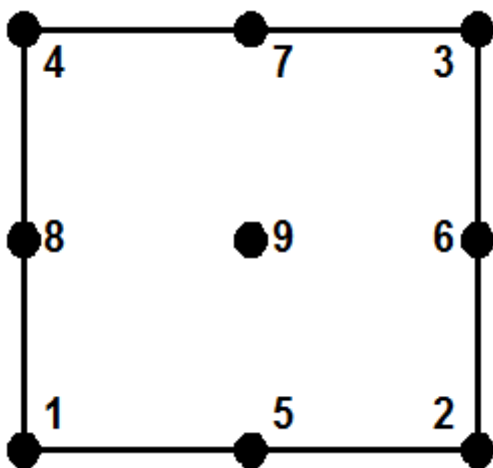
This command is used to construct an element and add it to the Domain.

Here follow the available element types:

- Zero-Length Elements
  - Truss Elements
  
  - Beam-Column Elements
  - Joint Elements
  - Link Elements
  - Bearing Elements
  
  - Quadrilateral Elements
  - Triangular Elements
-

- Brick Elements
- u-p Elements
  - UC San Diego u-p element (saturated soil)
    - Four Node Quad u-p Element
    - Brick u-p Element
    - bbarQuad u-p Element
    - bbarBrick u-p Element
    - Nine Four Node Quad u-p Element
    - Twenty Eight Node Brick u-p Element
  - Twenty Node Brick u-p Element
  - Brick Large Displacement u-p Element
  - SSPquadUP Element
  - SSPbrickUP Element
- Misc.
- Contact Elements

**Nine\_Four\_Node\_QuadUP** is a 9-node quadrilateral plane-strain element. The four corner nodes have 3 degrees-of-freedom (DOF) each: DOF 1 and 2 for solid displacement (u) and DOF 3 for fluid pressure (p). The other five nodes have 2 DOFs each for solid displacement. This element is implemented for simulating dynamic response of solid-fluid fully coupled material, based on Biot's theory of porous medium.



<b>\$eleTag</b>	A positive integer uniquely identifying the element among all elements
<b>\$Node1,...</b> <b>\$Node9</b>	Nine element node

<b>\$thick</b>	Element thickness
<b>\$matTag</b>	Tag of an NDMaterial object of which the element is composed
<b>\$bulk</b>	<p>Combined undrained bulk modulus <math>B_c</math> relating changes in pore pressure and volumetric strain, may be approximated by:</p> $B_c \approx B_f/n$ <p>where <math>B_f</math> is the bulk modulus of fluid phase (<math>2.2 \times 10^6</math> kPa for water), and <math>n</math> the initial porosity.</p>
<b>\$fmass</b>	Fluid mass density
<b>\$hPerm, \$vPerm</b>	Permeability coefficient in horizontal and vertical directions respectively.
<b>\$b1, \$b2</b>	Optional gravity acceleration components in horizontal and vertical directions respectively (defaults are 0.0)

**FourNodeQuadUP** is a four-node plane-strain element using bilinear isoparametric formulation. This element is implemented for simulating dynamic response of solid-fluid fully coupled material, based on Biot's theory of porous medium. Each element node has 3 degrees-of-freedom (DOF): DOF 1 and 2 for solid displacement ( $u$ ) and DOF 3 for fluid pressure ( $p$ ). The valid queries to a quadUP element when creating an ElementRecorder are force, stiffness, or material matNum matArg1 matArg2 ..., where matNum represents the material object at the corresponding integration point.

<b>\$eleTag</b>	A positive integer uniquely identifying the element among all elements
<b>\$iNode, \$jNode, \$kNode, \$lNode</b>	Four element node (previously defined) numbers in counter-clockwise order around the element
<b>\$thick</b>	Element thickness
<b>\$matTag</b>	Tag of an NDMaterial object (previously defined) of which the element is composed
<b>\$bulk</b>	<p>Combined undrained bulk modulus <math>B_c</math> relating changes in pore pressure and volumetric strain, may be approximated by:</p> $B_c \approx B_f/n$ <p>where <math>B_f</math> is the bulk modulus of fluid phase (<math>2.2 \times 10^6</math> kPa (or <math>3.191 \times 10^5</math> psi) for water), and <math>n</math> the initial porosity.</p>
<b>\$fmass</b>	Fluid mass density

\$hPerm, \$vPerm	Permeability coefficient in horizontal and vertical directions respectively.
\$b1, \$b2	Optional gravity acceleration components in horizontal and vertical directions respectively (defaults are 0.0)
\$t	Optional uniform element normal traction, positive in tension (default is 0.0)

#### TYPICAL RANGE OF PERMEABILITY COEFFICIENT

Gravel	Sand	Silty Sand	Silt	Clay
$>1.0 \times 10^{-1}$ cm/s	$1.0 \times 10^{-3}$ cm/s ~ $1.0 \times 10^{-1}$ cm/s)	$1.0 \times 10^{-5}$ cm/s ~ $1.0 \times 10^{-3}$ cm/s	$1.0 \times 10^{-7}$ cm/s ~ $1.0 \times 10^{-5}$ cm/s	$<1.0 \times 10^{-7}$ m/s

#### Quad element

This command is used to construct a FourNodeQuad element object which uses a bilinear isoparametric formulation.

\$eleTag	unique element object tag
\$iNode \$jNode \$kNode \$lNode	four nodes defining element boundaries, input in counter-clockwise order around the element.
\$thick	element thickness
\$type	string representing material behavior. The type parameter can be either "PlaneStrain" or "PlaneStress."
\$matTag	tag of nDMaterial
\$pressure	surface pressure (optional, default = 0.0)
\$rho	element mass density (per unit volume) from which a lumped element mass matrix is computed (optional, default=0.0)
\$b1 \$b2	constant body forces defined in the isoparametric domain (optional, default=0.0)

### Zero length element

This command is used to construct a zeroLength element object, which is defined by two nodes at the same location. The nodes are connected by multiple UniaxialMaterial objects to represent the force-deformation relationship for the element.

\$eleTag	unique element object tag
\$iNode \$jNode	end nodes
\$matTag1 \$matTag2 ...	tags associated with previously-defined UniaxialMaterials
\$dir1 \$dir2 ...	material directions: 1,2,3 - translation along local x,y,z axes, respectively; 4,5,6 - rotation about local x,y,z axes, respectively
\$x1 \$x2 \$x3	vector components in global coordinates defining local x-axis (optional)
\$yp1 \$yp2 \$yp3	vector components in global coordinates defining vector yp which lies in the local x-y plane for the element. (optional)
\$rFlag	optional, default = 0 rFlag = 0 NO RAYLEIGH DAMPING (default) rFlag = 1 include rayleigh damping

### Node command

This command is used to construct a Node object. It assigns coordinates and masses to the Node object.

\$nodeTag	integer tag identifying node
\$coords	nodal coordinates (ndm arguments)
\$massValues	nodal mass corresponding to each DOF (ndf arguments) (optional)

The optional -mass string allows analyst the option of associating nodal mass with the node

### EqualDOF command

This command is used to construct a multi-point constraint between nodes.

<b>\$rNodeTag</b>	integer tag identifying the retained, or master node (rNode)
<b>\$cNodeTag</b>	integer tag identifying the constrained, or slave node (cNode)
<b>\$dof1 \$dof2 ...</b>	nodal degrees-of-freedom that are constrained at the cNode to be the same as those at the rNode  Valid range is from 1 through ndf, the number of nodal degrees-of-freedom.

### Time series command

This command is used to construct a TimeSeries object which represents the relationship between the time in the domain,  $t$ , and the load factor applied to the loads,  $\lambda$ , in the load pattern with which the TimeSeries object is associated, i.e.  $\lambda = F(t)$

The type of time series created and the additional arguments required depends on the **seriesType?** provided in the command.

The following contain information about seriesType? and the args required for each of the available time series types:

- Constant TimeSeries
- Linear TimeSeries
- Trigonometric TimeSeries
- Triangular TimeSeries
- Rectangular TimeSeries
- Pulse TimeSeries
- Path TimeSeries
- PeerMotion
- PeerNGAMotion

### Path time series

This command is used to construct a Path TimeSeries object. The relationship between load factor and time is input by the user as a series of discrete points in the 2d space

---

(load factor, time). The input points can come from a file or from a list in the script. When the time specified does not match any of the input points, linear interpolation is used between points. There are many ways to specify the load path:

\$tag	unique tag among TimeSeries objects.
\$filePath	file containing the load factors values
\$fileTime	file containing the time values for corresponding load factors
\$dT	time interval between specified points.
{ list_of_times }	load factor values in a tcl list
{ list_of_values }	time values in a tcl list
\$cFactor	optional, a factor to multiply load factors by (default = 1.0)
-useLast	optional, to use last value after the end of the series (default = 0.0)
-prependZero	optional, to prepend a zero value to the series of load factors (default = false).
\$tStart	optional, to provide a start time for provided load factors (default = 0.0)

### Pattern command

The pattern command is used to construct a LoadPattern and add it to the Domain. Each LoadPattern in OpenSees has a TimeSeries associated with it. In addition it may contain ElementLoads, NodalLoads and SinglePointConstraints. Some of these SinglePoint constraints may be associated with GroundMotions.

The type of pattern created and the additional arguments required depends on the **patternType?** provided in the command. The following contain information about patternType? and the additional args required for each of the available pattern types:

1. Plain Pattern
2. Uniform Excitation Pattern
3. Multi-Support Excitation Pattern
4. DRM Load Pattern

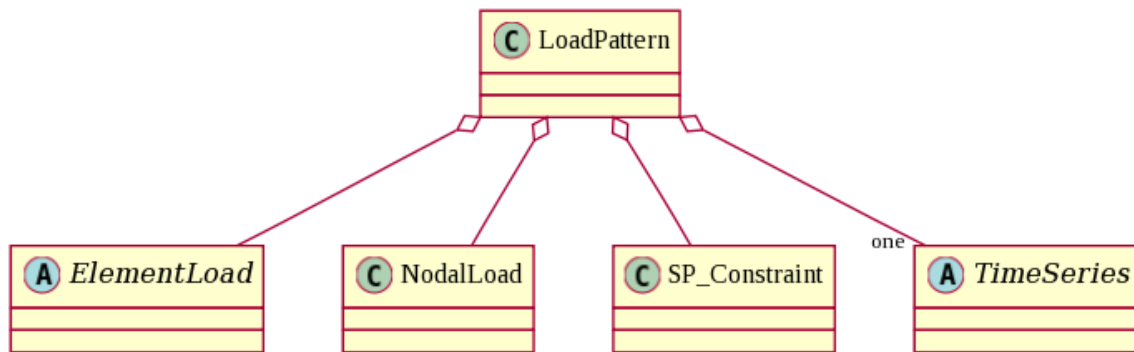
### Plain pattern

This command allows the user to construct a LoadPattern object. Each plain load pattern is associated with a TimeSeries object and can contain multiple NodalLoads,

---

ElementalLoads and SP\_Constraint objects. The command to generate LoadPattern object contains in { } the commands to generate all the loads and the single-point constraints in the pattern.

<b>\$patternTag</b>	unique tag among load patterns
<b>\$tsTag</b>	the tag of the time series to be used in the load pattern
<b>\$cFactor</b>	constant factor (optional, default=1.0)
<b>load...</b>	command to nodal load
<b>eleLoad ...</b>	command to generate elemental load
<b>sp ...</b>	command to generate single-point constraint



## 4.3 MATERIALS

### Uniaxial material command

This command is used to construct a UniaxialMaterial object which represents uniaxial stress-strain (or force-deformation) relationships.

The following contain information about matType and the args required for each of the available material types:

- Steel & Reinforcing-Steel Materials
- Concrete Materials
- Some Standard Uniaxial Materials
- Other Uniaxial Materials



**NDmaterial command**

This command is used to construct an NDMaterial object which represents the stress-strain relationship at the gauss-point of a continuum element.

The type of material created and the additional arguments required depends on the material type provided in the command.

The following contain information about matType and the args required for each of the available material types:

- Elastic Isotropic Material
  - Elastic Orthotropic Material
  - J2 Plasticity Material
  - Drucker Prager Material
  - Concrete Damage Model
  - Plane Stress Material
  - Plane Strain Material
  - Multi Axial Cyclic Plasticity
  - Bounding Surface Cam Clay Material
  - Plate Fiber Material
  - Plane Stress Concrete Materials
  - FSAM - 2D RC Panel Constitutive Behavior
  - Tsinghua Sand Models
    - CycLiqCP Material (Cyclic ElasticPlasticity)
    - CycLiqCPSP Material
  - Manzari Dafalias Material
  - Stress Density Material
  - Materials for Modeling Concrete Walls
  - Contact Materials for 2D and 3D
  - Wrapper material for Initial State Analysis
  - UC San Diego soil models
    - PressureIndependMultiYield Material
    - PressureDependMultiYield Material
    - PressureDependMultiYield02 Material
  - UC San Diego Saturated Undrained soil
    - FluidSolidPorousMaterial
  - Misc.
-

### 4.3.1 Stress Density material

This command is used to construct a multi-dimensional stress density material object for modeling sand behaviour following the work of Cubrinovski and Ishihara (1998a,b).

\$matTag	integer tag identifying material
\$mDen	mass density
\$eNot	initial void ratio
\$A	constant for elastic shear modulus
\$n	pressure dependency exponent for elastic shear modulus
\$nu	Poisson's ratio
\$a1	peak stress ratio coefficient ( $\eta_{\max} = a1 + b1 \cdot I_s$ )
\$b1	peak stress ratio coefficient ( $\eta_{\max} = a1 + b1 \cdot I_s$ )
\$a2	max shear modulus coefficient ( $G_{n\_max} = a2 + b2 \cdot I_s$ )
\$b2	max shear modulus coefficient ( $G_{n\_max} = a2 + b2 \cdot I_s$ )
\$a3	min shear modulus coefficient ( $G_{n\_min} = a3 + b3 \cdot I_s$ )
\$b3	min shear modulus coefficient ( $G_{n\_min} = a3 + b3 \cdot I_s$ )
\$fd	degradation constant
\$muNot	dilatancy coefficient (monotonic loading)
\$muCyc	dilatancy coefficient (cyclic loading)
\$sc	dilatancy strain
\$M	critical state stress ratio
\$patm	atmospheric pressure (in appropriate units)

Optional steady state line parameters:

<\$ssl1>	void ratio of quasi steady state (QSS-line) at pressure \$p1 (default = 0.877)
<\$ssl2>	void ratio of quasi steady state (QSS-line) at pressure \$p2 (default = 0.877)
<\$ssl3>	void ratio of quasi steady state (QSS-line) at pressure \$p3 (default = 0.873)
<\$ssl4>	void ratio of quasi steady state (QSS-line) at pressure \$p4 (default = 0.870)
<\$ssl5>	void ratio of quasi steady state (QSS-line) at pressure \$p5 (default = 0.860)
<\$ssl6>	void ratio of quasi steady state (QSS-line) at pressure \$p6 (default = 0.850)
<\$ssl7>	void ratio of quasi steady state (QSS-line) at pressure \$p7 (default = 0.833)
<\$ssl8>	void ratio of quasi steady state (QSS-line) at pressure \$p8 (default = 0.833)

- 
- <\$ssl9> void ratio of quasi steady state (QSS-line) at pressure \$p9 (default = 0.833)
  - <\$ssl10> void ratio of quasi steady state (QSS-line) at pressure \$p10 (default = 0.833)
  - <\$hsl> void ratio of upper reference state (UR-line) for all pressures (default = 0.895)
  - <\$p1> pressure corresponding to \$ssl1 (default = 1.0 kPa)
  - <\$p2> pressure corresponding to \$ssl1 (default = 10.0 kPa)
  - <\$p3> pressure corresponding to \$ssl1 (default = 30.0 kPa)
  - <\$p4> pressure corresponding to \$ssl1 (default = 50.0 kPa)
  - <\$p5> pressure corresponding to \$ssl1 (default = 100.0 kPa)
  - <\$p6> pressure corresponding to \$ssl1 (default = 200.0 kPa)
  - <\$p7> pressure corresponding to \$ssl1 (default = 400.0 kPa)
  - <\$p8> pressure corresponding to \$ssl1 (default = 400.0 kPa)
  - <\$p9> pressure corresponding to \$ssl1 (default = 400.0 kPa)
  - <\$p10> pressure corresponding to \$ssl1 (default = 400.0 kPa)

This nDMaterial object provides the stress density model for sands under monotonic and cyclic loading as set by Cubrinovski and Ishihara (1998a,b). The original formulation for this model was applicable to plane strain conditions. The current implementation also includes the extension for consideration of 3D conditions.

#### 4.3.2 PressureIndependentMultiYield material

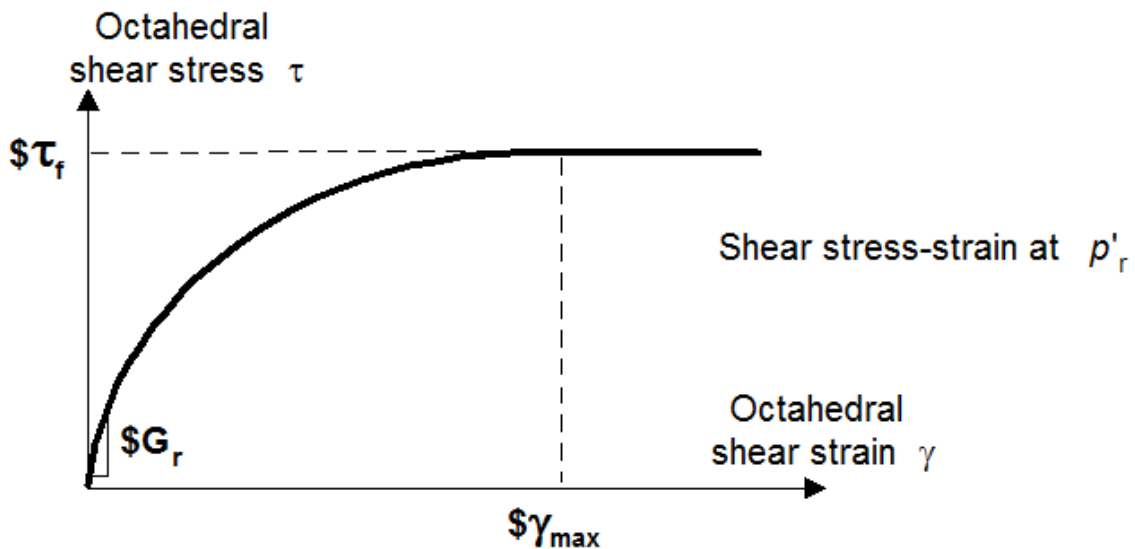
This material is an elastic-plastic material in which plasticity exhibits only in the deviatoric stress-strain response. The volumetric stress-strain response is linear-elastic and is independent of the deviatoric response. This material is implemented to simulate monotonic or cyclic response of materials whose shear behavior is insensitive to the confinement change. Such materials include, for example, organic soils or clay under fast (undrained) loading conditions. During the application of gravity load, material behavior is linear elastic. In the subsequent dynamic phase, the stress-strain response is elastic-plastic. Plasticity is formulated based on the multi-surface (nested surfaces) concept (Elgamal ....), with an associative flow rule. The yield surfaces are of the Von Mises type.

The parameters that may be extracted for this material at a given integration point, using the OpenSees Element Recorder facility are:

- stress
-

- strain
- backbone
- tangent

The "backbone" option records (secant) shear modulus reduction curves at one or more given confinements with a specific recorder command:



\$tag	A positive integer uniquely identifying the material among all nDMaterials.
\$nd	Number of dimensions, 2 for plane-strain, and 3 for 3D analysis.
\$rho	Saturated soil mass density.
\$refShearModul (G <sub>r</sub> )	Reference low-strain shear modulus, specified at a reference mean effective confining pressure refPress of p' <sub>r</sub> .
\$refBulkModul (B <sub>r</sub> )	Reference bulk modulus, specified at a reference mean effective confining pressure refPress of p' <sub>r</sub> .
\$cohesi (c)	Apparent cohesion at zero effective confinement.
\$peakShearStra (γ <sub>max</sub> )	An octahedral shear strain at which the maximum shear strength is reached, specified at a reference mean effective confining pressure refPress of p' <sub>r</sub> .
\$frictionAng (Φ)	Friction angle at peak shear strength in degrees, optional (default is 0.0).
\$refPress (p' <sub>r</sub> )	Reference mean effective confining pressure at which G <sub>r</sub> , B <sub>r</sub> , and γ <sub>max</sub> are defined, optional (default is 100. kPa).

\$pressDependCoe (d)	A positive constant defining variations of G and B as a function of instantaneous effective confinement $p'$ (default is 0.0)::  $G = G_r \left( \frac{p'}{p'_r} \right)^d \quad B = B_r \left( \frac{p'}{p'_r} \right)^d$
\$noYieldSurf	Number of yield surfaces, optional (must be less than 40, default is 20). The surfaces are generated based on a hyperbolic relation.
\$r, \$Gs	Instead of automatic surfaces generation users can define yield surfaces directly based on desired shear modulus reduction curve. To do so, add a minus sign in front of noYieldSurf, then provide noYieldSurf pairs of shear strain ( $\gamma$ ) and modulus ratio ( $G_s$ ) values. For example, to define 10 surfaces:  ... -10 $\gamma_1 G_{s1}$ ... $\gamma_{10} G_{s10}$ ...

A table is provided by the developers as a reference for selecting parameter values; when possible values obtained from dedicated tests on the investigated soils should be used.

	Soft Clay	Medium Clay	Stiff Clay
Rho	1.3 ton/m <sup>3</sup>	1.5 ton/m <sup>3</sup>	1.8 ton/m <sup>3</sup>
refShearModul	1.3x10 <sup>4</sup> kPa	6.0x10 <sup>4</sup> kPa	1.5x10 <sup>5</sup> kPa
refBulkModu	6.5x10 <sup>4</sup> kPa	3.0x10 <sup>5</sup> kPa	7.5x10 <sup>5</sup> kPa
Cohesi	18 kPa	37 kPa	75 kPa
peakShearStra (at $p'_r=80$ kPa)	0.1	0.1	0.1
frictionAng	0	0	0
pressDependCoe	0	0	0

#### 4.4 ANALYSIS COMMAND

### Rayleigh damping command

This command is used to assign damping to all previously-defined elements and nodes. When using rayleigh damping in OpenSees, the damping matrix for an element or node, D is specified as a combination of stiffness and mass-proportional damping matrices:

\$alphaM      factor applied to elements or nodes mass matrix

\$betaK        factor applied to elements current stiffness matrix.

\$betaKinit    factor applied to elements initial stiffness matrix.

\$betaKcomm   factor applied to elements committed stiffness matrix.

### Analysis commands

In OpenSees, an analysis is an object which is composed by the aggregation of component objects. It is the component objects which define the type of analysis that is performed on the model. The component classes, as shown in the figure below, consist of the following:

1. ConstraintHandler -- determines how the constraint equations are enforced in the analysis -- how it handles the boundary conditions/imposed displacements
2. DOF\_Numberer -- determines the mapping between equation numbers and degrees-of-freedom
3. Integrator -- determines the predictive step for time t+dt
4. SolutionAlgorithm -- determines the sequence of steps taken to solve the non-linear equation at the current time step
5. SystemOfEqn/Solver -- within the solution algorithm, it specifies how to store and solve the system of equations in the analysis
6. Convergence Test -- determines when convergence has been achieved.

The following Analysis commands are added to the interpreter to create the Analysis and perform the analysis:

- constraints Command
  - numberer Command
  - system Command
-

- test Command
- algorithm Command
- integrator Command
- analysis Command
- eigen Command
- analyze Command

### **Constraints command**

This command is used to construct the ConstraintHandler object. The ConstraintHandler object determines how the constraint equations are enforced in the analysis. Constraint equations enforce a specified value for a DOF, or a relationship between DOFs.

The following contain information about numbererType? and the args required for each of the available constraint handler types:

1. Plain Constraints
2. Lagrange Multipliers
3. Penalty Method
4. Transformation Method

### **Algorithm Command**

This command is used to construct a SolutionAlgorithm object, which determines the sequence of steps taken to solve the non-linear equation.

The type of solution algorithm created and the additional arguments required depends on the algorithmType provided in the command.

The following contain information about algorithmType? and the args required for each of the available algorithm types:

- Linear Algorithm
  - Newton Algorithm
  - Newton with Line Search Algorithm
  - Modified Newton Algorithm
  - Krylov-Newton Algorithm
  - Secant Newton Algorithm
-

- BFGS Algorithm
- Broyden Algorithm

### **Newton Algorithm**

This command is used to construct a NewtonRaphson algorithm object which uses the Newton-Raphson algorithm to solve the nonlinear residual equation. The Newton-Raphson method is the most widely used and most robust method for solving nonlinear algebraic equations. The Newton method used in finite element analysis is identical to that taught in basic calculus courses. It is just extended for the n unknown degrees-of-freedom.

### **Krylov-Newton Algorithm**

This command is used to construct a KrylovNewton algorithm object which uses a Krylov subspace accelerator to accelerate the convergence of the modified newton method.

### **Linear Algorithm**

This command is used to construct a Linear algorithm object which takes one iteration to solve the system of equations.

$$\Delta U = -K^{-1}R(U),$$

### **Integrator Command**

This command is used to construct the Integrator object. The Integrator object determines the meaning of the terms in the system of equation object  $Ax=B$ . The Integrator object is used for the following:

- determine the predictive step for time  $t+dt$
- specify the tangent matrix and residual vector at any iteration
- determine the corrective step based on the displacement increment  $dU$

The type of integrator used in the analysis is dependent on whether it is a static analysis or transient analysis.

---



Static Integrators:

- Load Control
- Displacement Control
- Minimum Unbalanced Displacement Norm
- Arc-Length Control

Transient Integrators:

- Central Difference
- Newmark Method
- Hilber-Hughes-Taylor Method
- Generalized Alpha Method
- TRBDF2

### **Newmark Method**

This command is used to construct a Newmark integrator object.

### **Analysis command**

This command is used to construct the Analysis object, which defines what type of analysis is to be performed. Currently 3 options are available:

1. Static - for static analysis
2. Transient - for transient analysis with constant time step
3. VariableTransient - for transient analysis with variable time step

Analyze Command is used to perform the analysis.

The commands used to get output from OpenSees are:

- recorder
    - record
  - print
  - printA
  - logFile
  - RealTime Output Commands
-

## **CHAPTER 5**

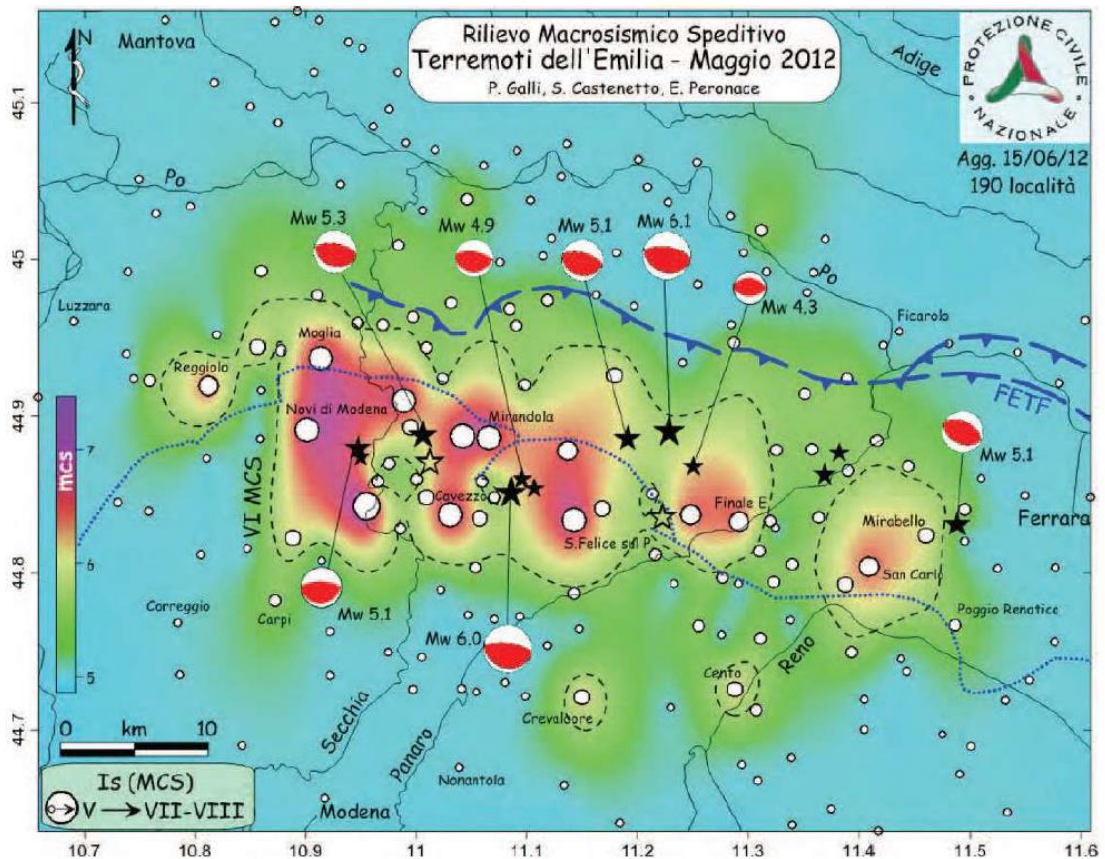
---

# Emilia earthquake sequence

## 5.1 General aspects

On May 20<sup>th</sup>, 2012 at 04:03 an earthquake of magnitude  $M_L=5.9$  struck the central Po valley mainly affecting Emilia region and partly of Lombardia region. The epicentre was located between Mirandola and Finale Emilia villages, in Modena province. The shaking was noticed in all northern Italy and the part of Modena, Ferrara, Bologna, Reggio Emilia and Mantova provinces reported severe damages. The ipocentre was located at a depth of 6,3 km. In the following days many aftershocks were recorded and two of them had a magnitude higher than 5. The 29<sup>th</sup> of May a second main seismic event occurred at 9:00 with  $M_L=5,8$  and epicentre close to Medolla village. The ipocentre was located at a depth of 10,2 km. Many aftershocks were recorded in the following weeks, a few of them with magnitude higher than 5 and with epicentre locations moving westwards. The earthquakes caused 27 deaths, of which 13 on industrial buildings. The area directly affected by the strong ground motion has a surface of approximately 500-700 km<sup>2</sup> and is densely populated and base of important industrial districts.

---



Date (dd/mm/yy)	Time (hh:mm:ss)	Lat (°)	Lon (°)	Depth (km)	M <sub>L</sub>	Directory
03/06/2012	19:20:43	44.899	10.943	9.2	5.1	20120603/192043
29/05/2012	11:00:25	44.879	10.947	5.4	5.2	20120529/110002_110025
29/05/2012	11:00:02	44.873	10.950	11	4.9	20120529/110002_110025
29/05/2012	10:55:57	44.888	11.008	6.8	5.3	20120529/105557
29/05/2012	08:27:23	44.854	11.106	10	4.7	20120529/082551_082723
29/05/2012	08:25:51	44.901	10.943	3.2	4.5	20120529/082551_082723
20/05/2012	17:37:14	44.876	11.382	3.2	4.5	20120520/173714
20/05/2012	13:18:02	44.831	11.490	4.7	5.1	20120520/131802
20/05/2012	03:02:50	44.860	11.095	10	4.9	20120520/030250
20/05/2012	02:07:31	44.863	11.370	5	5.1	20120520/020630_020731
20/05/2012	02:06:30	44.886	11.189	7.7	4.8	20120520/020630_020731

During the earthquakes 27 people died and hundreds were wounded. The material damages were considerable: 12,000 buildings were severely damaged and a preliminary evaluation estimated a damage of 12-13 billions of euro (martelli + ....). The buildings that were mainly struck by the shaking include monuments, historical sites, churches, towers, old rural constructions ecc.. (figure.....): these structures are mainly built with masonry and of big size and resists very poorly to the shaking.

Industrial buildings reported severe damages as well; part of fatalities occurred at work places. Most of factories had to interrupt their activity and the economical losses were massive. The peculiar construction characteristics of industrial building in the area, not

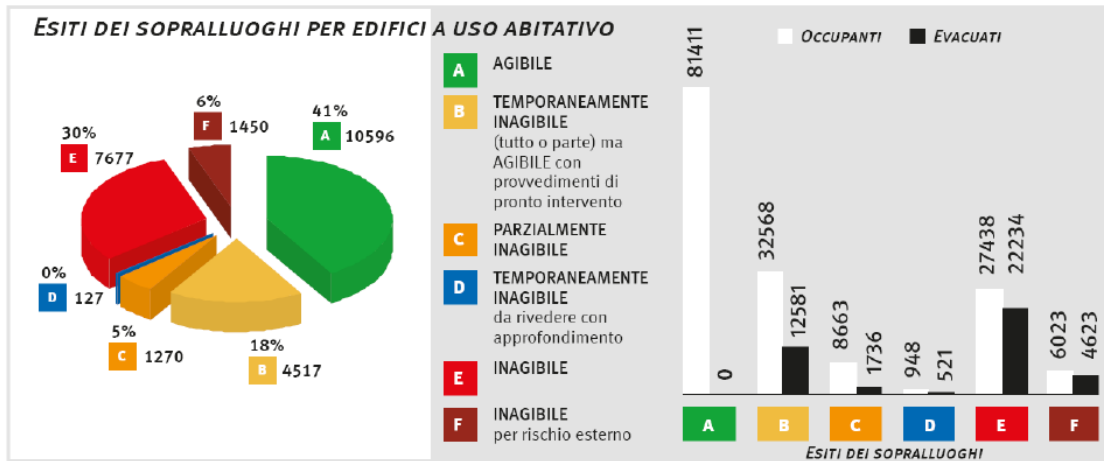
designed for earthquake loads, made them particularly vulnerable to seismic events, mainly because of poor connections between horizontal and vertical structural elements and weak foundations (fig....).



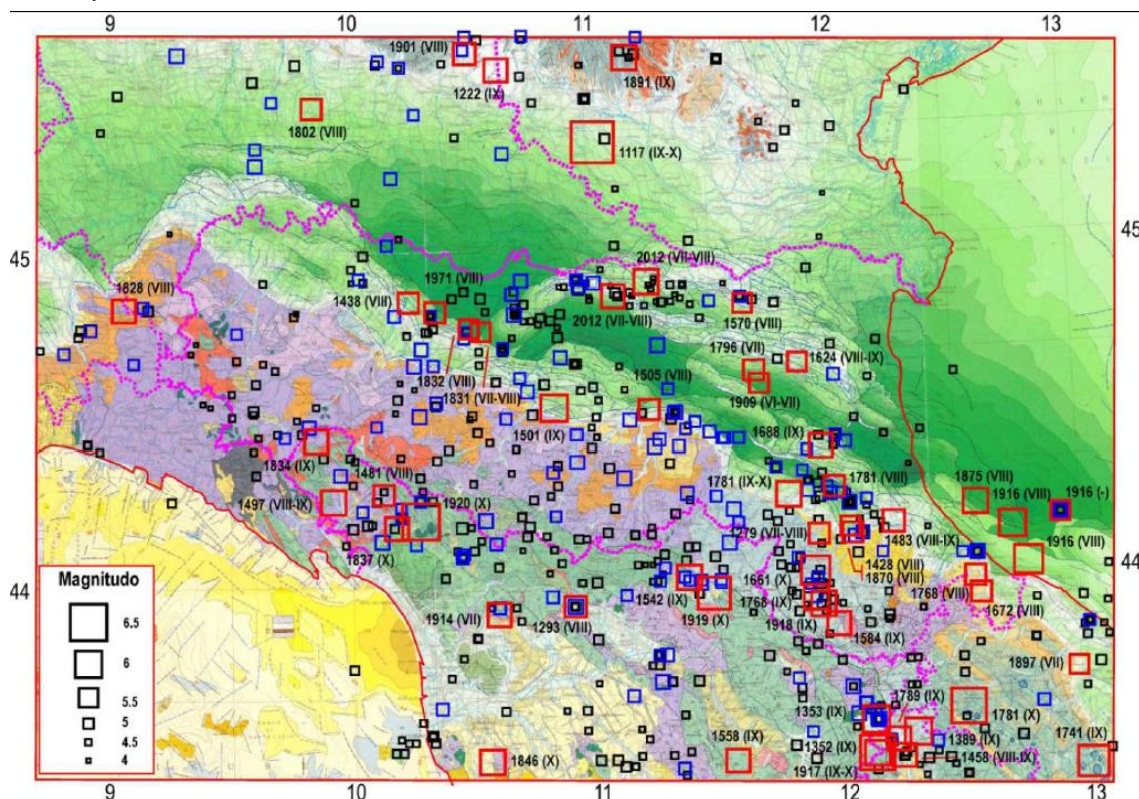




In figure... the results of the practicability controls on residential buildings are presented. The intensity is estimated by the authorities of VII-VIII degree.



The region struck by the earthquakes already experienced seismic events in the past. From historical documents events of similar intensity occurred in 1346, 1570 and 1796 (Locati et al., 2011). The event of 1570 in particular, has many analogies with the 2012 earthquakes.



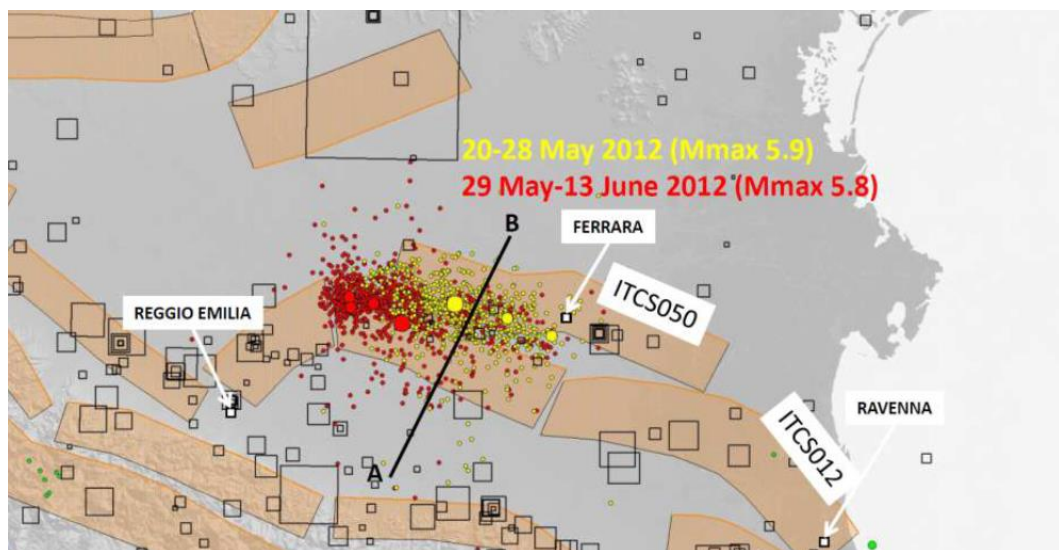
In rosso  $M \geq 5.5$ ; in blu  $5 \leq M < 5.5$

Da Mantovani et al. 2013

The Po plain is a valley filled with hundreds of meters of sediments carried by Po river and its branches. Underneath the young fluvial deposits the Appennines chain extends with covered dorsal until approximately the present Po river path. The hidden structures

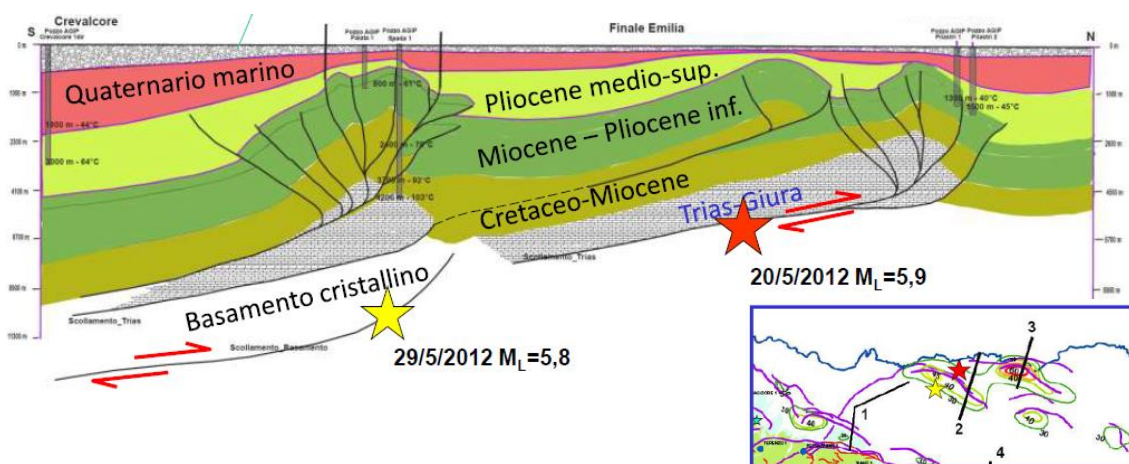
are geologically active and have a behaviour similar to the emerging Appennines located between Emilia Romagna region and Toscana. The collision between the African plate and the European plate generate a complex series of faults that are located along the Appennines chain.

In particular, the structure affected by the 2012 events is part of a direct faults system known with the name of "Pieghe Ferraresi" (fig.....). This system extends from Reggio Emilia to Ravenna, passing underneath the city of Ferrara. From figure.... it appears that there are two fault structures, an internal one (located more south) and an external one (located more north). The internal one is divided in the eastern, central and western area. Considering the main events and aftershocks location in figure... it is possible to derive that the first event took place in the external fault and the second event took place in the internal fault. This mechanism is quite common for these kind of fault system and consistent with historical events. In particular, the equilibrium overcoming in the external fault have caused a shaking and a consequent loading of the internal fault that has in a short time lead to a second seismic event.



The section of figure shows the two main faults with the rupture points.





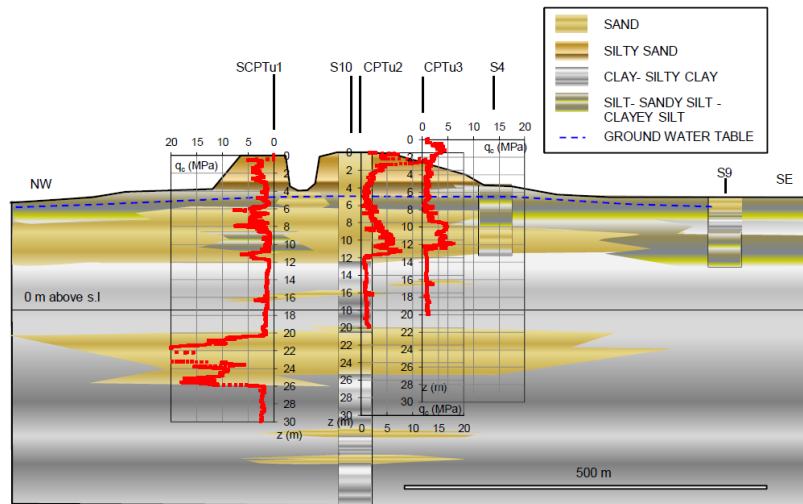
A peculiar aspect of the Emilia earthquakes is soil amplification and liquefaction phenomena. Due to the young age of the soils, to the depositional environment and to the presence of surficial water table the effects of ground motion have increased reaching the surface. The peak ground acceleration values have reached for example the level of 1,2g, while the maximum reference values for the area are equal to 1,15g. This occurrence is explained with the poor characteristics of the surficial soils that generated an amplification of the shaking, as well as, in some areas the manifestation of soil liquefaction.

## 5.2 Liquefaction

The Emilia earthquake has shown one of the first liquefaction phenomena occurred in recent Italian earthquakes, even though historical documents and paintings show in the same area features that are compatible with earthquake induced soil liquefaction, like cracks and sand boils.

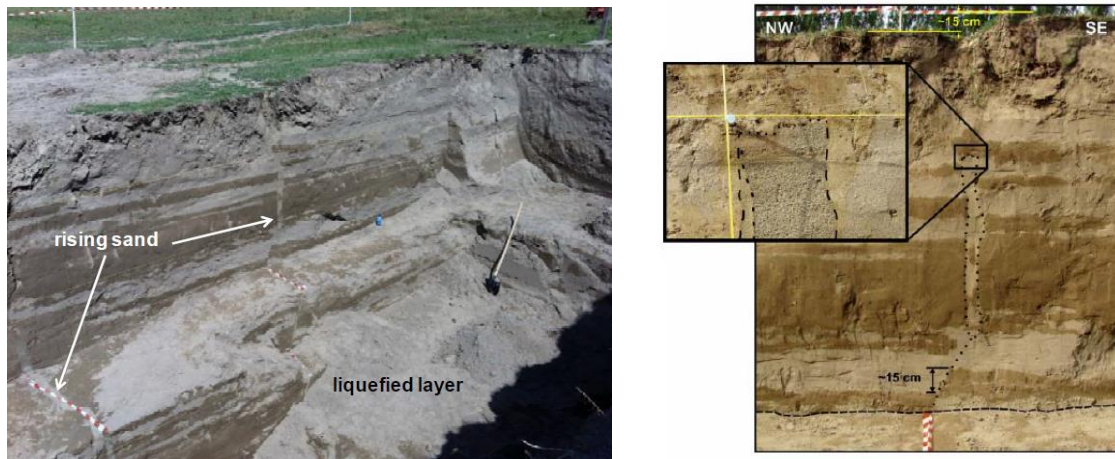
The most massive evidences and damages appeared along the paleochannel of Reno river, in the villages of San Carlo, Mirabello and Sant'Agostino. The river was in fact diverted from its previous path in the XVIII century and the mentioned villages developed on the abandoned embankment which had the advantage of being slightly higher than the surrounding fields.

As it appears clearly from figure... the first 8-10 m are made of sandy and silty-sandy soils, very loose and with water table located a few meters below the surface.



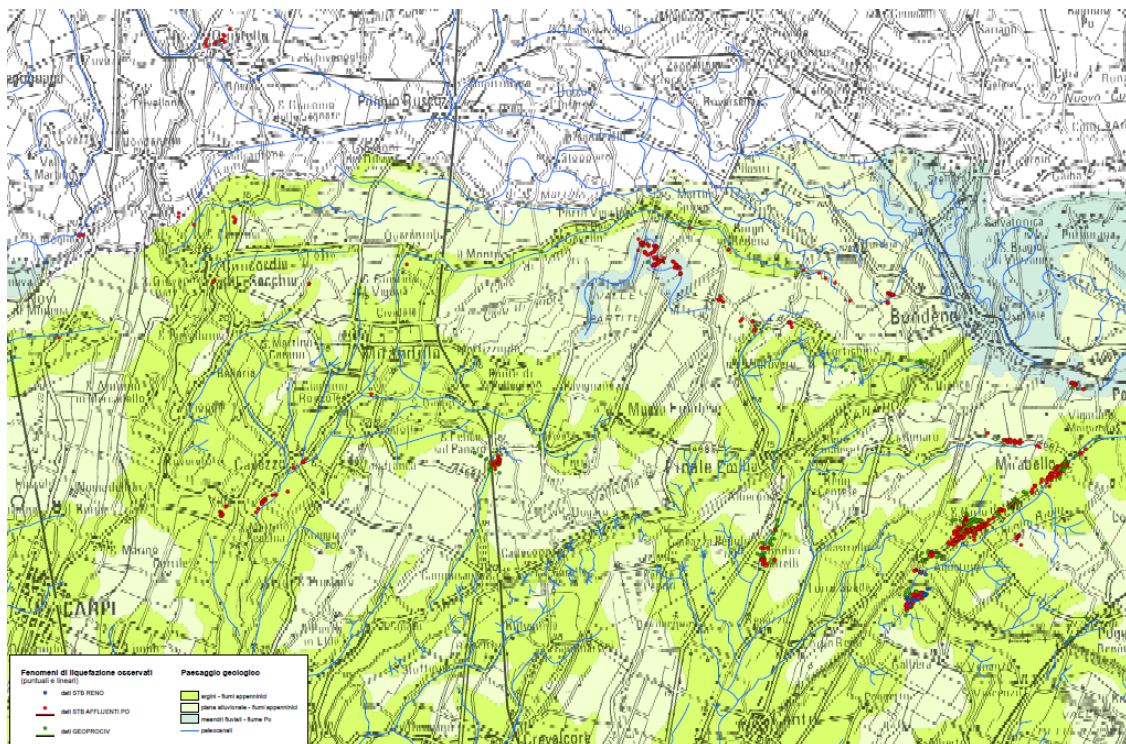
The main features observed consist in cracks with massive sand ejecta. The cracks were observed both on the paleochannel crest and in the surrounding fields. As it appears from figure.... the sand was driven on the surface by water with excess pressure. In the urban area many damages affected the buildings that showed tilting, deformations, differential settlements and fissures. Part of the buildings had to be demolished. Important consequences were observed for lifelines as well, with deformation and breakages in pipelines and uplifting of manholes.





Some trenches were dug in the surroundings and clearly showed the presence of rising material. From figure.... it is visible the paths followed by the sand ejecta as well as the thickness and the location of the liquefied layers, which are in this case quite superficial and can thus be easily detected, sampled and analysed with a trench.

In the map of figure.... all the liquefaction evidences are indicated, together with the geological characteristics of the area affected by the earthquake. Most of occurrence is located along the Reno paleochannel, as already described.



There were anyway other manifestations, of smaller entity and spatially limited but still evident and undoubtedly connected to soil liquefaction. In these cases damages were



similar to those already appeared in San Carlo area, even if of much smaller extension; this is due to the fact that sand boils, fissures and ground deformations were limited to small areas. All the evidences are related to the current or past presence of a river; it is interesting to note that soils carried by different rivers (Po river, Secchia river, Panaro river, among Reno river) experienced liquefaction. In table ... the main evidence locations are presented, including the connected river and the general soil characteristics (FC, % of sand and particles diameter). It appears that there is not uniformity in liquefied soils. In particular, most of soils show a high sand content and relatively low fine content but, in some cases, even soils with lower sand content liquefied. This is consistent with the possibility of detecting liquefaction even in soils that have mainly a silty content, as already mentioned in chapter 1 and 2.

Site	Fluvial domain	D50 (mm)	FC (%)	sand (%)
Case. S. Antonio	Po ancient riverbed	0.1-0.25	5-32	68-88
Uccivello di Cavezzo	Secchia ancient riverbed	0.15-0.3	11-25	68-88
S. Possidonio	Secchia ancient riverbed	0.22	4	96
Quistello	Po ancient riverbed	0.18-0.2	8-19	81-92
S. Felice sul Panaro	Panaro ancient riverbed	0.15-0.18	22	78
Mirabello	Reno ancient riverbed	0.18	16	84
S. Carlo	Reno ancient riverbed (fractures)	0.04-0.09	41-80	59-20
S. Carlo	Reno ancient riverbed (sand boils)	0.12-0.15	17-24	76-83

### 5.3 Liquefaction of river embankments

Apart from the events observed along the old path of Reno river, some liquefaction features were detected close to active river embankments. A first observation is from the surroundings of Sant'Agostino (FE) village, where Reno river flows nowadays. At the embankment toe an evident crack with sand ejecta was observed



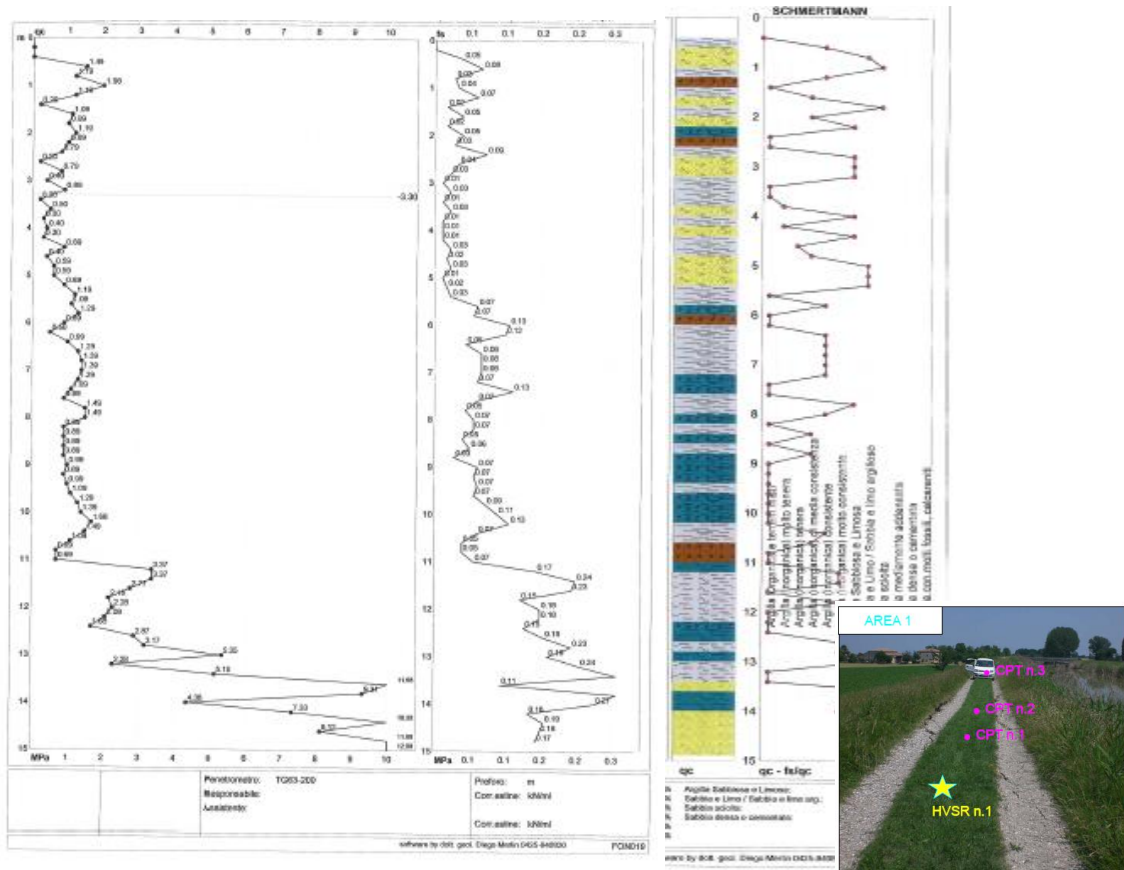
Some fissures were observed also along the embankment bank and the material ejection clearly indicate the occurrence of erosion consistent with what has happened in the close village of Scortichino. However, no relevant damages were detected on the earth structure. The responsible for the river maintenance (Sevizio Tecnico Bacino Reno), did not start any further and deep investigation.

Another manifestation that affected embankments structures occurred along the Diversivo channel (the channel history will be described more in detail in paragraph .....). A crack system made of two parallel fissures with semicircular projection appeared on the embankment crest. Two similar patterns were observed on the same embankment at a distance of some tens of meters.

This occurrence is of particular interest because the cracks location is on the same earth structure and at the close distance of a few kilometers from the Scortichino study area.



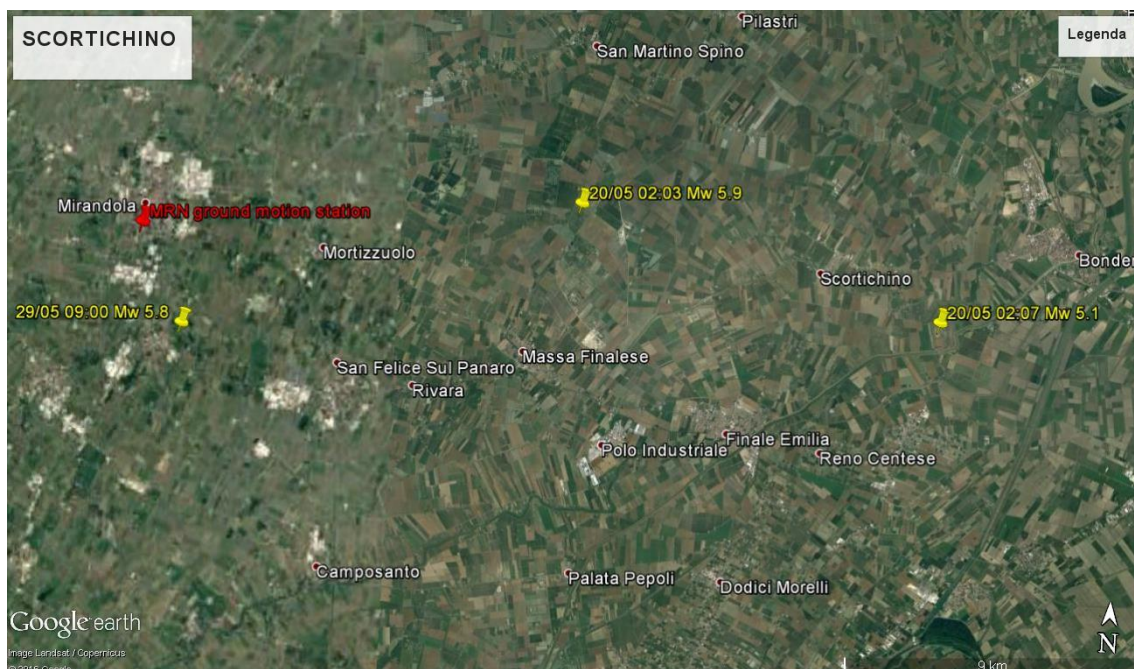
In this occasion the authority responsible for the channel (Consorzio della Bonifica di Burana) ordered some penetration tests (figure...) and quickly repaired the structure.



As a preliminary evaluation of the data available, it is not possible to define the cause of the damages. From the liquefaction occurrence map (fig.....), the surroundings experienced soil liquefaction but considering the cracks and the damage pattern it is not surely confirmed the occurrence in this case. In fact, no san ejecta were observed and the semicircular shape of the cracks is compatible also with an embankment stability problem. On the other hand, a first evaluation of the CPT does not show layers that appear clearly liquefiable. The deep sandy layer is place at an important depth and its role on the surficial damages appear quite unlikely. The more surficial layer made of mixed soils would need more tests to confirm the possibility of some reduction in bearing capacity connected to cyclic loading.

### 5.3.1 Scortichino case history

Scortichino is a village located quite close (less than 10 km) to the epicentre of the earthquake of the 20<sup>th</sup> of May (fig. ....). The area has suffered many earthquake induced damages on residential and industrial buildings, as all the areas close to the epicentre. Scortichino is also on the verge of a channel named “Canale Diversivo”, already mentioned in the previous paragraph and described in detail in paragraph .....



Canale Diversivo is a channel used for irrigation and for the drainage of rain water from the northern area of Modena province. In the proximity of Scortichino the channel



presents some enlargement of the embankment crest, obtained by filling older meanders, where during the years a few small groups of houses (6-7 groups) were built (fig. ....).



Following the earthquake the embankment reported some damages, in particular longitudinal fissures and some lateral deformations: these instabilities cause significant damages to the buildings placed in it. In particular, in 4 groups of houses the fissures in the embankment body opened (fig....) and cracks were induced in the overlying buildings (fig....). Some structures had to be demolished and some required relevant repairs.







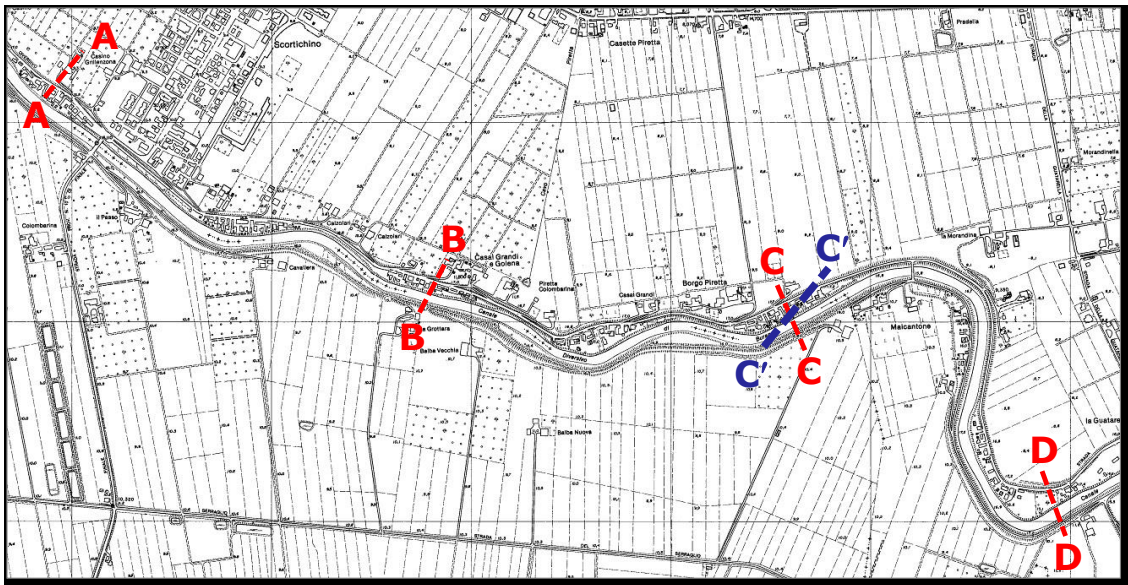
The damages are clearly related to the movement of the embankment and a detailed analysis of the cracks pattern will be presented in paragraph... Considered the presence of buildings on the embankment and the fact that the evidence appeared in more than one section, additional investigation were required by Regione Emilia Romagna, in order to decide if and how repair the buildings or relocate them somewhere else. A group of experts named "Gruppo di Lavoro AGI-RER" was created with the aim of organizing a proper investigation of the embankment structure and of the soil profile underneath it. The cause of the damages is not apparently obvious: in fact the cracks opened only in some section and not uniformly, implying that local conditions might play an important role. In addition on the field side close to the area of interest some soil liquefaction evidences like sand ejecta were observed. However not evident material expulsion were instead observed on the embankment. Consequently a detailed site and laboratory campaign was arranged to characterize properly the soil along the all study area. In the next chapter the experimental investigation and its results will be presented.

## CHAPTER 6

# Scortichino case study – in situ and laboratory investigations

### 6.1 Geotechnical investigations program

In the surroundings of Scortichino, along the Canale Diversivo path affected by earthquake damages, as described in the previous chapter, an investigation program was planned. The study area is approximately 3-3,5 km long and it includes all the groups of buildings that showed some damages and deformations in the embankment body. In particular 4 main cross-sections have been identified as the most representative (fig.....). On these sections all the field and laboratory tests arranged by “Gruppo di Lavoro AGI-RER sugli Argini” were performed.



The kind of tests performed are chosen with the aim of classifying in detail the soil profile under a static and dynamic point of view. The in-situ tests performed are coring with sampling, CPTU and SDMT. For each section the tests performed are summarized

in table.... with indication of the depth reached and the number of samples collected. In section C, where most of damages have occurred a more detailed investigation has been carried out with additional CPTU and coring down to 50 m, creating an additional cross-section of study named C'-C'.

TIPO DI PROVA	SEZIONE/ AREA DI INDAGINE	PROVA	PROFONDITÀ (m)	N° CAMPIONI
<b>SONDAGGI</b>	A - A	S1	30	5
	B - B	S2	20	6
	C - C	S3	50	7
	D - D	S4	20	6
	C - C	S5	20	5
<b>PROVE PENETROMETRICHE (PIEZOCONO)</b>	A - A	CPTU 1	28	-
	A - A	CPTU 2	29	
	A - A	CPTU 3	27	
	B - B	CPTU 4	27	
	B - B	CPTU 5	20	
	C - C	CPTU 6	31	
	C - C	CPTU 7	30	
	C - C	CPTU 8	26	
	C - C	CPTU 9	29	
	C - C	CPTU 10	31	
	D - D	CPTU 11	31	
	D - D	CPTU 12	31	
<b>PROVE DILATOM. SISMICHE</b>	A - A	SDMT A	35	-
	B - B	SDMT B	32	
	C - C	SDMT C	35	
	D - D	SDMT D	25	

The samples are divided between the laboratories of the universities involved in the group according to the specific laboratory test that on the samples must be performed. In table.... the samples collected for each coring with the depth of sampling are summarized, with the indication of the laboratory at which they were sent.

Campione	Profondità	Laboratorio
1	3,70 - 4,20	UniNA
2	6,20 - 6,80	UniRC

**S1**

Campione	Profondità	Laboratorio
1	3,20 - 3,70	UniFI
2	6,40 - 7,00	UniROMA

**S2**

3	10,85 – 11,60	UniFI
4	13,5 – 14,00	UniRC
5	23,00 – 23,60	UniNA
-	-	-

3	8,10 – 8,70	UniNA
4	10,40 – 11,00	UniNA
5	15,00 – 15,60	UniROMA
6	18,00 – 18,60	UniNA

Campione	Profondità	Laboratorio
1	3,00 - 3,50	UniFI
2	6,00 – 6,60	UniNA
<b>S3</b> 3	8,00 – 8,60	UniFI
4	11,00 – 11,60	UniFI
5	15,00 – 15,60	UniROMA
6	30,40 – 31,00	UniFI
7	40,00 – 40,50	UniROMA

Campione	Profondità	Laboratorio
1	3,10 - 3,40	UniNA
2	7,20 – 7,60	UniNA
<b>S4</b> 3	10,00 – 10,60	UniRC
4	12,00 – 12,60	UniROMA
5	14,00 – 14,60	UniNA
6	18,00 – 18,60	UniNA

Campione	Profondità	Laboratorio
1	3,00 - 3,60	UniNA
2	6,00 – 6,60	UniRC
<b>S5</b> 3	9,00 – 9,60	UniNA
4	11,20 – 11,80	UniNA
5	14,00 – 14,50	UniRC

## 6.2 In situ tests

As evident from table...., at each cross section one SDMT, one coring and two CPTU have been carried out, with exception of section C where additional tests have been performed.

For the analysis of a 2D or a 3D structure, the geometry is of particular importance, especially when there is the need of considering stability of slopes or lateral deformations; for this reason a detailed topographical survey was arranged along the all study area.



### 6.2.1 Topographical survey

The only available information related to the channel geometry come from the authority responsible for the channel know as “Consorzio di Bonifica”, that has available some not recently updated maps; those maps show a channel geometry that is quite similar to the present situation, even if the level of detail is not reliable enough to perform advanced analysis. In addition, in the maps some recent changes in the embankment shape and in the channel bed depth are not present; furthermore, the possible changes in the embankment shape due to the earthquake event are obviously not indicated on the maps, that were drawn some decades before.

Due to the size of the study area, to its morphology and to the level of accuracy required, the most suitable survey technology adopted is satellite based and know as GNSS (Global Navigation Satellite System), which allow a scatter of a few centimeters.

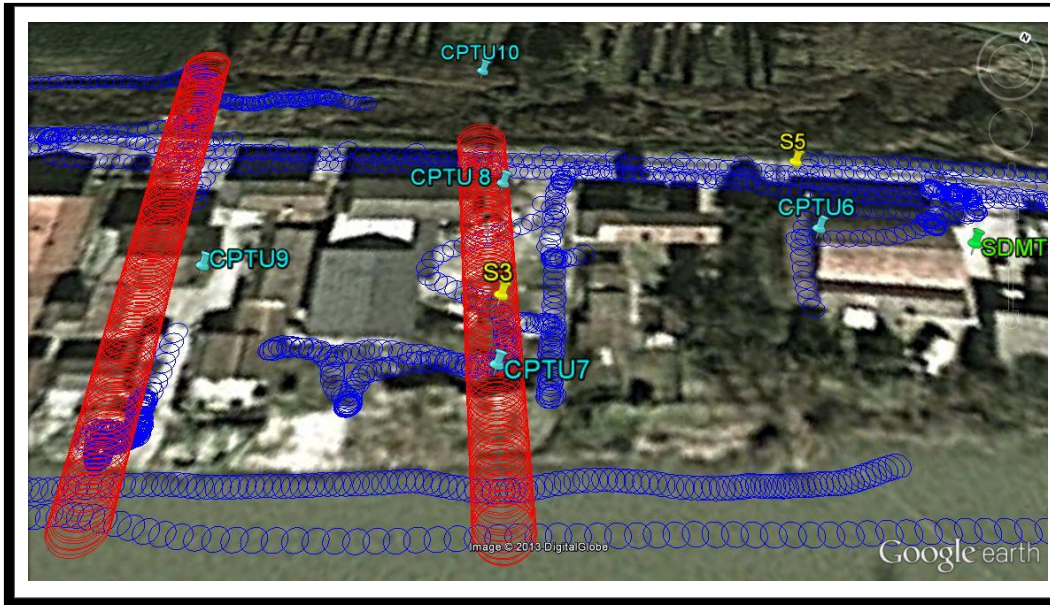
The survey was realized partly with a walking operator, partly by car and partly by boat, all equipped with a couple of Trimble R7 GNSS receivers with Zephyr Geodetic 2 GNSS antenna and a Bluetooth Trimble TSC2 controller (fig....).



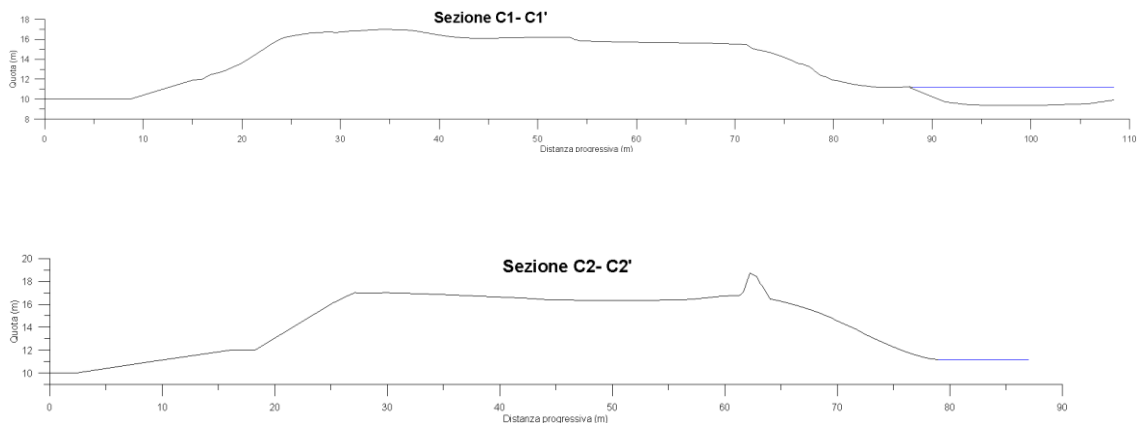
The main information required to the survey are:

- Mapping of the channel crest along the all study area, with care to the altitude change along the area;
- Mapping of the embankment shape along the cross-sections where the soil tests were performed;
- Detection of the channel shape and depth along the all area;
- Definition od the surface profile at the embankment toe on field side.

In figure ... it is represented the path followed by the instrument in section C in order to provide a topographical map of the area.

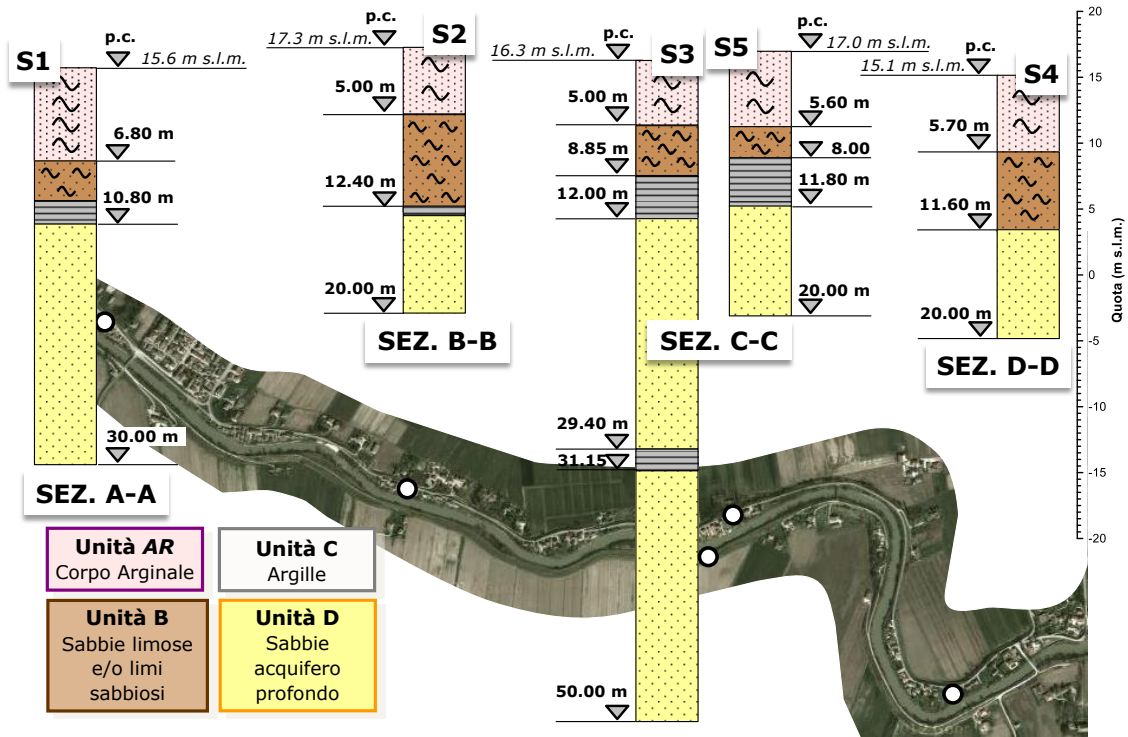


In figure .... The two cross-section resulting from the survey in section C are presented. The section try to correspond to the location of the field tests, with the aim of creating a detaild stratigraphy of the area.



### 6.2.2 Core drilling

The five coring performed are represented in figure.... S2-S3-S4 reached a depth of 20 m from ground surface, while S1 reached 30 m and S5 50 m respectively. A rough stratigraphy is shown in Fig. .... In principle there is a good uniformity along the all area of study for what concerns the deep layers (Unit A ). There is instead a certain variability for what concerns the surficial layers (Unit AR B and C).



With the name Unit Ar the embankment body has been identified and it is formed mainly by silt and sandy silt material, probably in a big part placed by mand activity. With the name Unit B the layer underneath Unit Ar is identified: it is the material lying immediately under the embankment body and composed by silts and sandy silts with small sandy lenses; Unit B is probably the deposition layer of Diversivo Channel when it was part of Panaro river (see paragraph ..... for more detail about this). Unit Ar and B are quite variable in thickness along the channel portion considered in the study.

Unit C is a relatively thin clayey layer dividing Unit B and Unit A; relevant to note that Unit C is not uniform in thickness along the study area. Unit A is a massive clean sandy layer formed by the deposition activity of Po river. Unit A hosts an important confined aquifer connected with Po river and known as “acquifero Padano”.

Figure .... shows the material drilled by the coring S5 and a more detailed stratigraphy. The samples location is also indicated. For the complete description of all the tests performed the report written by “Gruppo di Lavoro AGI-RER” can be examined.



Scala 1:100	P.P. I [daN/cm <sup>2</sup> ]	Vane Test [daN/cm <sup>2</sup> ]	Profondita' [m]	Stratigrafia	DESCRIZIONE	UNITÀ
1			0.20		Limo con radici ed erba, colore marrone	AR
2					Limo e limo sabbioso con sabbia limosa e sparsi apparati radicali. Colore marrone	
3	1.0	0.40				
4	1.2	0.50	3.70		<b>CAMPIONE INDISTURBATO</b>	
5			5.00		Limo e limo sabbioso alternato a livelli sottili di limo argilloso. Colore marroncino, rossiccio nella parte sommitale.	B
6	1.2	0.60	5.38		Sabbia fine e molto fine limosa marroncina. marroncina arigiastrea	
			5.45		Limo-argilloso marroncino grigiastro	
7			6.40		Limo e limo sabbioso alternato a livelli sottili di limo argilloso. Colore marroncino	
			7.00		<b>CAMPIONE INDISTURBATO</b>	
8	1.8	0.90	7.50		Limo e limo sabbioso con livelli < 1cm di limo argilloso. Colore marroncino	
			7.65		Limo e limo argilloso marroncino	
			8.10		Limo e limo sabbioso con livelli sottili di sabbia fine limosa. Colore marroncino	
9			8.70		<b>CAMPIONE INDISTURBATO</b>	
10	1.1	0.60			Limo e limo sabbioso alternato a livelletti di sabbia limosa di colore marroncino e livelli di limo argilloso di colore grigiastro.	
11			10.25		Sabbia fine limosa marroncina	C
			10.40		<b>CAMPIONE INDISTURBATO</b>	
12			11.00		Alternanze di limo e limo sabbioso con sabbia fine limosa e debolmente limosa.	A
13	1.2	0.60	12.40		Argilla grigia e grigio scura con livello mm di gusci madreperlacei	
			12.50		Limo e limo argilloso grigio con livelli di limo sabbioso.	
14			12.80			
15					Sabbia medio-grossolana, localmente media, grigia	
16			15.00		<b>CAMPIONE INDISTURBATO</b>	
17			15.60			
18					Sabbia grossolana e molto grossolana, subordinatamente media, di colore grigio	
19			18.00		<b>CAMPIONE INDISTURBATO</b>	
20			18.60			
			20.00		Sabbia grossolana e molto grossolana, localmente media, grigia	

### 6.2.3 Cone penetration tests (CPTU)

The cone penetration tests (CPTU) are the in situ tests that were performed mostly. This kind of tests, among many positive aspects, is particularly suitable and of common use

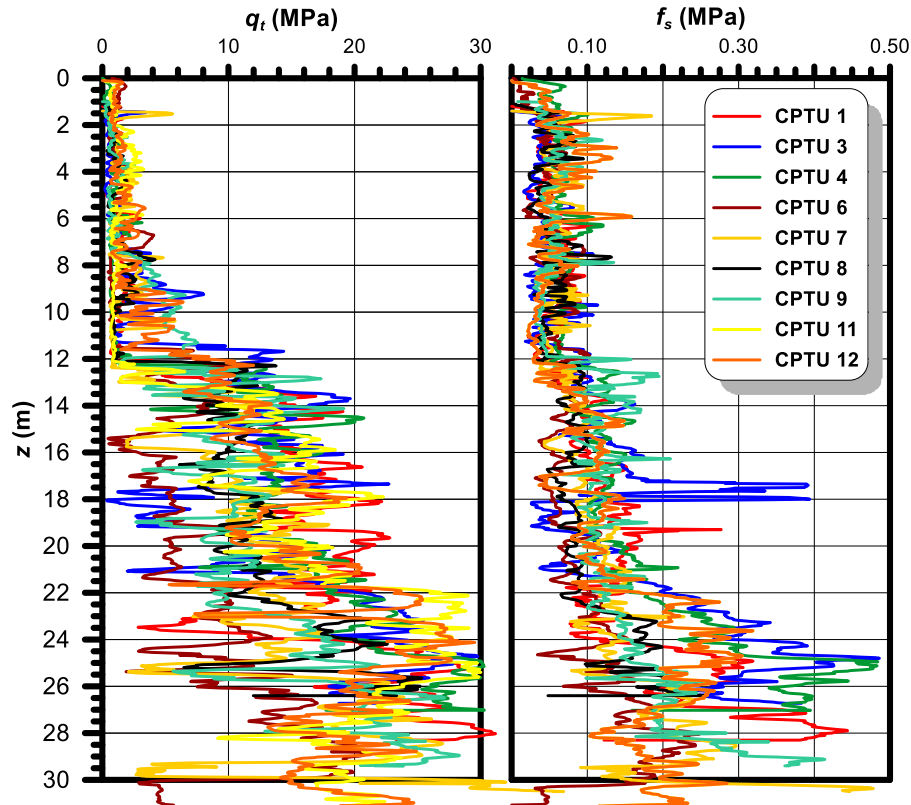
for evaluating liquefaction susceptibility using semi-empirical methods. This aspect is described in detail in chapter 7.

In table .... the CPTU for each cross-section, with the position respect to the embankment and the depth reached are reported.

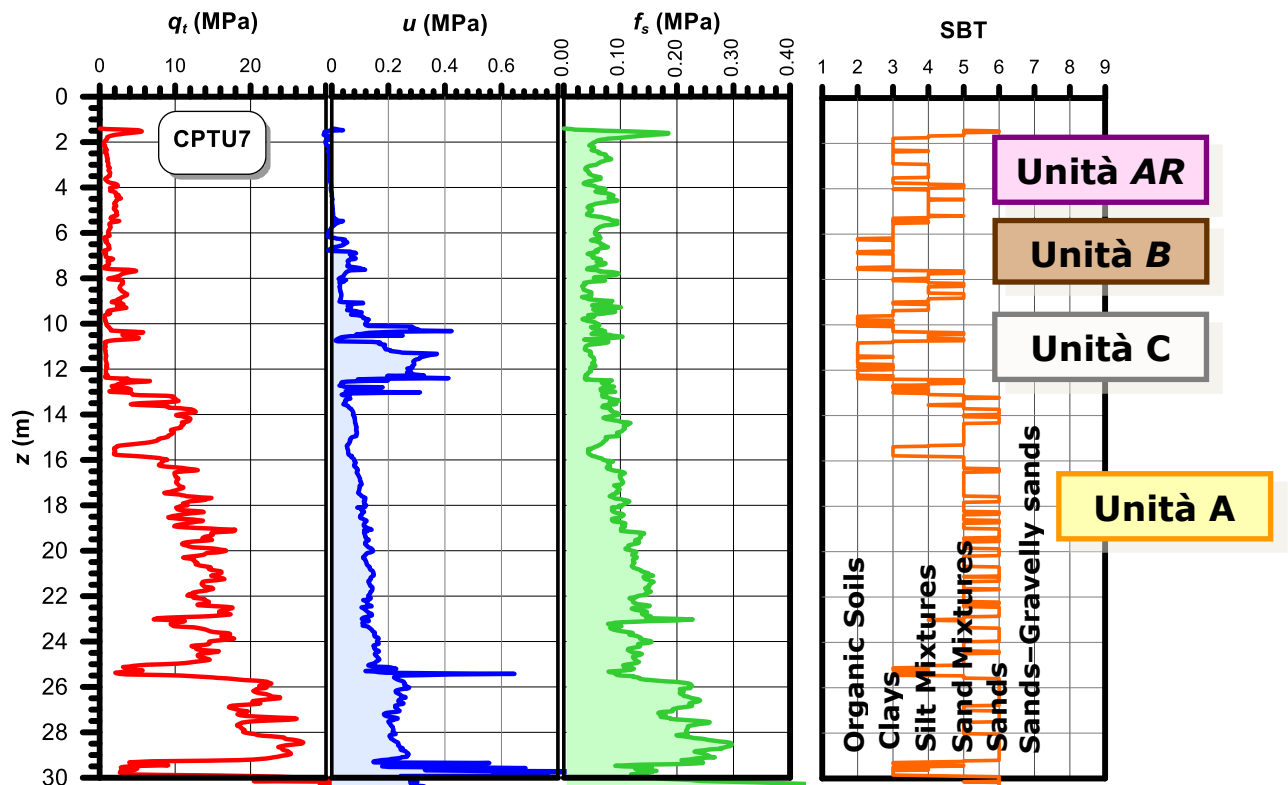
Sezione/ Area di indagine	Prova	Profondità raggiunta (m)	N° dissipazioni	Posizione	Coordinate Planimetriche Approx. (°)
A – A	CPTU 1	28	4	Sommità argine	N 44.878693 E 11.321536
	CPTU 2	29	1	Lato campagna	N 44.878430 E 11.323062
	CPTU 3	27	2	Sommità argine	N 44.878019 E 11.322562
B – B	CPTU 4	27	2	Sommità argine	N 44.873653 E 11.334087
	CPTU 5	20	3	Lato campagna	N 44.873841 E 11.334624
C – C	CPTU 6	31	2	Sommità argine	N 44.873198 E 11.345988
	CPTU 7	30	2	Sommità argine	N 44.872872 E 11.345649
	CPTU 8	26	2	Sommità argine	N 44.873097 E 11.345491
	CPTU 9	29	3	Sommità argine	N 44.872840 E 11.345159
	CPTU 10	31	1	Lato campagna	N 44.873265 E 11.345323
D – D	CPTU 11	31	1	Sommità argine	N 44.868590 E 11.353405
	CPTU 12	31	1	Sommità argine	N 44.868270 E 11.353311

All the recorded  $q_t$  and  $f_s$  values are represented in figure .... All the tests overlying each other do not allow a careful interpretation of the data, but can provide a general overview of the soil properties along the all area of study. The main outstanding aspects are a relevant and general change in the soil properties at a depth of around 12 m, which corresponds to the upper boundary of Unit A where the  $q_t$  goes from values generally lower than 4-6 MPa to values higher than 10 MPa. Above this boundary the  $q_t$  values are below 2 MPa until 5 m and go from 2 to 6 MPa from 5 to 12 m below the surface. It is important to note that there is an important variability in  $q_t$  values especially between 5 and 12 m, which correspond to the variability in the thickness of Unit Ar and B already

observed in paragraph..... For what concerns Unit A, a good level of variability, not in terms of the layer thickness, but in terms of  $q_t$  values can be observed.



As an example, CPTU 7 is considered in detail. CPTU 7 is located in section C, which is the section where most of tests were carried out and were most of damages were observed. Unit A is identified from 12 to 30 m below surface as a sandy layer with some lenses of silty-clayey material. Unit C is not uniform in this section; it appears to be located between 10 and 12 m, with a silty inclusion. From ground level down to 10 m Unit Ar and B are present. Unit B is the most difficult to detect, since the difference from Unit Ar is sometimes very subtle; however, a reasonable evaluation of the thickness of Unit B would place it between 7 and 10 m approximately from the ground surface.

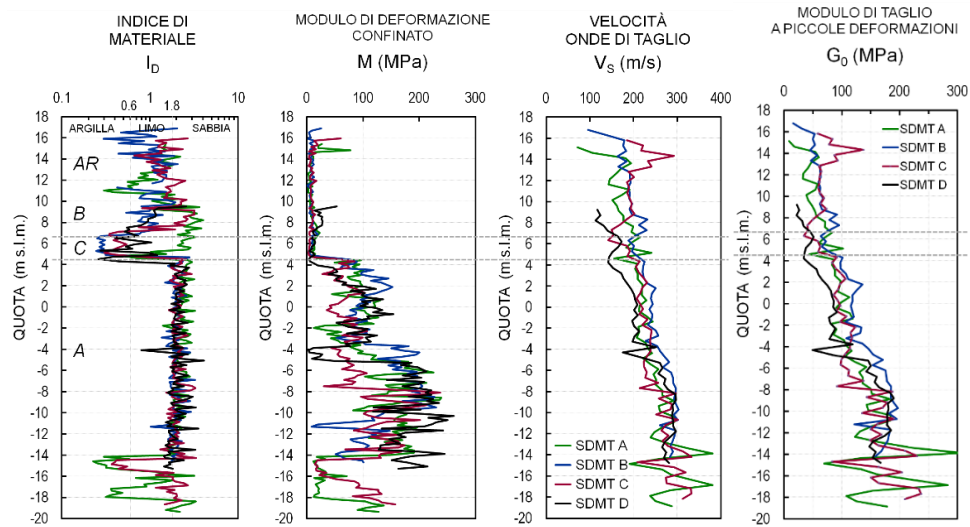


#### 6.2.4 Seismic dilatometer tests (SDMT)

The seismic dilatometer tests have been performed to find and confirmation about the results obtained from CPTU for what concerns the static properties of the soil, and to provide information about the dynamic properties. In Table ... the SDMT performed and the depth reached are summarized.

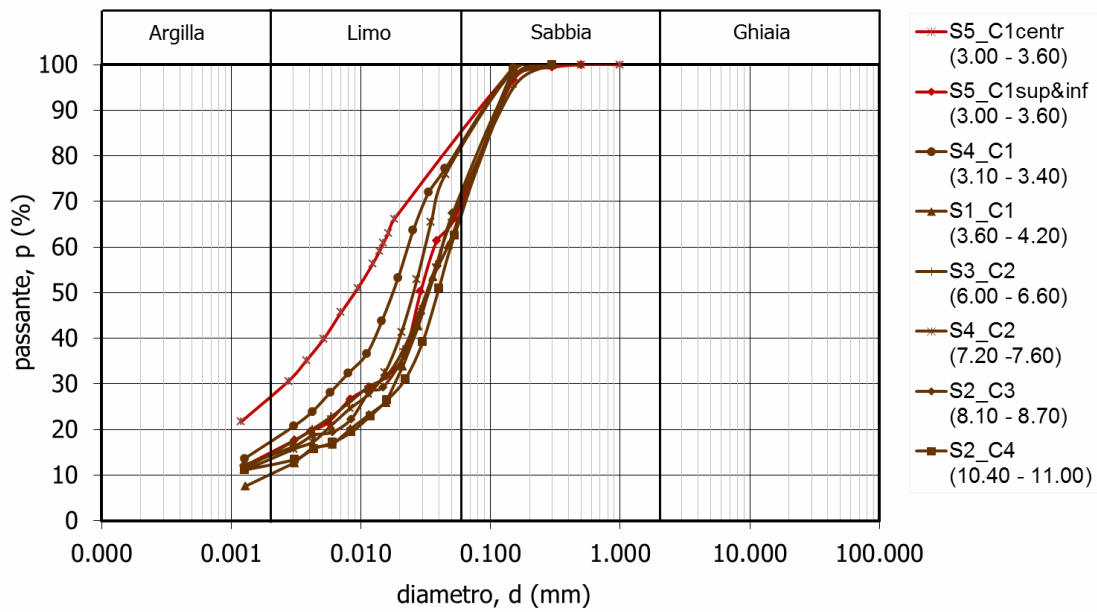
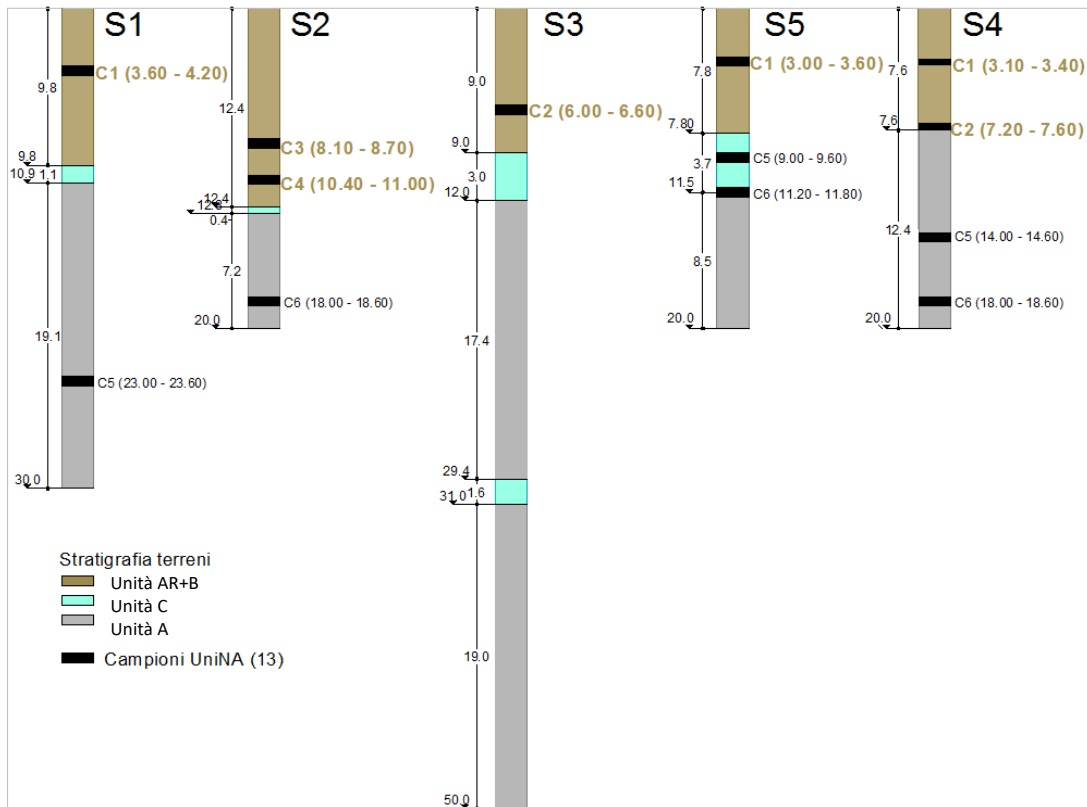
Ubicazione	SDMT #	Max profondità di prova dal p.c. (m)	Quota assoluta (approx) del p.c. (m s.l.m.)
Sez. A-A	SDMT A	35.00	15.63
Sez. B-B	SDMT B	32.00	17.30
Sez. C-C	SDMT C	35.00	16.33
Sez. D-D	SDMT D	25.00	9.72

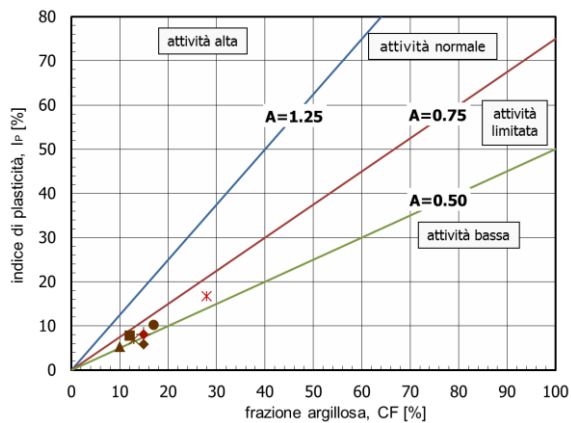
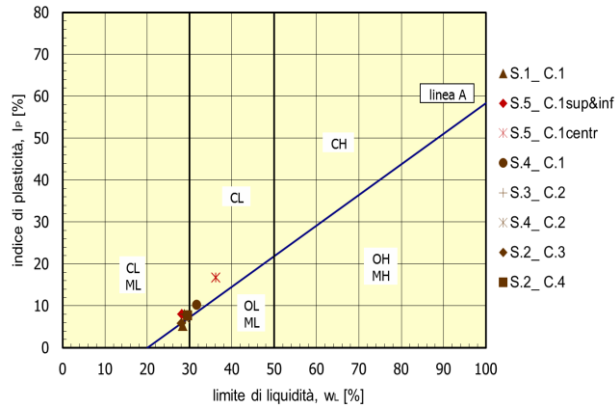
In figure.... the main results from SDMT are represented. In particular, considering the  $I_d$  (material index) values, it appears the uniformity of Unit A among the different sections as well as the variability of Unit Ar and B. Good consistency is observed as well



### 6.3 Laboratory tests

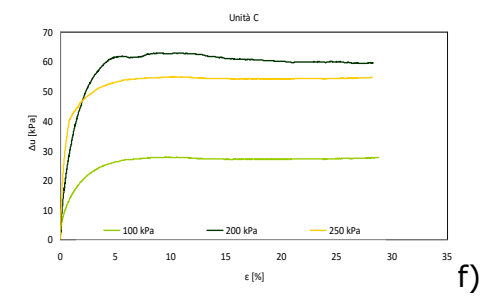
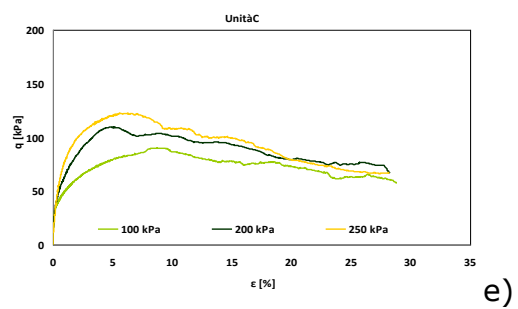
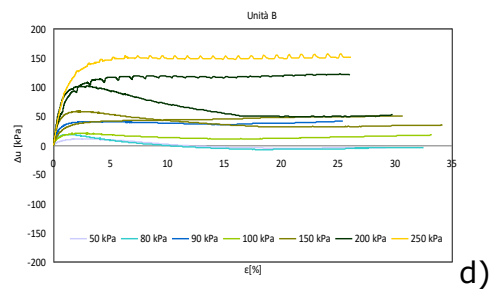
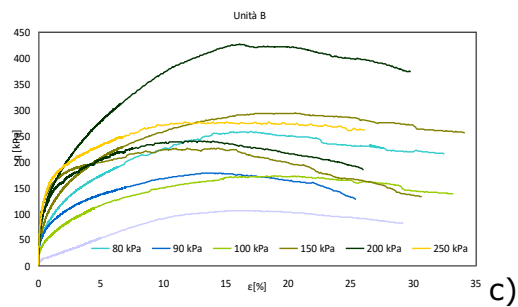
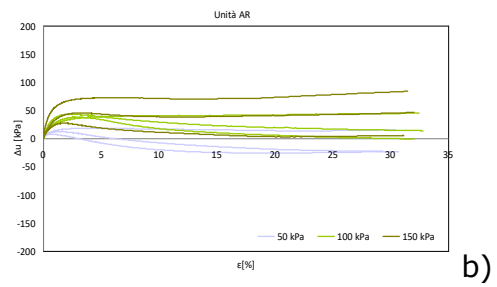
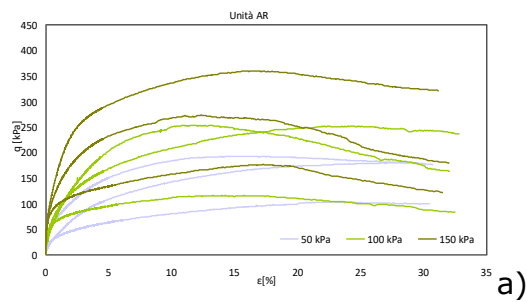
Sondaggio	Campione	Profondità [m]	Unità
S1	C1	3.60-4.20	Ar-B
	C5	23.00-23.60	A
S2	C3	8.10-8.70	Ar-B
	C4	10.40-11.00	Ar-B
	C6	18.00-18.60	A
S3	C2	6.00-6.60	Ar-B
S4	C1	3.10-3.40	Ar-B
	C2	7.20-7.60	Ar-B
	C5	14.00-14.60	A
	C6	18.00-18.60	A
S5	C1	3.00-3.60	Ar-B
	C5	9.00-9.60	C
	C6	11.20-11.80	A



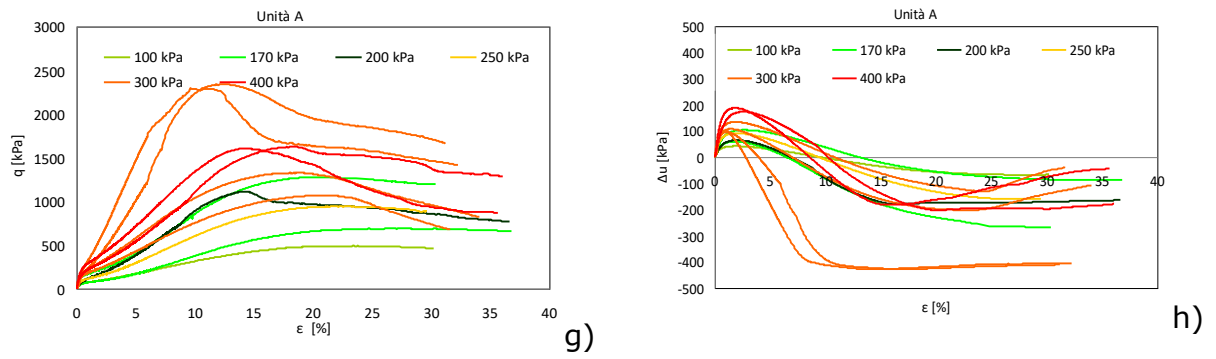


Campione	Unità	Prof. M	Argilla %	limo %	sabbia %	w <sub>L</sub> %	I <sub>p</sub>	w %	γ kN/m <sub>3</sub>	γ <sub>s</sub> kN/m <sub>3</sub>
S1-C1	Ar-B	3.60-4.20	10	59	31	28.4	5.2	31	18.44	26.58
S1-C5	A	23.00-23.60			100			22	19.20	26.71
S2-C3	Ar-B	8.10-8.70		56	28	28.1	5.8	29	19.87	26.82
S2-C4	Ar-B	10.40-11.00	12	55	33			28	20.09	26.65
S2-C6	A	18.00-18.60			100			24	20.44	26.56
S3-C2	Ar-B	6.00-6.60	15	57	28	28.8	8.0	29	19.82	26.82
S4-C1	Ar-B	3.10-3.40	17	70	13	31.6	10.3	21	19.21	26.60
S4-C2	Ar-B	7.20-7.60	13	69	18	29.1	7.0	26	20.28	26.74

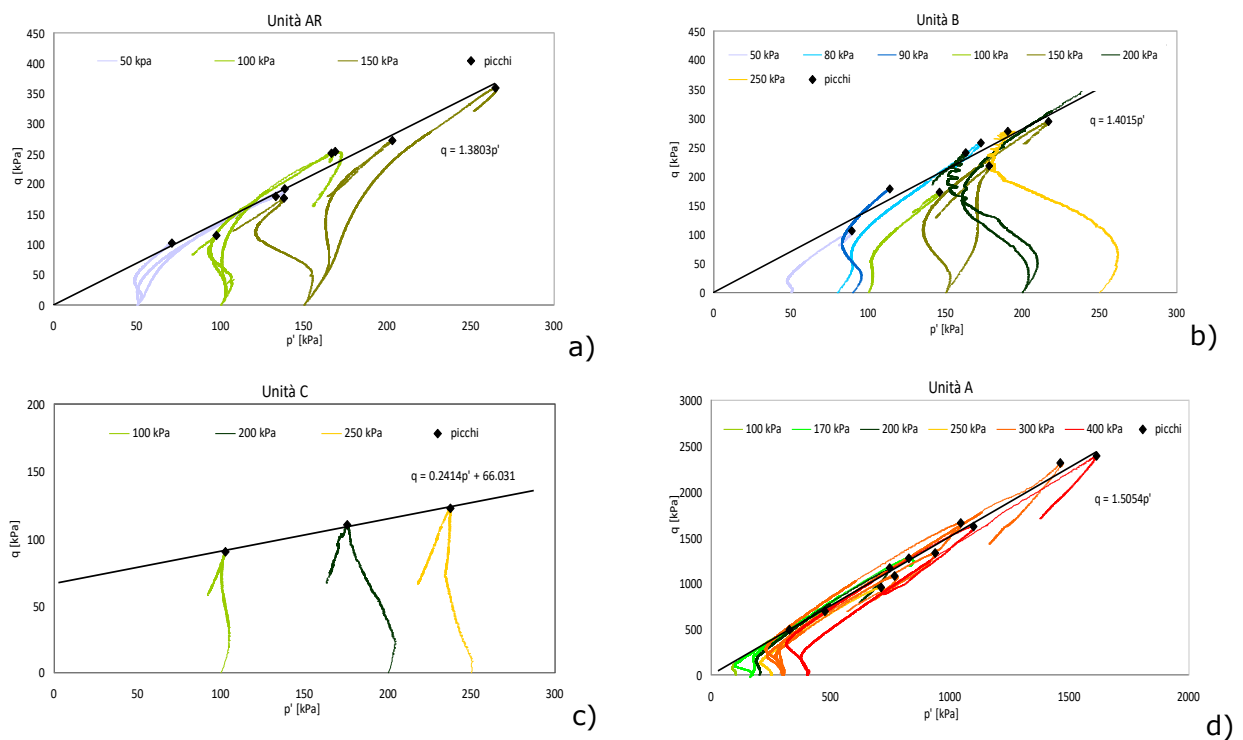
S4-C6	A	18.00 - 18.60			100			2 5	18.21	26.81
S5-C1	Ar-B	3.00- 3.60	15	55	30	28. 2	8.0	2 6	20.17	26.68
S5-C5	C	9.00- 9.60	67	29	4	70. 7	45. 4	5 3	16.68	26.88
S5-C6	A	11.20 - 11.80			100			2 9	18.54	26.74







**Figura 5.9:** Risultati delle prove TX CIU eseguite sui campioni prelevati dalle diverse unità: sx) diagramma ( $q:\epsilon_a$ ) e dx) diagramma ( $\Delta u:\epsilon_a$ ).



**Figura 5.10:** Percorsi tensionali e relativi involucri di rottura.

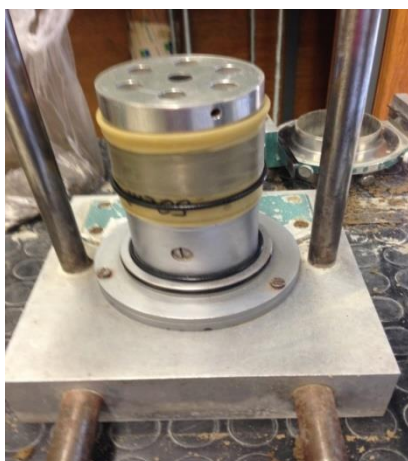
sondaggio	campione	Profondità [m]
1	3	10.90 – 11.50
2	1	3.20 – 3.70
3	1	3.00 – 3.60
3	3	8.00 – 8.60
3	4	11.00 – 11.60
3	6	30.40 – 31.00

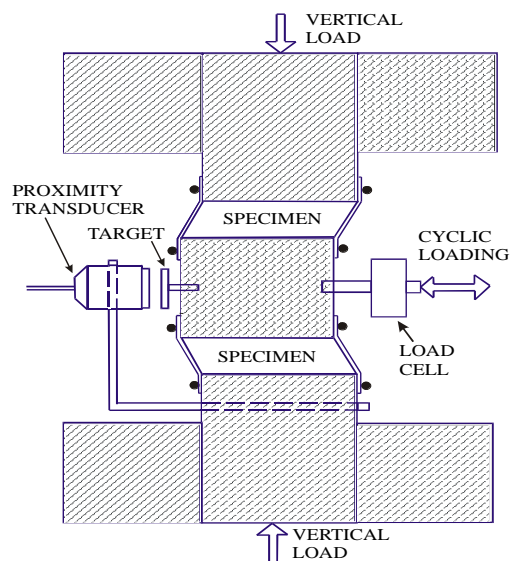
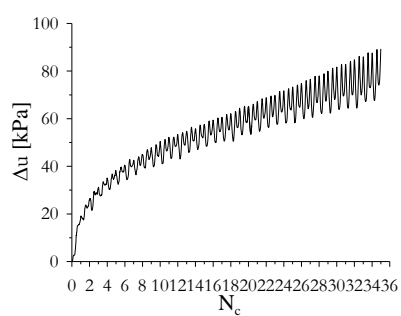
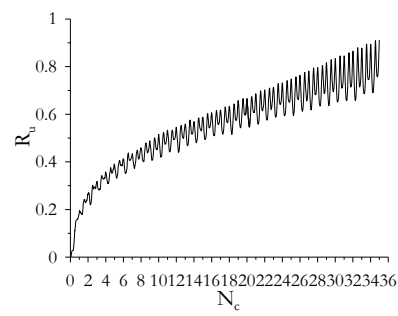
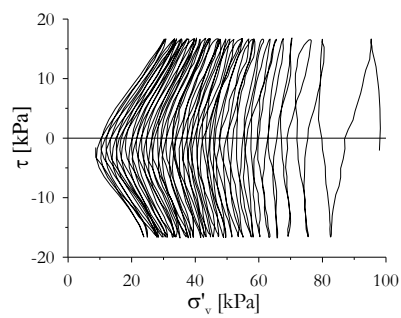
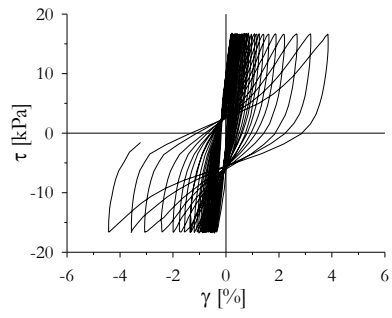
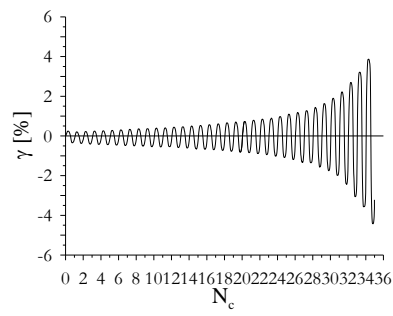
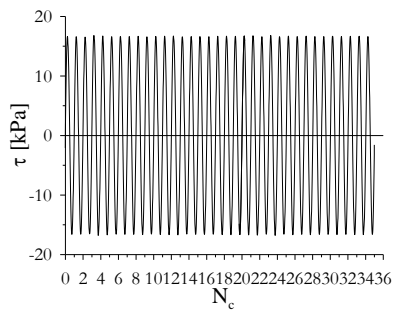
**Tabella 5.IX:** Elenco campioni esaminati

SONDAGGIO	CAMPIONE	PROFONDITA' (m) dalla sommità dell'argine	PROFONDITA' (m) s.l.m.	% Fine
1 (sez. A)	2	6.20-6.80	10.38-9.58	40
1 (sez. A)	4	13.50-14.00	2.88-2.38	4
5 (sez. C)	2	6.00-6.70	10.38-9.68	72
4 (sez. D)	3	10.00-10.60	5.00-4.40	42

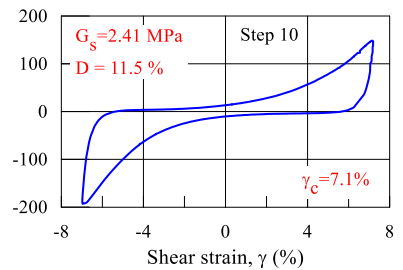
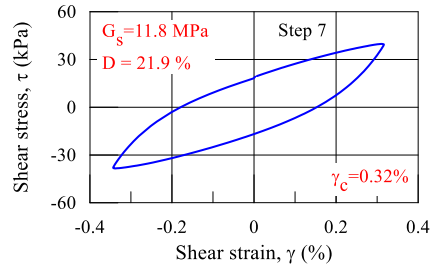
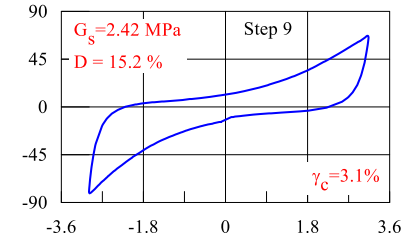
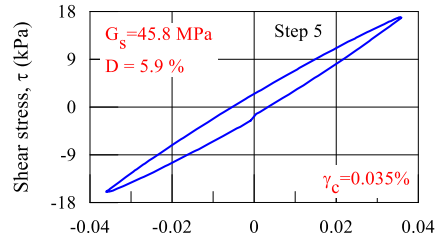
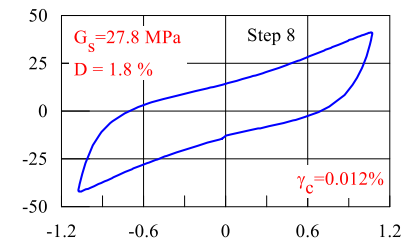
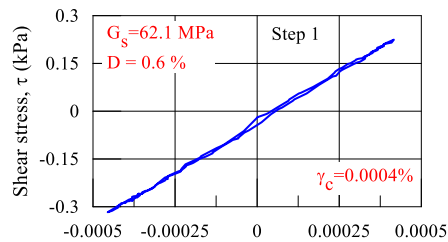
**Tabella 5.X:** Programma di prove di taglio semplice non drenate cicliche

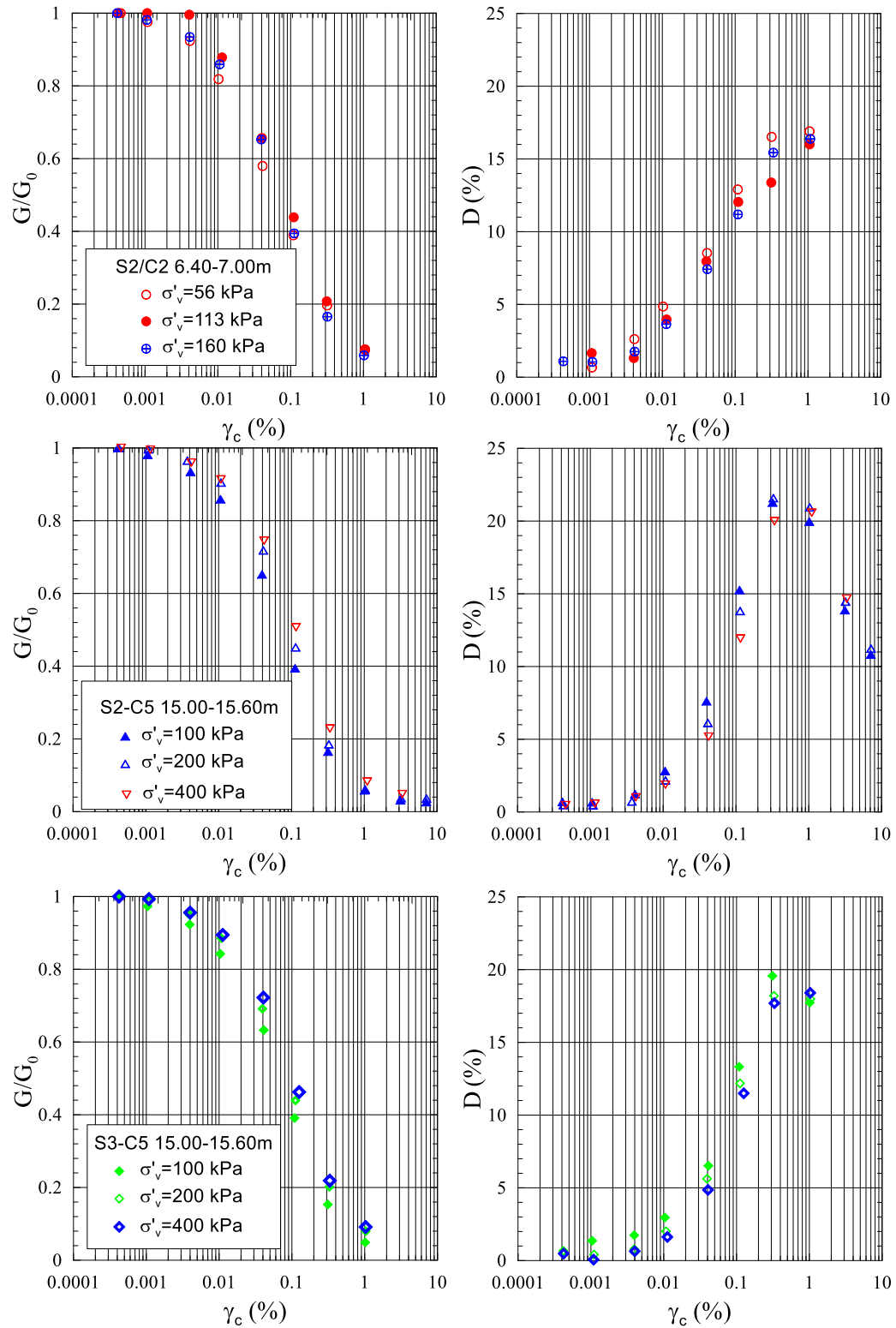
Sondaggio	Campione	Prof. (m)	Tipo di materiale/ Strato di appartenenza	Stato materiale	Provino	Metodo di ricostituzione	$\sigma_{vo}$ (kPa)	D <sub>r</sub> (%)	Rapporto tensionale ciclico (CSR)
1	2	6.20-6.80	Sabbia con limo	Indisturbato	1	-	130	-	0.20
					2	-	130	-	0.20
					4	-	130	-	0.17
					5	-	130	-	0.25
					6	-	130	-	0.26
					1	4	13.50-14.00	Sabbia medio-fine pulita 7 unità sabbiosa profonda	Ricostituito
					4		100	65	0.16
					5		100	63	0.13
					6		100	60	0.23
4	3	10.00-10.60	Sabbia fine con limo	Indisturbato	1	-	150	-	0.17
					2	-	150	-	0.20
					4	-	150	-	0.13
					5	-	150	-	0.24
					5	2	6.00-6.60	Limo sabbioso	Indisturbato
					4	-	100	-	0.21
					5	-	100	-	0.17
					6	-	100	-	0.23





Sondaggio/Campione	Profondità (m)	$\sigma'_v$ (kPa)	$\gamma$ (%)
S2-C2	6,40-7,00	56	0,0005-1,05
		113	0,0004-1,05
		160	0,0004-1,08
S2-C5	15,00-15,60	100	0,0004-7,13
		200	0,0004-7,13
		400	0,0005-3,33
S3-C5	15,00-15,60	100	0,0004-1,02
		200	0,0004-3,13
		400	0,0005-3,16
S3-C7	40,00-40,50	180	0,0005-1,05
		360	0,0005-1,08
S5-C5	9,00-9,60	70	0,0005-1,09
		115	0,0005-1,10
		200	0,0005-1,10





## **CHAPTER 7**

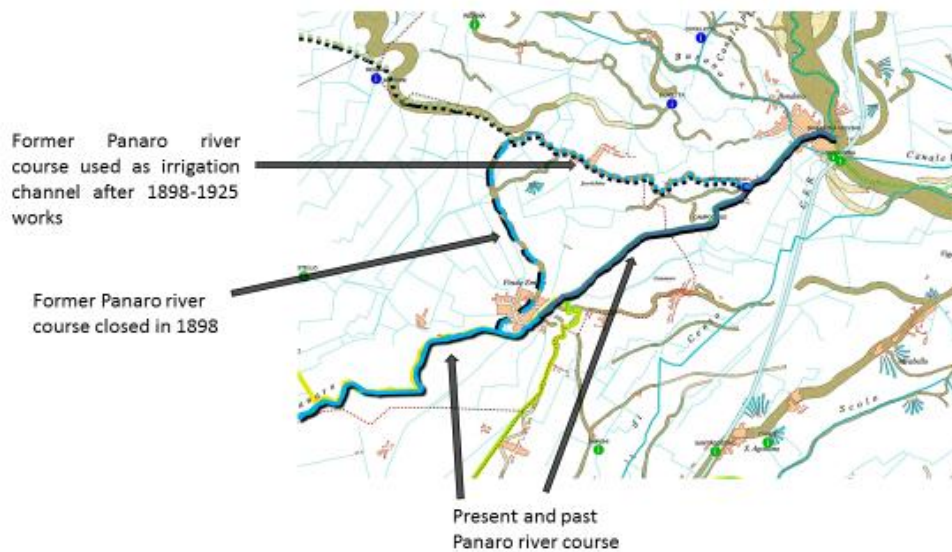
# **Scortichino case study – liquefaction evaluation based on in situ tests**

### **7.1 Preliminary evaluation of liquefaction susceptibility based on historical and geological criterion**

#### **7.1.1 History of Canale Diversivo and of the surrounding areas**

The study area involves part of what is now called “Canale Diversivo di Burana” and is part of the channels net that collects rain water in the northern part of Modena Province. The channel net has been improved and developed from the middle age till nowadays in order to reduce the flood risks and to improve the water drainage especially in the area between Bondeno and Mirandola, which was mainly occupied by swamps till the XIX century. It is relevant to note that, before being reclaimed, this area was a net of channels connected with Po river, with a various depositional environment with swamps and sandy and silty deposits. The present channel net, reorganized and regulated, is managed by Consorzio di Burana, which provides in summer The channels are also used for irrigation of cultivated fields in summer.

---



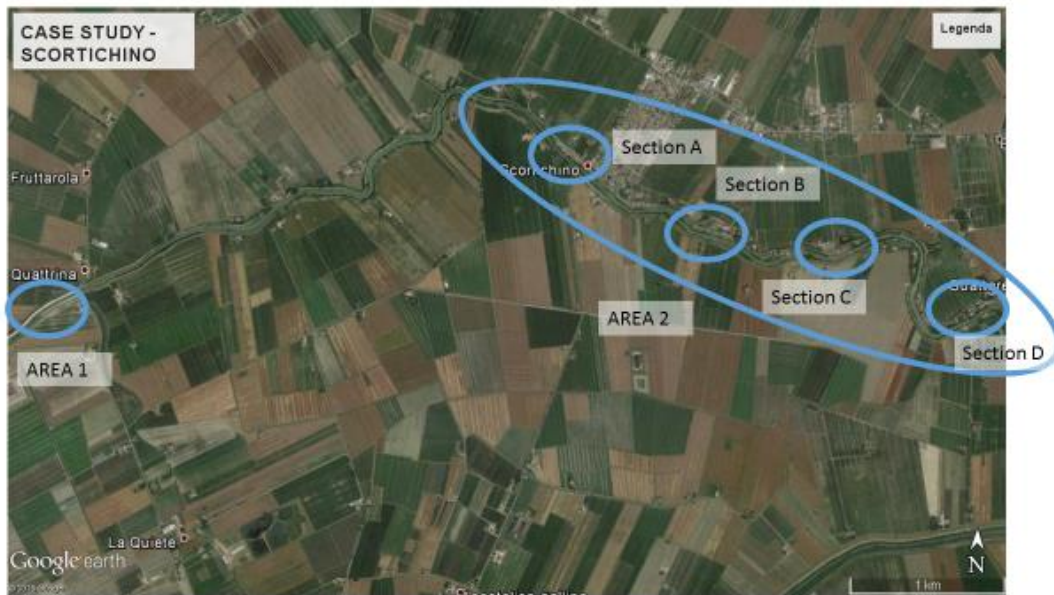
For what specifically concerns the part of Canale Diversivo of interest for this study, the historical aspects are a bit more complex and more critical under the point of view of soil liquefaction. Until the end of the XIX century, the Panaro river was dividing in two parts immediately before Finale Emilia. One part was flowing in north-east direction, reaching Bondeno and after it merging with Po river. The second branch was flowing through the centre of Finale Emilia in north-west direction and after a relevant curve reaching Bondeno and merging again with the other branch. This second branch was called “Ramo della lunga di Panaro” and was source of many problems, due to frequent flooding of the village and of the surrounding areas. For this reason the Duke Francesco IV gave start to an important improvement of hydraulic structures. Among this works the “Ramo della lunga di Panaro” was partly closed and all the waters carried by Panaro river were forced along the branch going straight to Bondeno in north-east direction. The part of the branch going through the centre of the village was completely closed till the village called Quattrina. The part of the branch from Quattrina to Bondeno was instead maintained active and connected to other channels in order to create a net able to drain pluvial water in rainy season and provide irrigation during summer. Thus “Canale Diversivo” between Quattrina and Bondeno is flowing inside the old Panaro river bed and the embankments are still those of Panaro river in XIX century, with some small changes. This aspect is particularly important to the purpose of this study. In fact it comes out from the historical reconstruction, and it is confirmed by geological maps available, that the area of interest has experienced river deposition, leading to the formation of loose sandy and silty layers.



### 7.1.2 Cracks map

The first preliminary field survey was performed by “Gruppo di Lavoro AGI” in June 2012, a few weeks after the main seismic event. In October 2012 a second and more detailed field reconnaissance trip took place. A series of cracks was reported along the top of the embankment of “Canale Diversivo”. The reconnaissance activity has been focused on the places above the channel embankment occupied by houses. There are in fact on the top of the embankment some small groups of houses that were built on floodplains or on meanders of the former Panaro river. The fact that, after the closure of the “Ramo della lunga di Panaro”, the remaining part from Quattrina to Bondeno was a channel with regulation of the water level, has encouraged the urbanization of part of the river embankment. All the buildings are located on the left side of the embankment, close to Scortichino centre, along a section approximately 2 km long. In order to understand which mechanism has caused the damages observed on the embankment body and on the building located on the top of it, it is extremely important to perform critical and thoughtful study of the damages and cracks itself.





Starting from the pictures taken during the first and the second reconnaissance field trip it is possible to identify a series of cracks located on the top of the embankment with orientation approximately parallel to the channel path. In some sections, usually those where the embankment is wider, there are more than one parallel fissures. The fissures are accompanied by lateral movements of the embankment body. The width of the fissure is .... and the lateral movements can vary from some cm to ... In some specific point the lateral movement is more relevant and shows a partial detachment of part of the embankment.

On the building damages have been observed too. In particular, there are important cracks affecting some of the buildings. The creation of cracks maps makes quite clear that the cracks on the buildings are associated to the fissures on the ground. It appears evident that the building damages is related to and caused by the movements occurred inside the embankment body. The movement appear to be a lateral deformation on both sides, towards the channel and towards the field. From the surficial observation has not been possible though to understand if the deformations are related to a phenomenon occurred inside the embankment body or inside the layers underneath it. It is important to note that only in one point out of the urbanized zones those kind of fissures have been observed. This point has been named AREA A (figure....). This can be due to the fact that most of the attention has been focused on damages on buildings, also considering that the fissures width is in some points very modest. The absence of a complete survey of all the channel section from Quattrina to Bondeno doesn't allow to state that only the urbanized parts of the embankment in the surroundings of

Scortichino have been affected by this damage pattern. Anyway, no complete collapses has been observed.

For what concerns the right embankment, no damage has been reported. On this side no buildings are present. It is important anyway to note, comparing figure.... and figure..... that probably the right side has been in the past history of the river less affected by sediment deposition, which was instead a more relevant aspect on the left side.

There are no detailed topographic surveys that allow to compare the geometry of the embankment before and after the event and consequently it is not possible to evaluate accurately the deformations occurred. The only evaluation of the deformations can be done considering the cracks width which varies from a few centimetres to some tens of centimetres in the worst situation (fig.....).



On the field close to section C some cracks have been observed, oriented perpendicularly to the embankment direction.

---





The last important element to consider is the eventual ejection of sandy material from the fissures formed in the soil, both on the top of the embankment and on the ground field. Some sand ejecta have been certainly observed in the cracks located on the field outside the channel, close to section C. Despite the first survey was performed some weeks after the event it has been possible to recognize sand ejecta. For what concerns the fissures on the top of the embankment there are no sure reports about sand ejecta. Apparently, from local inhabitants attestation, some sand ejecta were observed along the fissure present in section B.





## 7.2 Liquefaction potential computation based on in situ tests

### 7.2.1 Choice of input parameters

Considering the Seed&Idriss procedure, and using the three of the most used simplified methods, liquefaction analysis have been performed for different sections. The methods adopted are I&B2014, NCEER (Robertson&Wride 1996) and Andrus&Stokoe 2001. All the methods considered in this section are based on in situ tests: the first two methods are based on CPTU tests and the last one are based on SDMT tests. For all the tests available the liquefaction analysis have been performed using all the formentioned methods.

The analysis has been developed using the CLiq software.

During the field test campaign 12 CPTU and 4 SDMT tests have been performed. The analysis with the above mentioned methods have been performed for each test. In addition to the values directly provided by the in situ tests, there are other parameters that are needed to perform the analysis with each method. Not all the parameters are

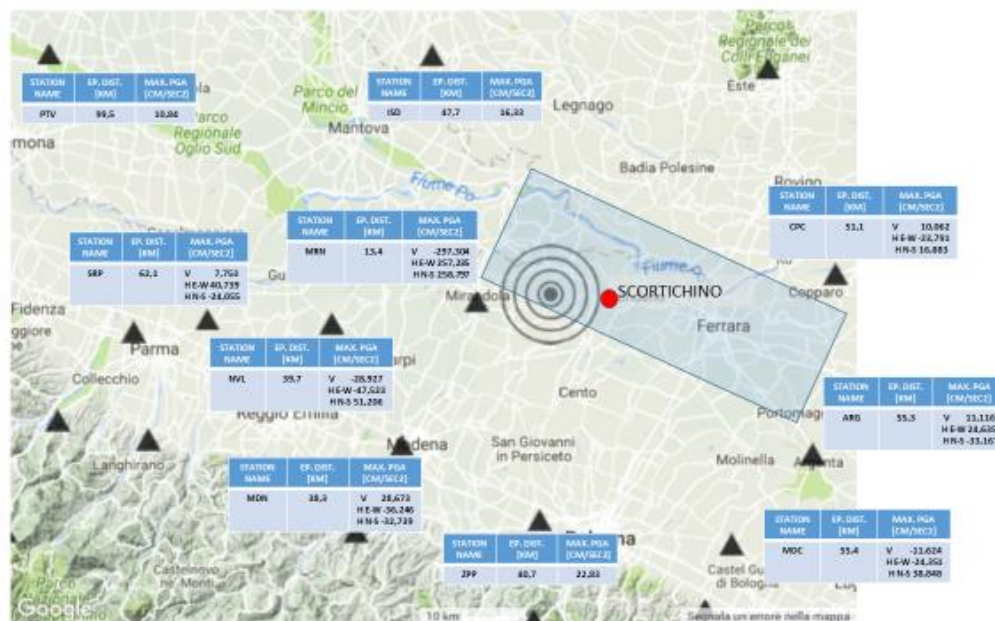


uniquely defined, and in particular there is some concern in defining the ground motion input, the water table level and the fine content.

### 7.2.1.1 Ground motion

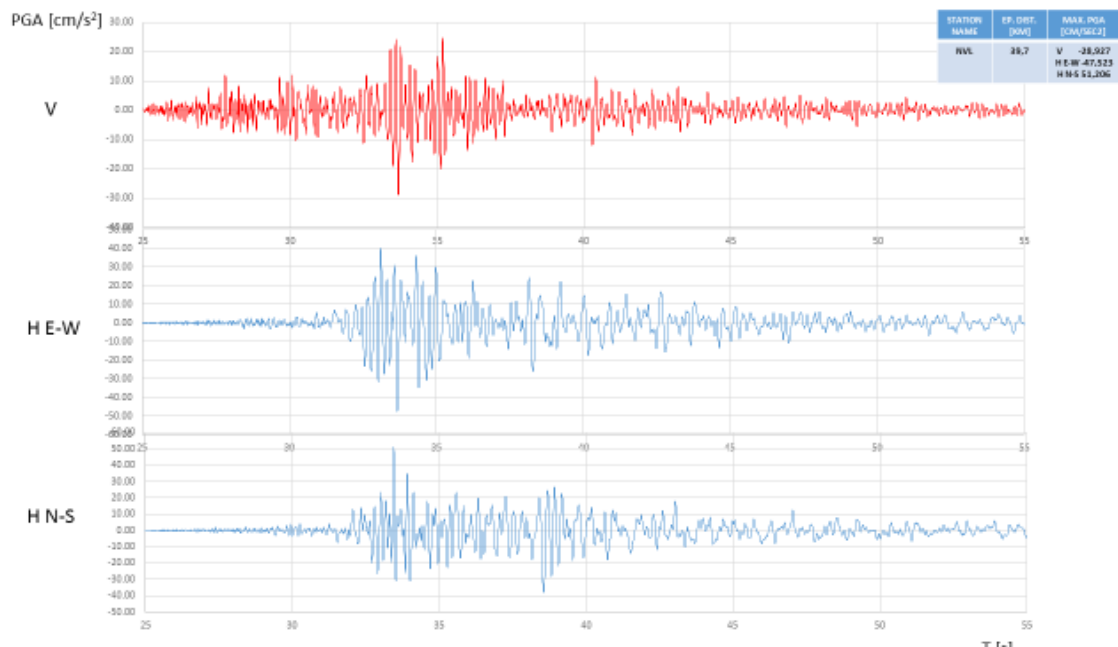
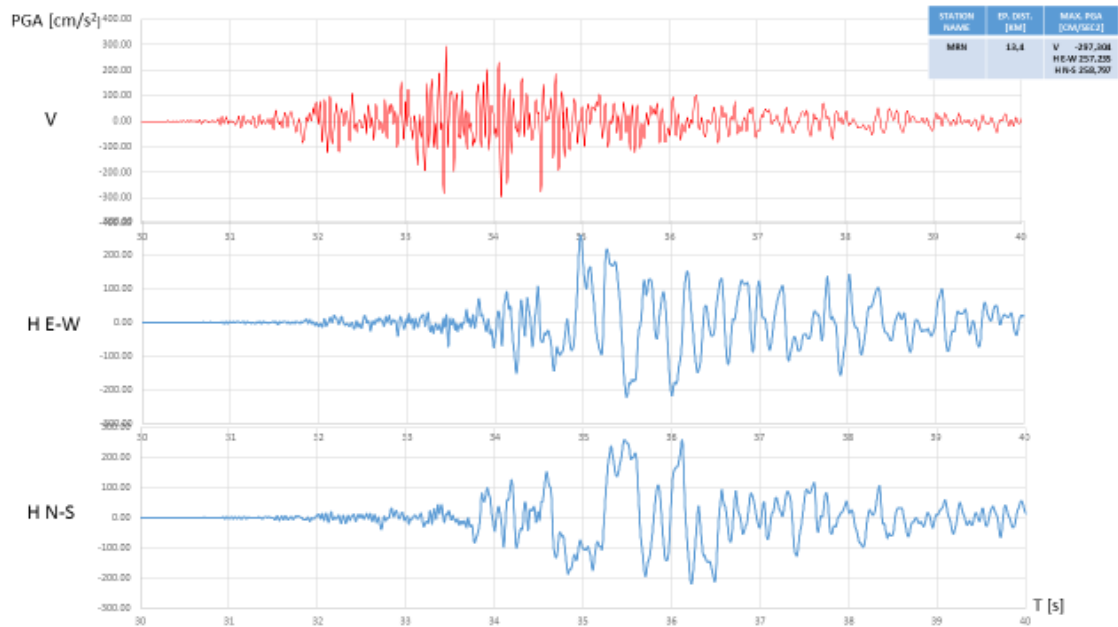
The simplified Seed&Idriss method requires to know the magnitude of the event and the maximum peak ground acceleration in horizontal direction. This is needed in order to calculate CSR, that is the earthquake load applied to the soil profile in the considered point.

For the event considered in this study, that is the main shock of the 20<sup>th</sup> of May 2012 the magnitude is known and in the analysis the value of 6.14 has been used. Unfortunately there are no records for the PGA values close to Scortichino site. The national ground motion station net for the region of interest is reported in figure....



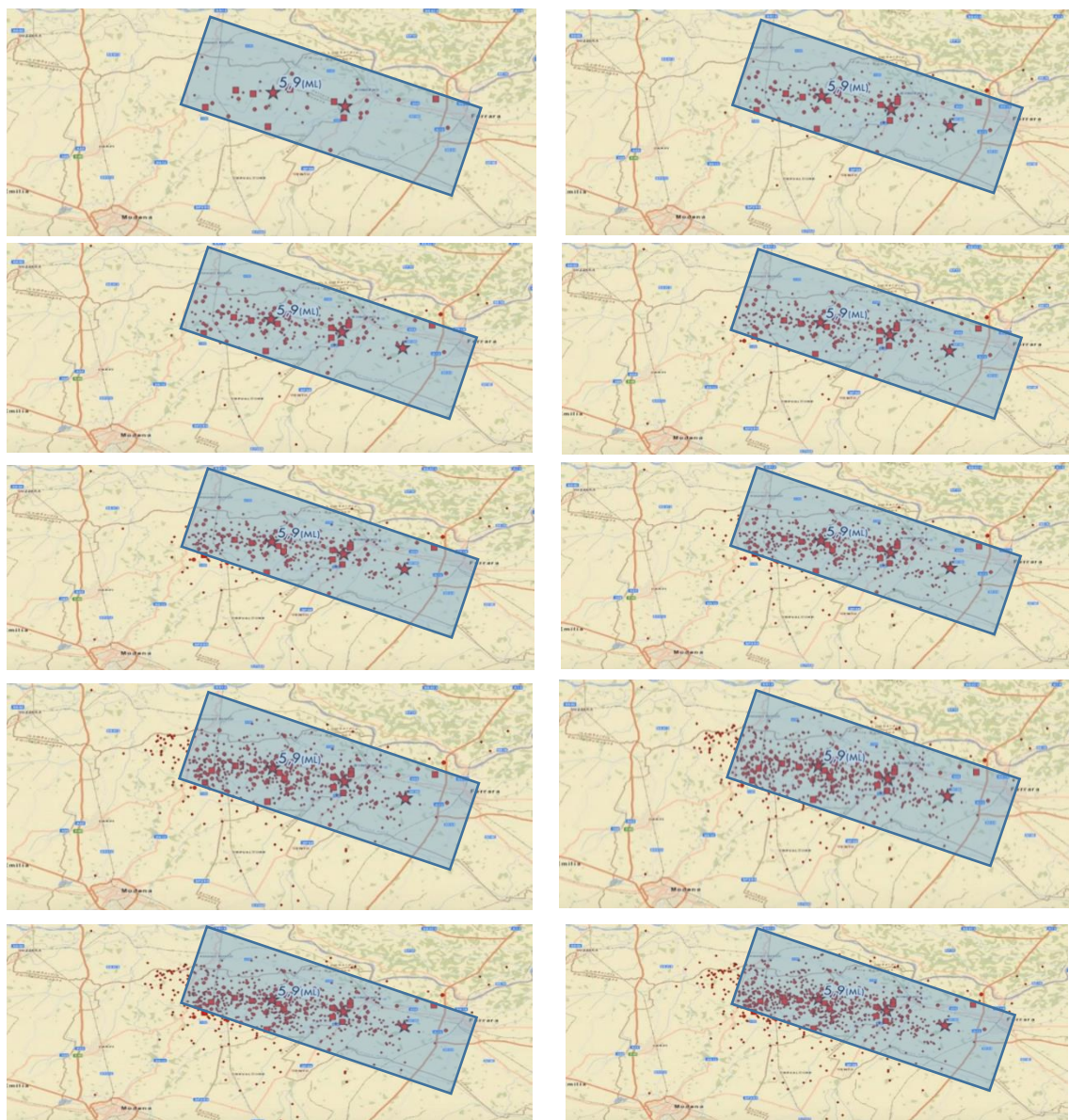
Considering the map where the epicentre, the study site and all the ground motion stations of the national net are indicated, it appears clear that the epicentre is quite close to Scortichino site (less than 10 km) and the closest ground motion station is the one located in Mirandola (MRN) placed at more or less 15 km from Scortichino. It is also evident that the epicentre lies between Mirandola ground motion station and the study site, approximately at the same distance. The location of the fault plane generating the seismic event has been indicated in the figure as well. There are no stations available east north and south from Scortichino that are at a similar distance to the one of Mirandola. Copparo (CPC), Argenta (ARG), Zola Predosa (ZPP) and Isola della Scala (ISD) are all located around 50 km from the epicentre. It is not easy to obtain in a simplified

way a reasonable PGA value for Scortichino site. The values recorded in Mirandola are surely the most useful.

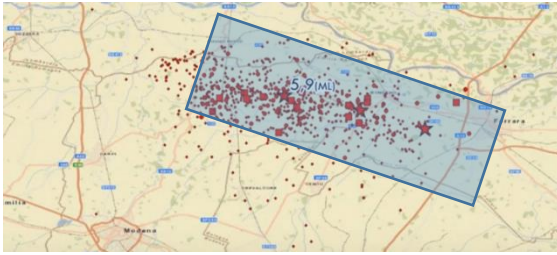


In order to obtain proper PGA values a site response analysis should be performed. In this preliminary phase anyway, an attempt to derive a reliable value of PGA with simple deductions will be considered, with the awareness that the uncertainties and the

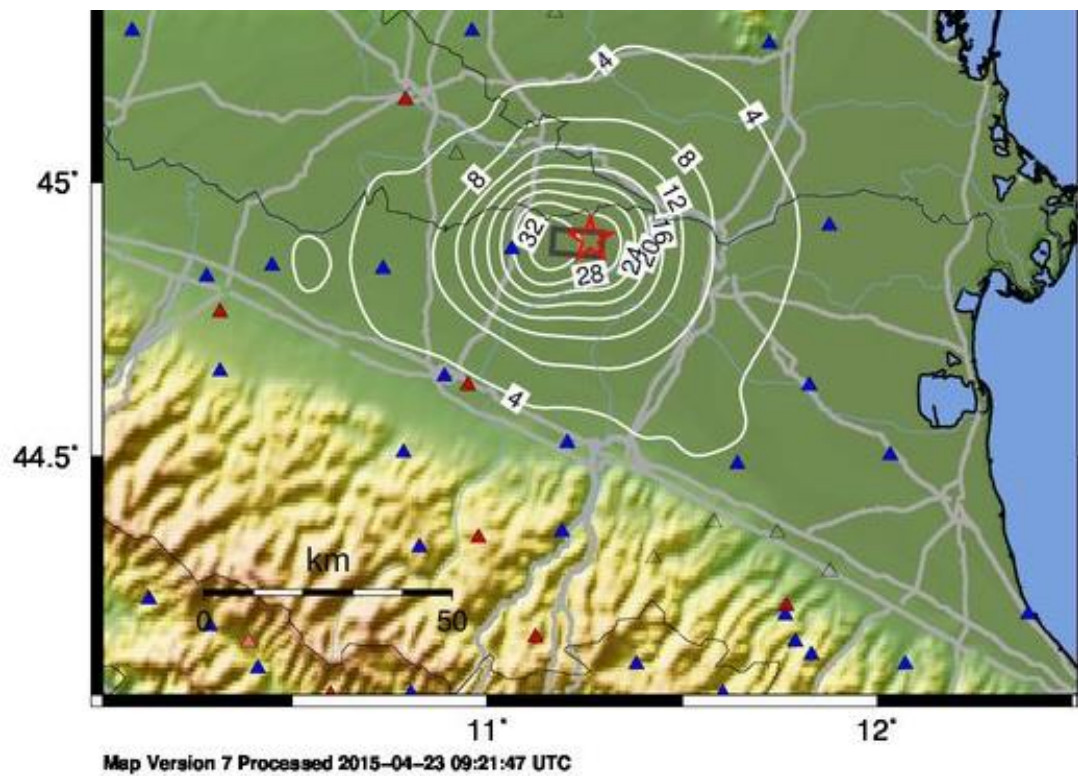
approximations inherent in deductions are not larger than those inherent in the simplified methods in which the values will be used. Some considerations can however be made in order to obtain a more realistic estimation of PGA. Considering that the ground motion can be strongly dependent on the rupture direction, it is useful to evaluate the location of the aftershocks epicentres and their time history. In figure ... the epicentre time history that considers all the aftershocks of the 2 main events (20<sup>th</sup> and 29<sup>th</sup> of May) divided for each day, until around a week after the second event, is shown. It appears clearly that the area interested by the shaking is mainly east-west oriented, and that the epicentres move constantly from east to west during the period where most of the aftershock have occurred. This is consistent with the fault structure known as "Pieghe Ferraresi".



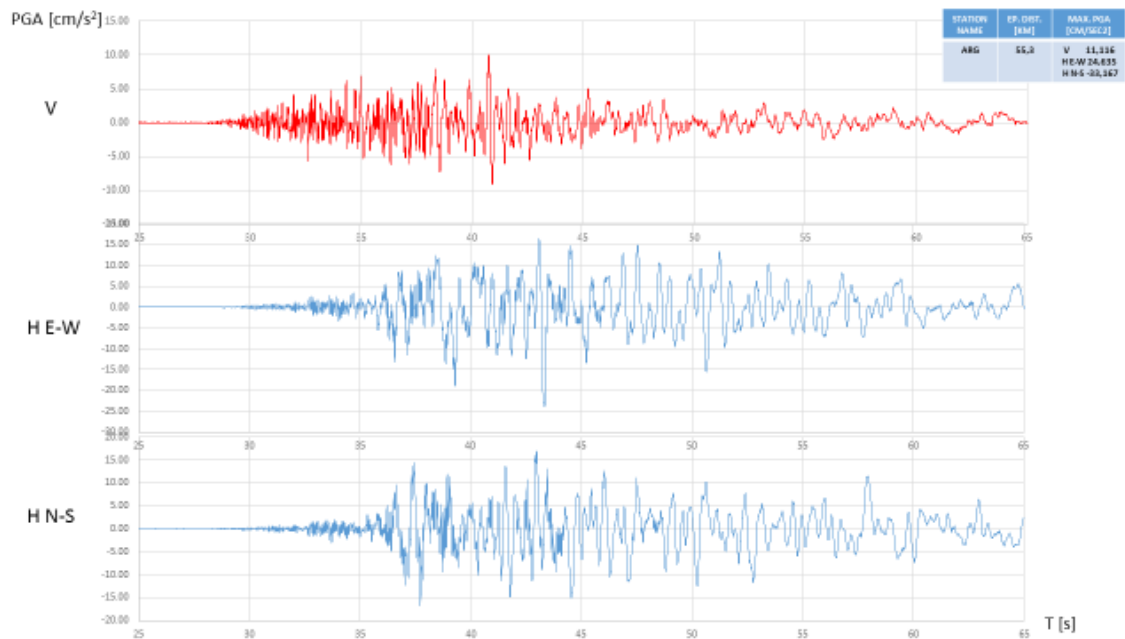




Considering that the distance between Mirandola station and the epicentre is slightly bigger than the distance between the epicentre and Scortichino it can be assumed that considering as PGA value for Scortichino the one recorded at Mirandola ground motion station is quite conservative. Respect to the epicentre Mirandola record station is located westwards and Scortichino is located eastwards and they are somehow in the east-west direction that is the one where most of the aftershocks are located. A confirmation of the considerations here expressed comes from the shake map realized by INGV (figura...). A value that appears to be reliable, considering the position of Scortichino (figura...), might be 0,29 g. In paragraph .... a sensitivity analysis to check how a slight variation of PGA values can affect the liquefaction susceptibility of the site has been performed.







### 7.2.1.2 Water table level

Another key element for the liquefaction analysis response is the depth of the water table. As described in detail in chapters 1 and 2, the presence of the water table is one of the fundamental elements that can make a specific soil profile liquefiable or not. A big attention has been paid to define the water table level at Scortichino site. In particular the elements considered in order to obtain a reliable value are:

- Water level in the channel
- Water level in an existing well
- Water level measured from piezometers
- Water level derived from in situ tests

Part of the values mentioned above were not available referred to the day of the event: the piezometers and the in situ tests had in fact been performed months later; for what concerns the measurements of the channel level and of the water level into the well, the first were performed time after the event. The information that probably can give the most precise value is the measurement of the water channel level. In fact the channel level is artificially controlled and kept approximately constant; the authority delegate to manage the channel informed that..... during the..... After the earthquake, when the “Gruppo di Lavoro AGI” started its work a measurement of the channel level has been performed at different sections of the study area. The

measurement was carried out with a good level of detail and was included in the topographical survey.

It is important to note that the water table level is not constant in the study area, since there is a gentle slope that, considering the area about 2 km long, the channel level has a difference of about .....

Once the channel measurements have been clarified, some considerations about the water table system in the site need to be done. Based on the field tests (CPTU and coring) and on the geological information about the area which is quite well-known and has a stratigraphic profile which is in principle rather uniform, there is a confined aquifer in Unit A, known as "acquifero Padano". Unit C, the clayey layer placed above Unit A, is confining the aquifer. There is then no doubt about the fact that inside Unit A water table is constantly present. A more sophisticated analysis should instead take into account that the aquifer is confined and for that reason in Unit A the water pressure has an excess respect to the hydrostatic values. In this chapter the confinement effects will not be taken into account.

For what concerns the water table inside Units B and Ar, it is more difficult to detect the exact water level. Unit A and Unit B are divided by an impermeable layer (Unit C) which extends also under the channel and on the field side (figure....). This element might imply that there are 2 different water tables in the site: a confined one, referred to Unit A and a phreatic one referred to the surficial layers B and Ar. The surficial water table involves both layers since there is no impermeable separation between them and actually Unit B and Ar are often overlying and interconnected. The well located on the top of the embankment close to section D (figure ...) has a depth of .... m, which means that it is connected to the surficial water table. The level measured is around .....

Considering the stratigraphy and the water level measured inside the well and on the channel, it can be inferred that the surficial water table is connected to the channel which is somehow determining its level (fig. ....). A gross evaluation of the water table level can thus be performed considering the above mentioned measurements, that need to be interpolated in order to obtain a value for each of the study sections that are, as pointed out before, located along an area 2 km long with a gentle inclination. Focusing on section C, which is the one mainly considered in this study, a reasonable value for the water table depth of ..... has been derived interpolating the ..... And .....

While a gross value of the water table has been identified, there is some uncertainty in obtaining a precise value. In fact small seasonal variations, which are allowed, and the water table surface inside the river embankment that might be not strictly horizontal at the same channel level (Figure ...) let a variation from some tens of cm up to 1 m being considered realistic. This aspect is not of small importance, considering that the soil at that depth might have a composition critical for soil liquefaction, if there is full

---

saturation. For this reason, starting from the value assumed (...) a second analysis with change in the water table depth has been performed, in order to evaluate how the soil place close to the water table surface can be affected by water presence and in general how a liquefaction susceptibility analysis can be inferred by a small change of 1 m in the water table depth. The value assumed to perform the main analysis, is a value that according to the author was not in excess during the event, with a good level of certainty. The sensitivity analysis will consider instead a water table level 1 m higher (...) which is a scenary that cannot be considered certain but possible in reference to the seismic event studied and it can provide as well some considerations for future events where slightly different considitions might be taken into account.

#### 7.2.1.3 Fine content

As described in detail in paragraph ..... the method proposed by Boulanger and Idriss (2014) and that will be used in the next paragraph for a liquefaction susceptibility analysis is strongly dependent on the fine content. In the method there is a formulation that allows to derive the FC (fine content, considered as the percentage passing the N° 200 AASHTO (0.075 mm) sieve) from the CPTU values. There is also the possibility, when data are available, to use a FC content defined by the user.

The samples taken at each section during the in situ tests campaign might suggest that FC derived from the tests can be used. Though, a scrupolous evaluation of the data shows that care must be use in order to choose proper values. The samples in fact show a significant variability in fine content in Unit Ar and B, especially if this information is combined with plasticity.

Some key elements need to be considered: first, Boulanger and Idriss (2014) method is dependent on fine content; second, soils with high fine content can be liquefiable only if they have low plasticity (< 5-8%) while this doesn't apply to soils with low fine content which can be in general liquefiable; third, in Scortichino there is a high variability in Ar and B units as it appears from the CPTU profiles. The samples analysed show in some cases soil with high fine content (>80%) and low plasticity (<8%), in other cases soil with high fine content and plasticity around.... and in other cases soils with low fine content. In order to apply Boulanger and Idriss (2014) method using a fine content defined by the user, it is necessary to assign a fine content for the all soil profile referred to a specific CPTU used for each of the analysis. Considered that it is not possible to assing a specific and different FC value for each single point of the CPTU, Units Ar and B have been divided into sublayers to which the same value of FC has been assigned. The criterion used to assign the same FC content is based on the Ic values obtained from the CPTU. Starting from the samples available for each coring, even in different sections, the FC have been considered and assigned to the layers at the same depth of the CPTU

---

performed in the same location of the coring. Then, for CPTU located at some distance from the coring, comparing the  $I_c$  values, the correspondent FC values obtained on other sections has been assigned. This procedure is considered reasonable since the soil is not homogeneous horizontally and vertically in Units Ar and B due to the fact that the embankment is made of a combination of depositional and manmade material, but the difference is not in the soil composition which is the same, but in the distribution and in the layering of the material itself. In other words a same kind of soil, identified by a certain  $I_c$ , can be found along the site sections at different depth and with different thickness, but the material itself is the same found in the other sections and for that reason the FC values, obtained from coring in other sections, can be used with reasonable accuracy. The procedure here explained has allowed to obtain enough values to define the fine content along all the CPTU profile, especially for what concerns Units Ar and B. For Units A and C the problem is much easier and less questionable, since those Units are far homogeneous and there is no variability in FC inside the units. However, analysis using FC obtained with the formulation suggested by Boulanger and Idriss (2014) has been performed as well, in order to evaluate how the procedure here defined might have affected the results and at which size.

### **7.2.2 NCEER method (Robertson and Wride 1998 – Youd et al. 2001)**

Analysis n°: 3 – method: NCEER (Youd et al. 2001)

Ground motion input: PGA 0,29g Mw= 6,1

water table (m from 0 level of each test):

CPTU7 6,80

CPTU9 6,90

Advanced parameters:

average results interval 1

cone area ratio 0,58

limit analysis at depth 20,00

auto unit weight calculation (yes)

default unit weight 19,00

calculate dry settlement NO

use factor 2 in dry settlement (yes)

use custom CSR data NO

weighting factor for  $e_v$  NO

aging factor for CRR NO

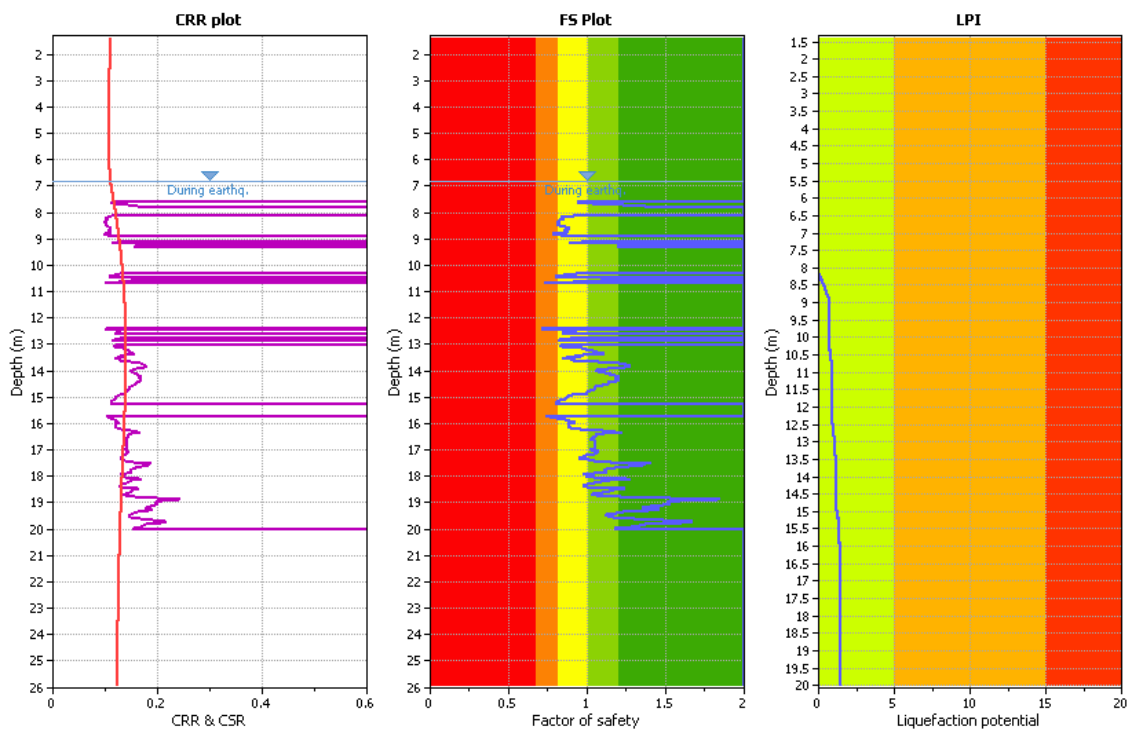
PL based volumetric strain NO

---

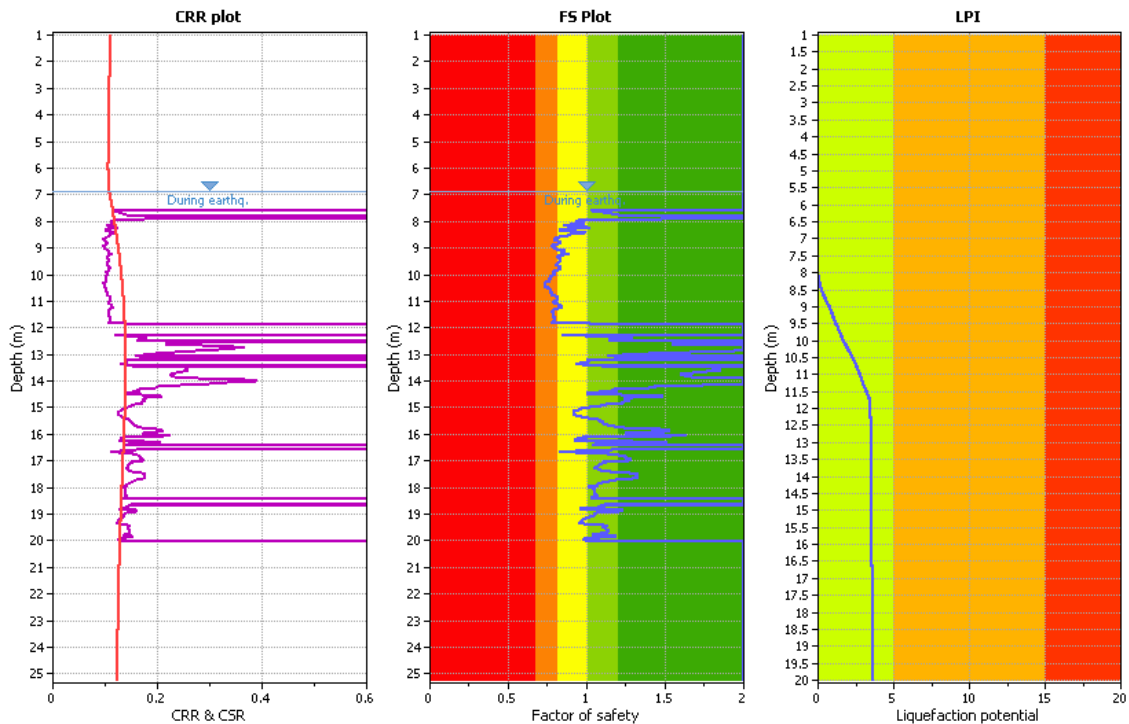
apply  $K(\sigma)$  correction (yes)  
 auto transition layer detection NO  
 remove loose sand criteria NO  
 $I_c$  cutoff value 2,7  
 $C_n$  limit value 1,70  
 user FS 1,00  
 weighting depth limit 18,00  
 $N_{kt}$  14,00  
 $K(\alpha)$  0,90  
 $\Delta I_c$  0,00  
 stress exponent calculation --> based on selected method  
 MSF --> based on selected method

site conditions: same as initial

lateral displacements: level ground



CPTU7



## CPTU9

### 7.2.3 Boulanger & Idriss method (2014)

Analysis n° 4 - method B&I 2014

Ground motion input: PGA 0,29g Mw= 6,1

water table level (m from 0 level of each test):

CPTU7 6,80

CPTU9 6,90

advanced parameters:

average results interval 1

cone area ratio 0,58

limit analysis at depth 20,00

auto unit weight calculation (yes)

default unit weight 19,00

calculate dry settlement NO

use factor 2 in dry settlement (yes)

use custom CSR data NO

weighting factor for ev NO

aging factor for CRR NO

PL based volumetric strain NO

apply K( $\sigma$ ) correction (yes)

---

auto transition layer detection NO

remove loose sand criteria NO

Ic cutoff value 2,7

Cn limit value 1,70

user FS 1,00

weighting depth limit 18,00

Nkt 14,00

K(alfa) 0,90

Delta Ic 0,00

stress exponent calculation --> based on selected method

MSF --> based on selected method

site conditions: same as initial

lateral displacements: level ground

FC (quote in m from 0 level of each test)

CPTU7 0-3,50 80%

3,50-5,50 40%

5,50-7,50 72%

7,50-9 40%

9-12,50 87%

12,50-20 10%

CPTU9 0-3,30 80%

3,30-4,80 40%

4,80-8 72%

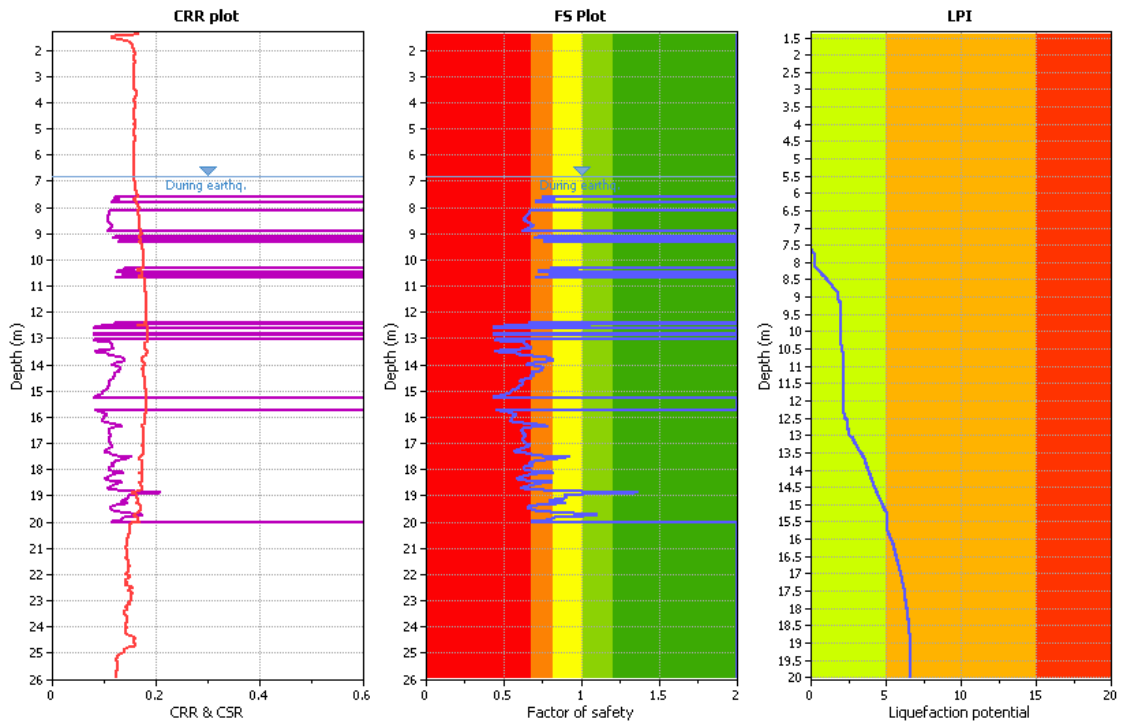
8-12 40%

12-13,50 87%

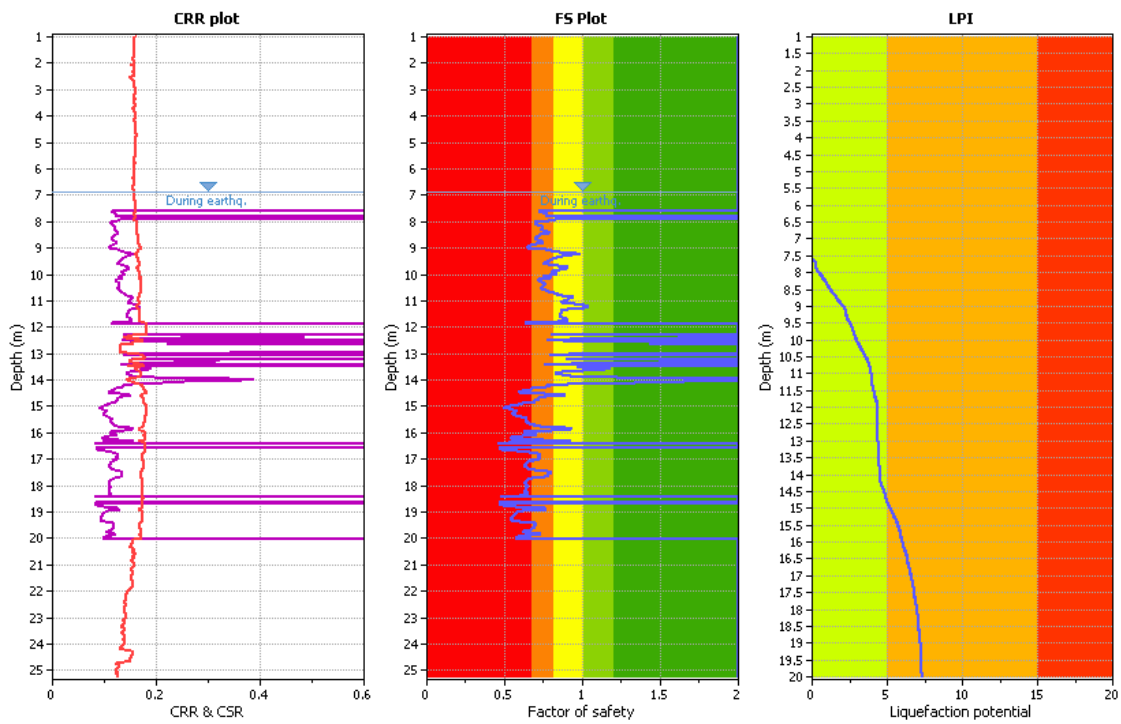
13,50-20 10%

---





**CPTU7**



**CPTU9**

Analysis n° 8 - method B&I 2014

Ground motion input: PGA 0,29g Mw= 6,1

water table level: (m from 0 level of each test)

CPTU7 6,80

CPTU9 6,90

Advanced parameters:

average results interval 1

cone area ratio 0,58

limit analysis at depth 20,00

auto unit weight calculation (yes)

default unit weight 19,00

calculate dry settlement NO

use factor 2 in dry settlement (yes)

use custom CSR data NO

weighting factor for ev NO

aging factor for CRR NO

PL based volumetric strain NO

apply K(sigma) correction (yes)

auto transition layer detection NO

remove loose sand criteria NO

Ic cutoff value 2,7

Cn limit value 1,70

user FS 1,00

weighting depth limit 18,00

Nkt 14,00

K(alfa) 0,90

Delta Ic 0,00

stress exponent calculation --> based on selected method

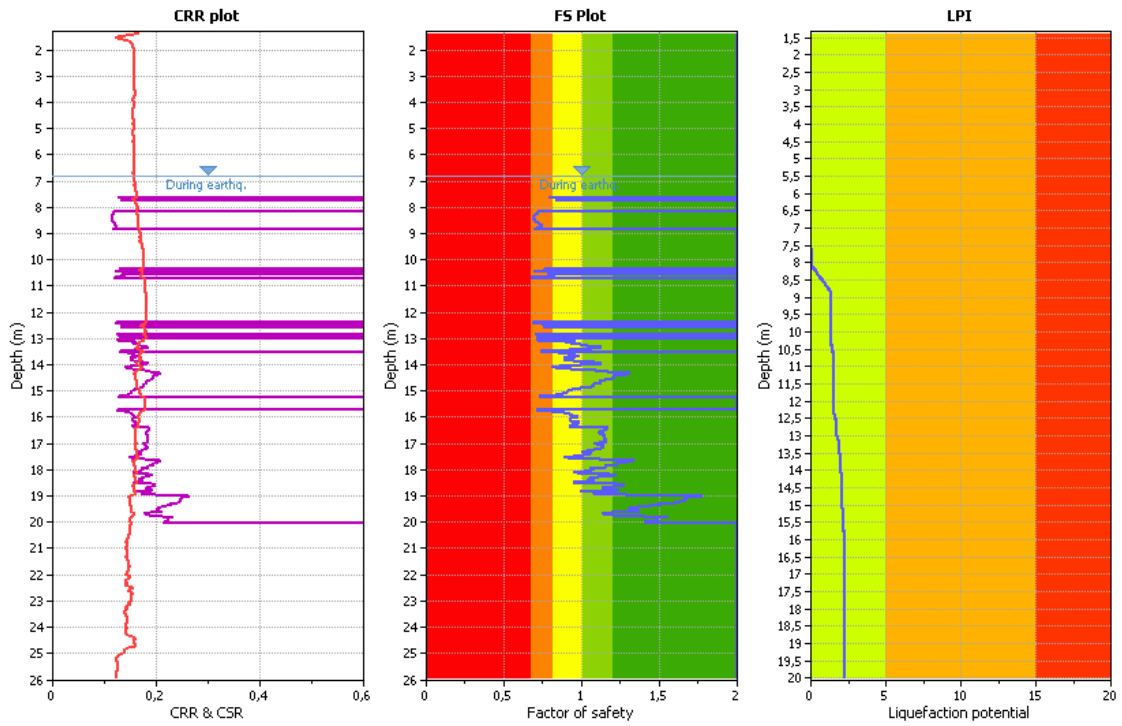
MSF --> based on selected method

site conditions: same as initial

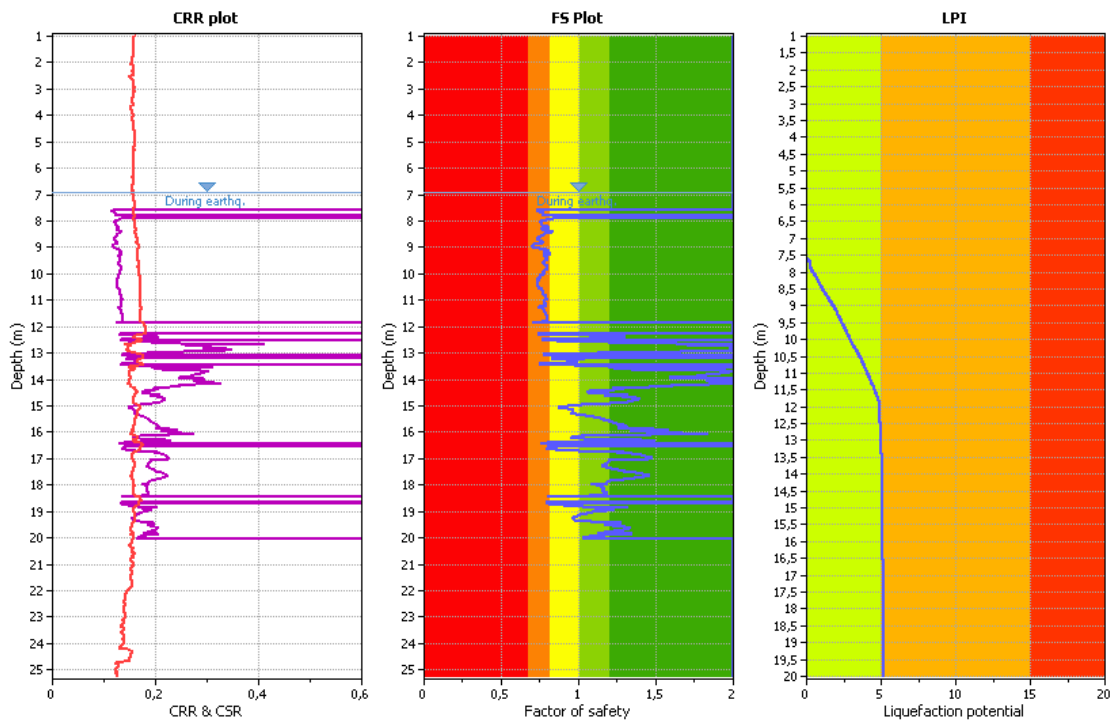
lateral displacements: level ground

FC according Idriss&Boulanger

---



CPTU7 – FC according BI2014

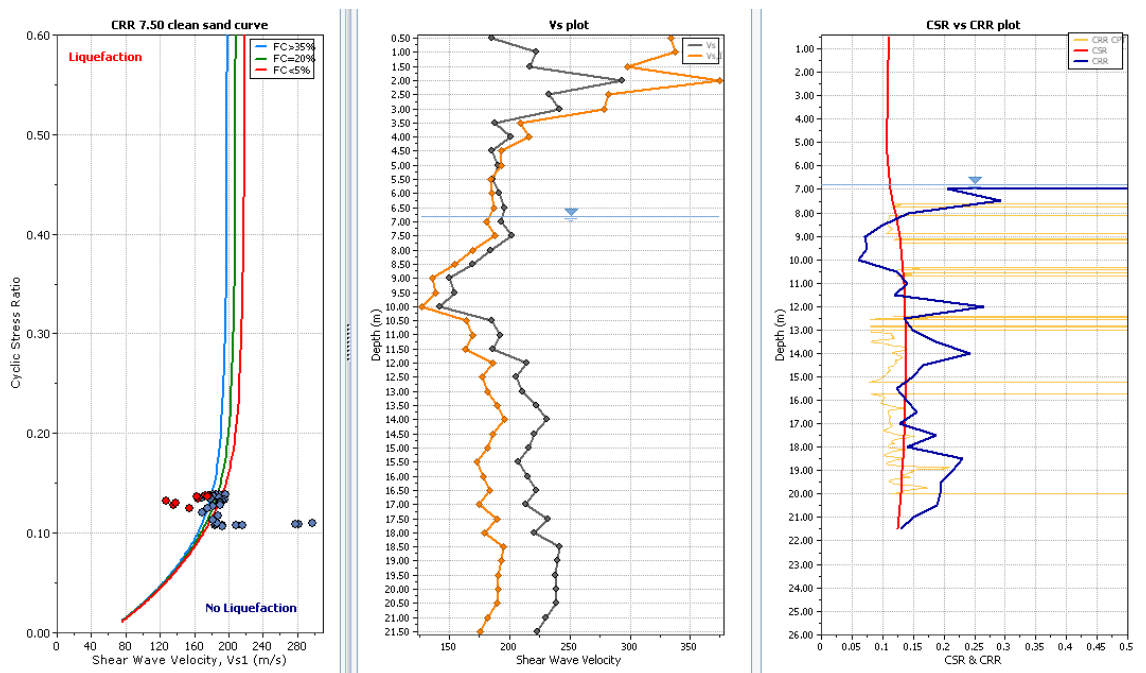


CPTU9 – FC according BI2014

## 7.2.4 Andrus & Stokoe (2000) method

The Andrus and Stokoe method, presented in chapter 2 is used to evaluate liquefaction susceptibility using the  $V_s$  directly measured during the SDMT tests performed. In Figure ... the values obtained by SDMT C (see chapter 6) are plotted. In the right diagram CSR is plotted in red, CRR calculated with Andrus and Stokoe method is plotted in blue and, as comparison CRR calculated with NCEER method for the closest CPTU tests to the SDMT is plotted in yellow.

There is a similarity between the two methods (NCEER and Andrus and Stokoe) in the sense that both show a boundary condition, where CRR is partly and slightly lower than CSR, at least in some layers or sublayers. This is also a main difference: while for the CPTU based method the layer that appears to be more liquefiable is Unit A, for the SDMT based method, Unit B is far more critical. It is relevant to note that, generally, the NCEER method is based on a much richer database and consequently is usually more reliable than Andrus and Stokoe method. Nevertheless, this result points out the importance of performing analysis with different methods, due to the uncertainties of the subject, and for this specific case shows the need of using more advanced tools.

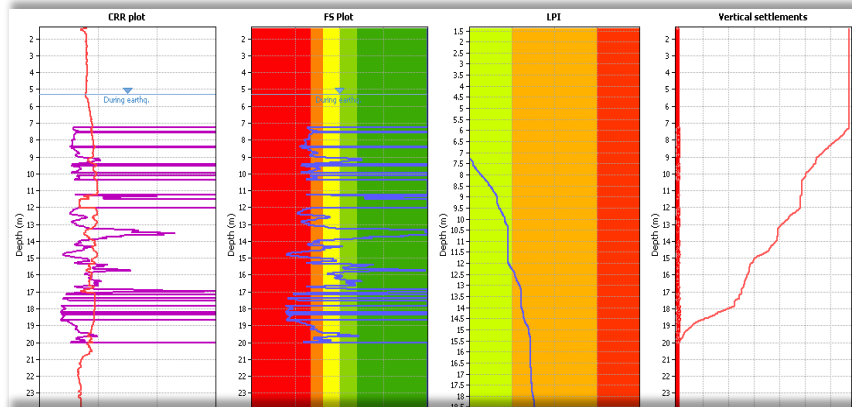


7.2.5 Sensitivity analysis for variation of PGA and water table level...

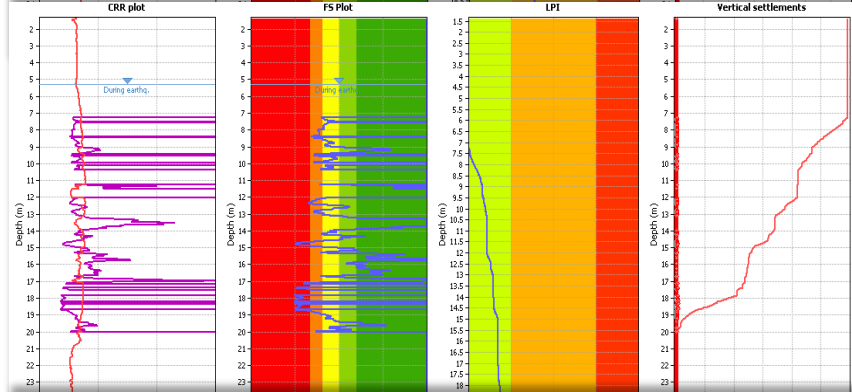
CPTU3

BI14

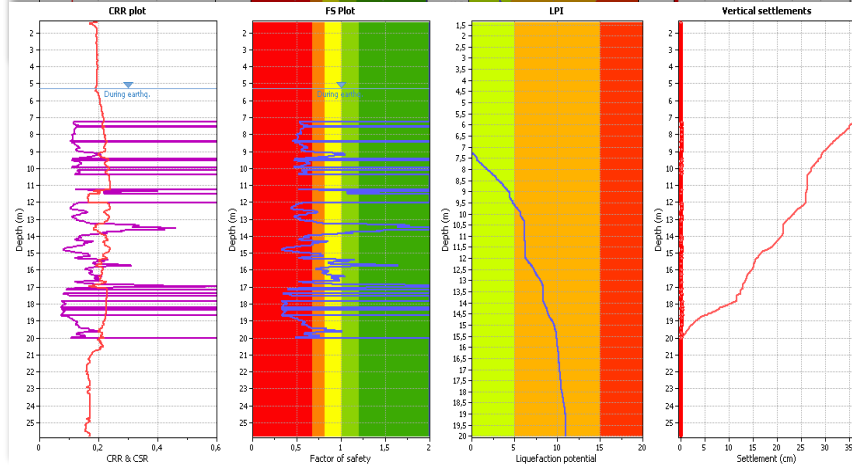
PGA = 0,29 G



PGA = 0,23 G



PGA = 0,35 G



from [m]	to [m]	FC [%]	NOTE
0	4.5	55	
4.5	5.5	78	sample
5.5	6	40	sample
6	8	55	
8	10	40	
10	12	78	

12      20      8      sample-A

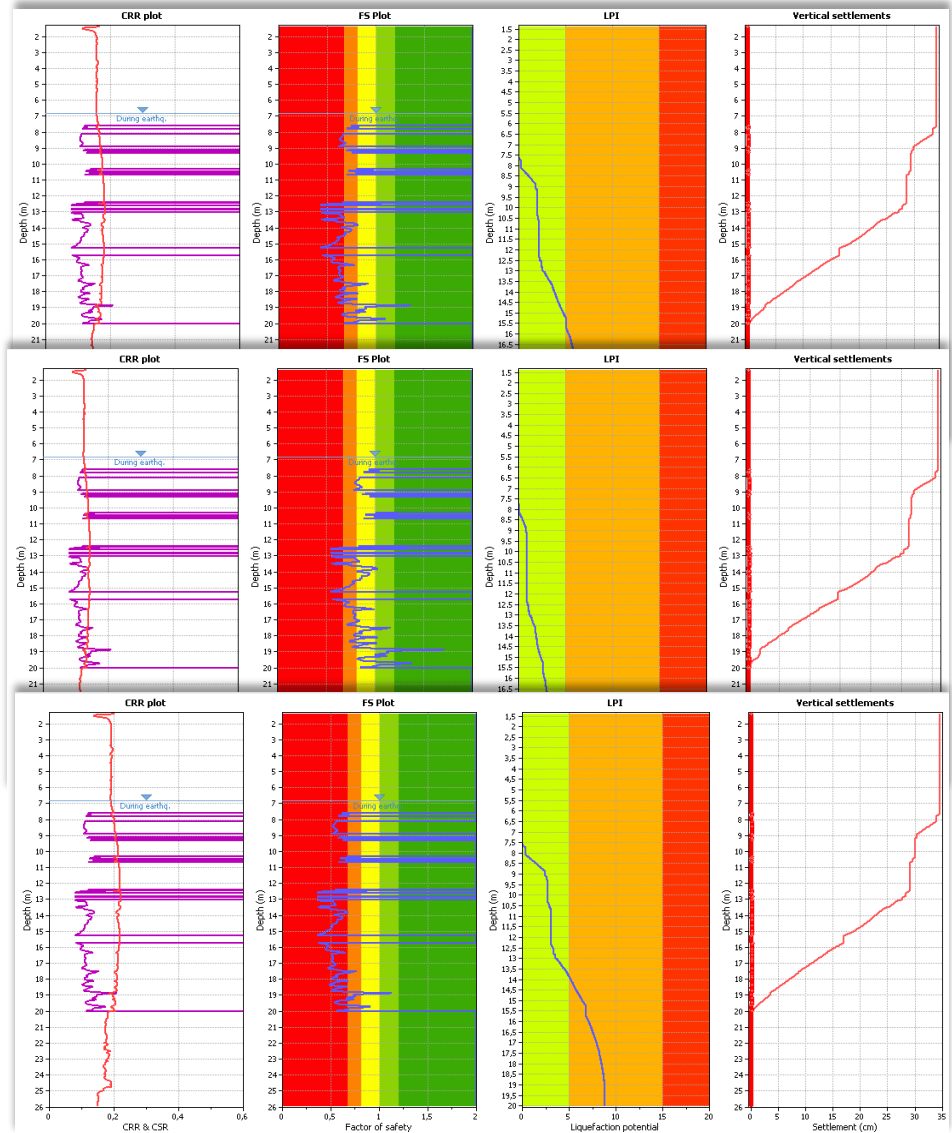
**CPTU7**

BI14

PGA = 0,29 G

PGA = 0,23 G

PGA = 0,35 G



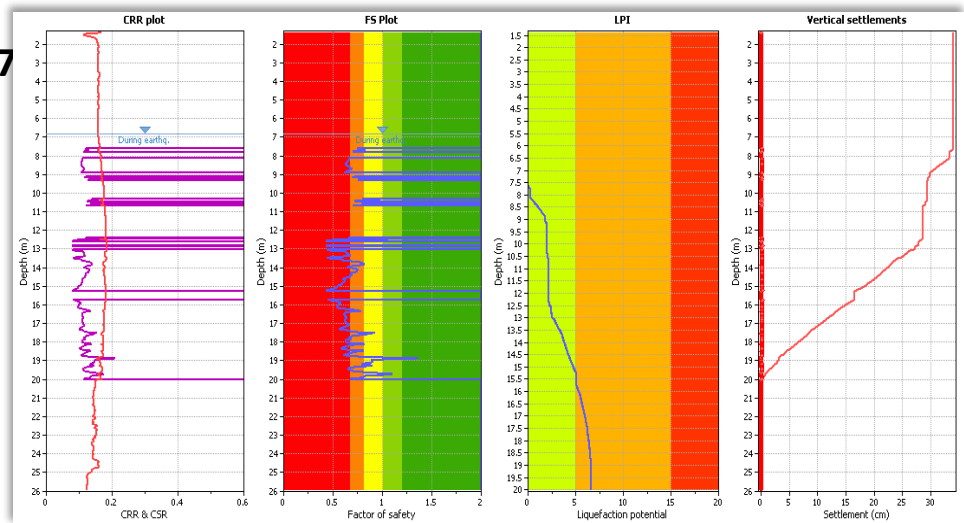
from [m]	to [m]	FC [%]	NOTE
0	3.5	80	sample-A
3.5	5.5	40	
5.5	7.5	72	sample
7.5	9	40	
9	12.5	87	sample-A
12.5	20	10	sample-A

CPTU7

BI14

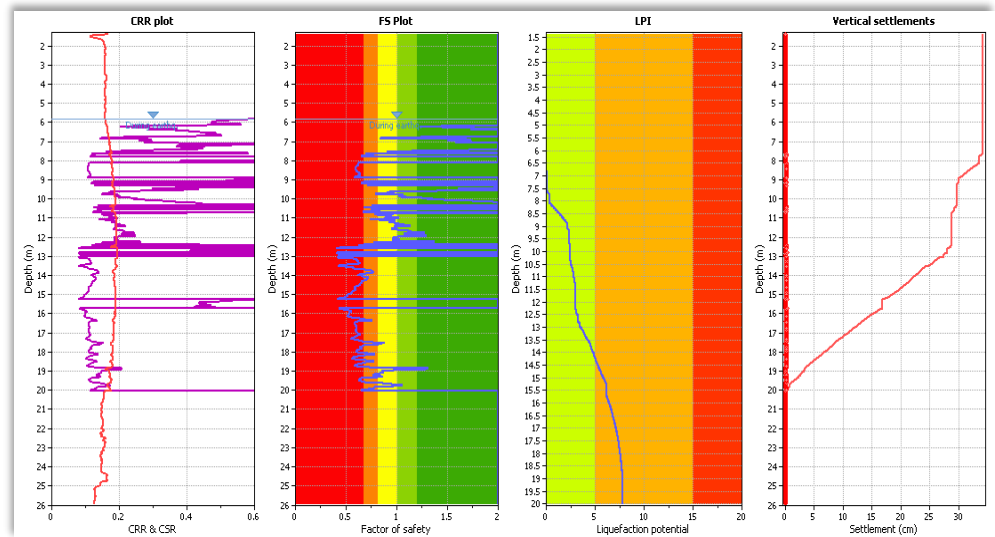
PGA = 0,29

WATER TABLE  
UNCHANGED



PGA = 0,29

WATER TABLE  
INCREASED of 1 m  
AFTERSHOCK  
(including claylike)



from [m]	to [m]	FC [%]	NOTE
0	3.5	80	sample-A
3.5	5.5	40	
5.5	7.5	72	sample
7.5	9	40	
9	12.5	87	sample-A
12.5	20	10	sample-A

### 7.3 Final remarks on simplified methods

Liquefaction susceptibility analysis have been performed using three different methods (NCEER 2001, Boulanger and Idriss 2014, Andrus and Stokoe 2000) through the program



CLiq. The analysis involved all the in-situ tests, that is all the CPTU for the NCEER and Boulanger and Idriss methods and all the SDMT for the Andrus and Stokoe method. In appendix all the analysis performed are reported, while in the previous paragraphs only a representative number had been considered, mainly referred to section C, which is the one of more interest.

The main peculiar aspects for each CPTU or SDMT location are due to the fact that some tests were performed on the top of the embankment while other were performed on the field side at the embankment toe: in this case, Unit Ar and B are not present, and the water table level is much higher, around 2 m depth compared to approximately 7 m for the tests located on the top of the embankment. There is obviously, in addition, a difference due to variability in the soil profile especially in Units Ar and B, as clearly expected and already mentioned in previous paragraphs.

From the different methods applied, considering the PGA reference value of 0,29 g, the results are quite different along the sections and on the same sections as well. It is anyway consistent the result obtained from different methods on the same test location and the slight difference given by each method is acceptable and reasonable, since it has to be taken into account that the methods here used are affected by a degree of uncertainty.

In general, it can be considered the Unit A shows a factor of safety against liquefaction almost everywhere below 1 and usually around 0.6-0.7. Unit Ar and B show instead a more variable behaviour, and in some locations the factor of safety is always higher than 1 and in other locations it assumes the value around 0.7-0.8. It is relevant to note that the thickness of liquefiable layers in Unit B is quite variable and usually there is an alternation of small sublayers with factor of safety below 1 and sublayers with factor of safety above 1.

For what concerns the estimation of vertical settlements and horizontal movements, the empirical methods used provide estimations that are not realistic and not comparable with what has been observed after the earthquake.

The sensitivity analysis to the variation of pga has shown that for what has been considered a lower value of pga equal to 0.23 g the factor of safety against liquefaction is below 1 mainly for Unit A while it is usually above 1 in Unit B. On the other side, for the higher value of pga equal to 0.35 both Unit A and B show a factor of safety significantly below 1.

The sensitivity analysis to the variation of water table level has shown that only for some CPTU this has affected the thickness of liquefiable layers. This is due to the variability of the composition of the embankment body. In general almost half of the tests have shown a difference in the liquefaction susceptibility with an increase of the water table level of 1 m, but in all these cases the liquefiable layers are the first meter below water

---

table are extremely thin and probably do not particularly affect the overall behaviour of the embankment body.

No more information can be obtained by the preliminary analysis carried out in this chapter. The fact that there are two soil Units (A and B) that show some susceptibility to liquefaction is consistent with the effects experienced by the embankment during the seismic event. It is also remarkable that the factor of safety is not dramatically below the unit confirms that the liquefaction phenomenon was not massive, as it appear by the surficial manifestation that didn't show important sand ejecta and lateral spreading. Understanding if only one or both Units liquefied is a relevant aspect in the analysis, and an essential element to arrange a mitigation project; though, it is not possible to clarify this issue with the simplified analysis performed and, on the other hand, no sand boils, or at least no samples of ejected material have been collected and consequently it is not even possible to have a field confirmation about this aspect.

Essentially, all the preliminary analysis presented in this chapter are consistent in showing that the damages observed at the Scortichino site a compatible with a slight liquefaction phehomena; nevertheless it is not possible to evaluate which layer is responsible for the observed evidences. A numerical analysis with the use of an advanced soil constituve model will then be performed in the next chapter, with the aim of improving the understanding of the occourence.

---

## CHAPTER 8

# Scortichino case study – numerical analysis

### 8.1 General aspects of the model

#### 8.1.1 Model structure

#### 8.1.2 Geometrical aspects and boundaries

An embankment structure should be considered a three dimensional structure, wanting to perform a rigorous analysis. However, considering the shape of the embankment, which has one dimension (length) significantly bigger than the other two (width and height), it is considered reasonable and acceptable to perform a 2D-analysis. A 3D analysis might be useful to study the embankment behaviour especially where the channel path is not straight and curves and direction changes are present. On the other hand, a 3D analysis is conceptually similar to a 2D analysis except for a more complex model structure and a heavier computational load. A future development of this project might involve a 3D analysis.

For the present purpose a 2D numerical analysis is considered an advanced tool able to simulate a seismic event and to capture liquefaction occurrence. In particular, a 2D analysis can give information about the settlement of the embankment and the deformations along the slopes connected to lateral spreading.

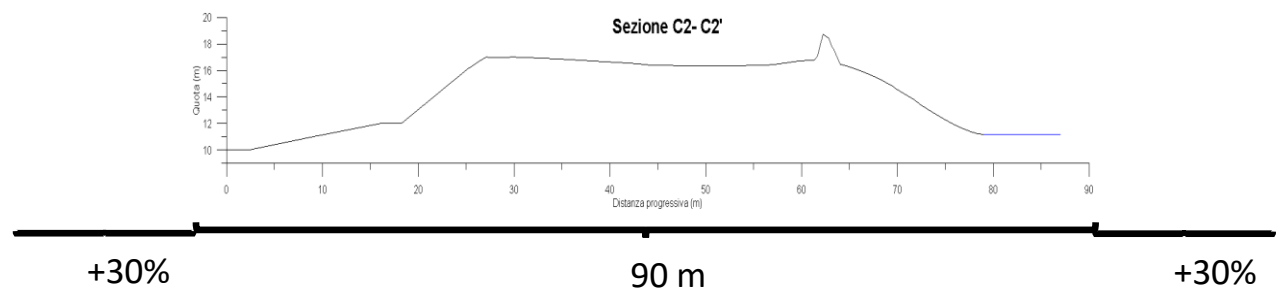
The 2D geometric model represents a cross-section which is considered of relevant interest for the understanding of the embankment behaviour. In particular section C-C is considered since many data for defining soil properties are available and, at the same time, in this section most of damages have been observed.

The geometry of the section is well-known because of the topographical survey performed and already described in paragraph .....

---

In the model the dimension of the investigated area are chosen in order not to affect the analysis results with boundary effects. The region of main interested for the overall analysis is the embankment body, including the crest and the slopes (field side and river side) and, in addition, the region next to the embankment toe with a width of approximately 10 meters. The complete area of interest is object of the survey and for this reason the shape is known in detail.

In order to study correctly this area with an Opensees model the boundary of the model must be far enough from the area of interest, in order to have anomalous response due to the presence of the edge effects. Based on previuos experiences (.....) a precautionary choice would locate the boundary at a distance from the edge of the area of interest equal to two times the width of the area itself (fig.....). There might be an alternative, which will not be considired in this project, in order to avoid the use of such a large area of study through the use of dasphpot placed on the boundaries in order to simulate the presence of soil for a large distance outside the boundaries. This choice need though a careful calibration of the dashpot properties, and for this reason will not be considered here.



Considering an area of interest equal to approximately 90 m, the complet width of the model will be of approximatel 450 m. In order to reduce the computational load in area that are not of main interest the size of elements will be kept quite large, and it will be reduced in the area of interest with the aim of refining the quality of the results.

For what concerns the depth of the model it has been considered a depth of 60 m and more details about this choice will be given in paragraph.....

### 8.1.3 Stratigraphy and soil constitutive models

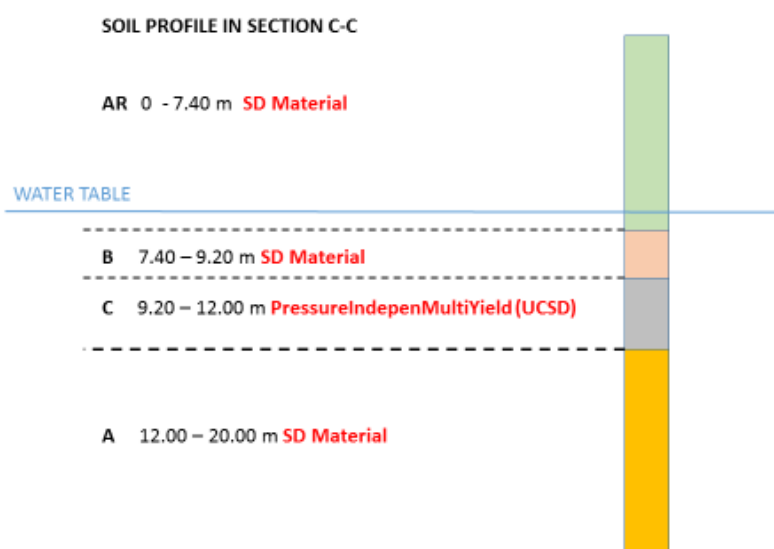
Based on the in-situ investigation and on the soil profile obtained a reference stratigraphy is defined for the model (figure ....). It is important to note that for a first

analysis the soil profile used is simplified: the horizontal variability is well known and was clearly pointed out in chapters 6 and 7.

This study is focused on liquefaction phenomena, and for this reason most of attention is given to the layers that, from the preliminary evaluations of chapter 7, might be critical for this aspect. In particular Unit Ar is of limited interest since it is mainly located above the water table level and the same minor role is played by Unit C, which appears clearly not liquefiable. Most of interest is instead focused on Unit B and Unit A.

The soil profile represented in Figure.... is obtained by an interpretation of the more complex stratigraphy referred to the same section obtained by in situ tests and represented in chapter 6. The non-cohesive layers are studied as SD material; for Unit AR this choice has a limited relevance since the layer is mainly above the water table. The cohesive material of Unit C is modelled as a PressureIndependentMultiYield (USCD) material, developed by Elgamal (...) at the University of California San Diego. Unit A is assumed to start at a depth of -12 m from the embankment crest and is studied until a depth of -20 m. The layer goes deeper but for liquefaction studies, especially because this work is focused on the surface induced deformations, the depth considered is more than sufficient to perform a reliable result.

The model is not limited at a depth of -20 m, though and the reason for the need of a deeper model is explained in the next paragraph. However, the area of main interest, where the values of deformations and excess water pressure must be accurate to perform a good analysis, goes from the crest level to -20 m.



For what concerns the water table level, considering what already discussed in chapter 7, a value of -7 m from the embankment crest is assumed. The water surface is assumed

horizontal, even if from the data collected it might be slightly inclined going from the channel to the field outside the embankment. Due to the small inclination and to the fact that there are some uncertainties about the exact position of the surface, a horizontal direction is assumed. In addition, keeping a horizontal direction, the level of the water table can be easily changed in the model and the effects of a variation in the water table table on the analysis results can be easily evaluated with a small computational effort.

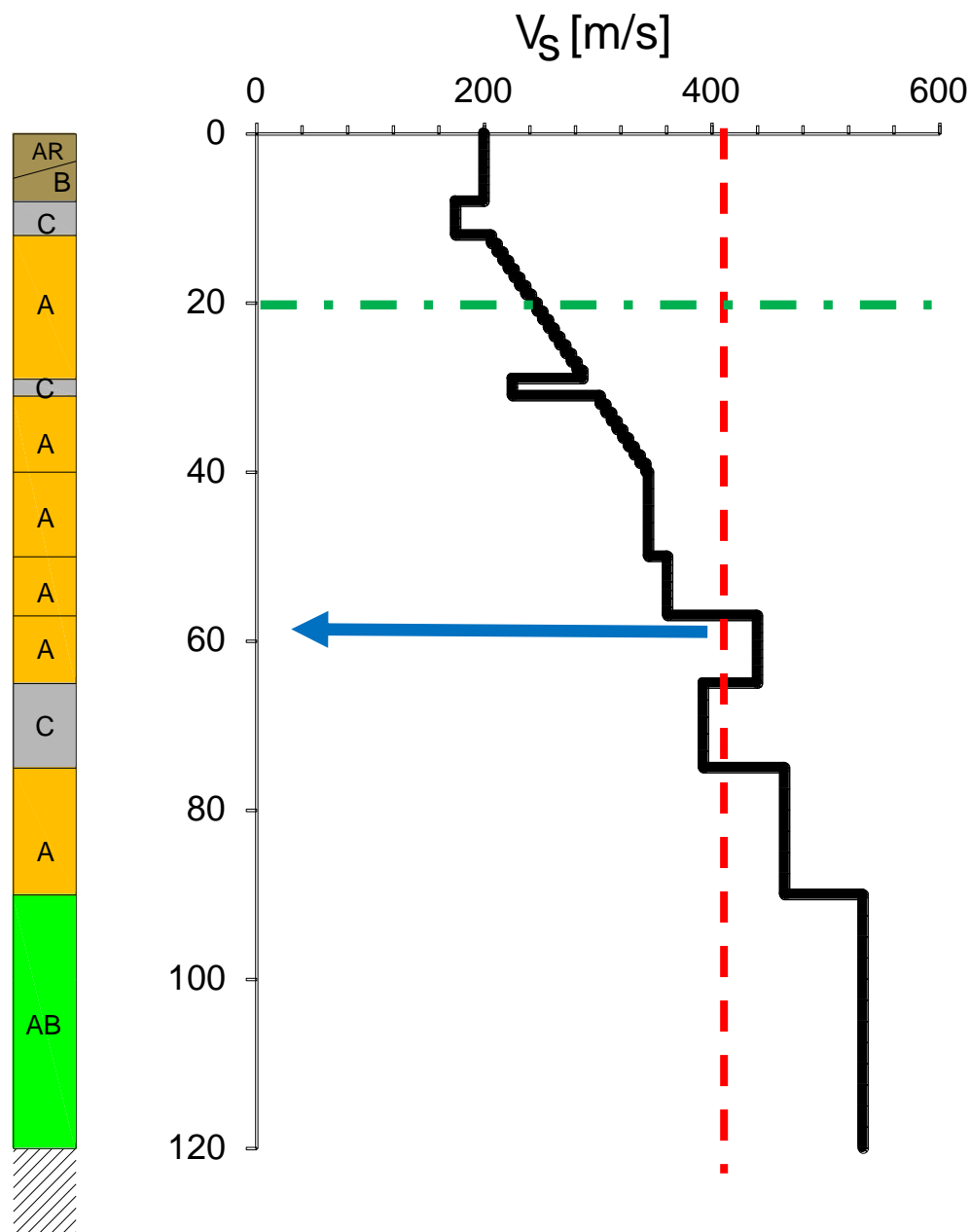
#### **8.1.4 Ground motion**

As indicated in figure ... the area of interest is limited to a depth of 20 m from the embankment crest. The model boundary cannot be limited to that depth because at the base of the model the ground motion input must be applied.

For a rigorous site response analysis the model should reach the bedrock, usually identified with a  $V_s$  value  $>800$  m/s. From the deep soil tests data available for Mirandola, the bedrock is located at approximately 120 m from the ground level (fig. ....). In Scortichino, which is located at less than 20 km from Mirandola, considering the geological structure of the area, it is reasonable to assume the bedrock located at a similar depth.

Under a computational point of view the use of such a depth is particularly heavy and there is not an important benefit in terms of results (Markham.....). A valid depth to locate a ".....bedrock" is considered the depth where the  $V_s$  reaches the value of 400 m/s. Assuming a similar soil profile, at least broadly, between Mirandola and Scortichino the deep tests from Mirandola can be used and a value of 400 m/s is reached at a depth of around 60 m.

---



The model between 20 and 60 m below the embankment crest will have a low degree of detail since its function is simply that of letting the signal reach the real area of interest (0 – 20 m) from the “..... bedrock” and there is no interest in specific aspects such as deformations and water pressure. For this reason a rough stratigraphy will be adopted for the layers below – 20 m and SD material will be used for sandy layers and PressureIndepenMultiYield material will be used for clayey layers. Since the most of test in Scortichino site are limited to a depth of 30 m, and only one coring has reached the



depth of 50 m (S5) the available data will be used to determine the soil parameters for deep layers using critical comparison with available literature data (.....).

It is important to point out that, despite the small number of information available for the deep layers, the surficial layers are quite carefully classified and enough information are provided for a valid analysis in the area of interest (0-20 m).

## **8.2 Site response analysis**

Specifically, the deconvolution of surface acceleration time series is performed to provide representative equivalent-bedrock soil input motions for seismic site response analyses. The site response analysis will be performed by Opensees itself.

The ground motion stations close to the epicentre in Emilia earthquake are not located on bedrock. The closest outcropping bedrock is in fact many tens of km far from the area of interest. For this reason there is the need to obtain a ground motion signal at the bedrock (within) from a ground motion record on the surface. As explained in the previous paragraph an equivalent bedrock or stiff-enough soil profile has been identified with a  $V_s=400$  m/s at a depth of approximately 60 m. The general characteristics of the area, under a geological point of view, can be considered roughly similar and, on the other hand there are no more detailed information to perform a more detailed analysis. The real bedrock depth (>120 m) is assume to be too far to allow reasonable computational load.

### **8.2.1 Choice of strong motion records**

Records from a ground motion station have been choosed. The closest station is the Mirandola station. Other stations are significantly farer and consequently less useful for evaluating the strong motion signal. In fact Mirandola station is close both to the epicentre and to Scortichino site, as already mentioned in chapter 7. In addition, the soil profile at Mirandola and Scortichino can be considered roughly similar and the transfer of signal from the equivalent bedrock in Mirandola and the equivalent bedrock in Scortichino has less uncertainties compared to other ground motion stations. To perform a more detailed analysis it would be useful to consider more than one ground motion station and repeat the same procedure for all the stations in order to refine the results. In this case only the Mirandola station have been considered.

---

The event analysed is the main shaking of the 20<sup>th</sup> of May, which is the event that caused the main damage system pattern in Scortichino.

In figure ... it appear the ground motion records from Mirandola station, as published by ... Website. The Opensees model requires as input the velocity time history, but all the site repsonsed analysis will be performed considering peak ground acceleration, and finally it will be converted in velocity.

### 8.2.2 Signal filtering

### 8.2.3 Soil properties

In table ... the soil properties of the layers underneath Miranola site are presented, including shear wave velocity values (source....). Only the marked layers will be considered, due to the assumption of the equivalent bedrock located at 60 m of depth.

Soil type	Layer	Thickness (m)	z(m)	V <sub>s</sub> (m/s)
AR + B	Ar+B	8	0.0	200.0
			8.0	200.0
C (clay)	C	4	8.0	175.0
			12.0	175.0
A (sand)	A	17	12.0	204.0
			29.0	289.0
Clay	C	2	29.0	225.0
			31.0	225.0
Mainly sand	A	9	31.0	299.3
			40.0	344.5
Mainly sand	A	10	40.0	344.5
			50.0	344.5
Mainly sand	A	7	50.0	361.3
			57.0	361.3
Mainly sand	A	8	57.0	440.1
			65.0	440.1
Mainly clay	C	10	65.0	392.8
			75.0	392.8
Mainly sand	A	15	75.0	463.9

---

			90.0	463.9
Silt and sand	AB	30	90.0	532.9
			120.0	532.9
Bedrock	-	-	120.0	800.0
			125.0	800.0

#### 8.2.4 Signal deconvolution

#### 8.2.5 Definition of motion input parameters for the numerical model

### 8.3 Calibration of soil constitutive models

#### 8.3.1 Stratigraphy

#### 8.3.2 Calibration of clayey layers

#### 8.3.3 Calibration of sandy and silty layers

#### 8.3.4 Calibration of deep layers

### 8.4 Graphical pre and post-processing

#### 8.4.1 model boundaries

#### 8.4.2 mesh

### 8.5 Analysis

### 8.6 Discussion

---

## CHAPTER 9

# Conclusions

The 20<sup>th</sup> and 29<sup>th</sup> of May 2012 Emilia region was struck by two main earthquakes having ML=5,9 and 5,8 respectively and epicentres located close the villages of Finale Emilia and Mirandola, in Modena province. The earthquake induced soil liquefaction, concentrated on some areas built on the paleochannel of Reno river and minor areas in Modena province.

In particular, the left embankment of an irrigation channel called “Canale Diversivo” showed a damage pattern along a section of its path close to the village of Scortichino. The section interested by the evidences is approximately 2 km long and some groups of houses are located on the embankment crest and showed cracks and deformations. The damages appear to be related to lateral movement affecting the embankment body, with formation of longitudinal fissures. The damage pattern appears compatible with occurrence of soil liquefaction, especially at the light of a detailed in-situ and laboratory investigation campaign organized by “Gruppo di Lavoro AGI-RER”.

After introducing the main theoretical aspects of soil liquefaction, with focus on case histories of liquefaction on river embankments, details about the Scortichino case history are presented in chapter 5.

Chapter 6 has introduced the investigation program organized by “Gruppo di Lavoro AGI-RER” that provided all the data used to perform the analysis of the case history. In particular, the results from in situ tests and laboratory tests are briefly presented. A topographic survey is of particular importance considering the two-dimensional nature of the structure object of the study. A detail survey made with the GNSS (Global Navigation Satellite System) technology has provided the ground surface used to locate the in-situ tests and to perform the preliminary and numerical analysis.

Based on other reconnaissance experiences performed in USA, Japan and New Zealand a careful evaluation of the damage pattern observed along Canale Diversivo embankment has been performed in chapter 7. The study of the surface evidences is based on pictures taken in the weeks and in the months after the earthquake. The pictures representing the damages observed, mainly fissures on the embankment body and cracks on buildings, are located on a map of the area. Zones where sand ejecta was observed are also reported on the map. The result is a crack map that gives a global spatial overview of the evidences. It is possible to realize in an unbiased way which

---

sections were more affected by the damages and how they are distributed along the area. For liquefaction detection the field reconnaissance is of great importance and the realization of a crack map is the first step to perform a reliable analysis. In the Scortichino case, unfortunately, the photographic survey was not organized immediately after the event and consequently some evidences, such as possible small sand ejecta, might have been not detected. For what emerges from the crack map, the damage pattern is compatible with a slight occurrence of lateral spreading or some cyclic softening effect. The absence of sand ejecta on the embankment body and the impossibility to sample it, in case it occurred without being visible, implies the need of additional investigations to ensure the occurrence of soil liquefaction. A further important preliminary research described in chapter 7 is the reconstruction of the history of "Canale Diversivo" and of the surrounding area. Liquefiable soils requires specific characteristics in terms of composition, fabric, stress history ecc..., as described in detail in chapter 1. In particular, river paths and abandoned river path present soils typically liquefiable due to the young age and to the grain properties of the depositional environment. From the research it results that the present channel was previously (until a century ago) an active river capable of carrying sediments along its paths. The geological maps of the area clearly confirm this assumption, showing a significant zone with silty material deposition. In summary, the soil layering and the historical features of "Canale Diversivo" add information that confirms the hypothesis of soils prone to liquefaction.

Considering what emerged from the preliminary evaluation of the damage pattern and from the historical features of the area, the research has been carried on considering the data obtained from in-situ tests. All the cross sections investigated during the in-situ and laboratory tests program have been considered. Particular attention is given to section C where most of damages are reported. Available data allow to define the soil profile through the section: the embankment body is made by a quite mixed material (Unit Ar) mainly silty and probably rearranged by human activity; underneath Unit Ar a layer classified as sandy silt is located at the base of the embankment (Unit B). Unit B has a composition partly similar to Unit Ar but it is not uniformly present on all the investigated area: its presence is detected only on some sections. The thickness of Unit B is quite variable but it appears not to exceed the 2 m of depth. Underneath Unit B a clayey layer named Unit C is found, with a thickness variable from 0 to 2 m. Unit C is more uniform than Unit B and is present on almost all the sections investigated. At the base of Unit C and thick sandy layer named Unit A is located. Unit A extends at around 30 m from ground surface and reaches the maximum depth of interest for the purpose of this study. The surficial water table is connected with the channel level and passes through the embankment base with a slight inclination in the direction of the field side.

---

Details about water table are provided in chapter 6. A deeper and confined aquifer is located in Unit A.

Liquefaction susceptibility analysis have been performed using methods based on in-situ tests: 2 methods based on CPT were chosen (NCERR and Boulanger&Idriss 2014) among the most used in practice; in addition, having  $V_s$  direct measurements from the SDMT a method that relies on  $V_s$  values was used (Andrus and Stokoe 2000). All the CPTU and SDMT tests performed have been used for analysis. However, attention is focused on cross section C. There are some uncertainties that can affect the results of the analysis.

First of all the ground motion input applied is not certain and for this reason it is difficult to reproduce the conditions caused by the event of the 20<sup>th</sup> of May 2012. Some simplified assumptions based on the epicentral position respect to the site location and to the closest ground motion station of Mirandola have provided a reference  $p_{ga}$  value for the analysis equal to 0,29g. Additional considerations are suggested to evaluate the sensitivity of the liquefaction susceptibility to the variation of acceleration.

A second uncertainty source is the depth of water table: the level expected during the seismic event has been evaluated through different assumptions based on the measured level of the channel, the level of a water well located close to the embankment and the information obtained by in situ tests. A sensitivity analysis to control the influence of the variation in water table level on the results has been performed: this aspect requires particular attention because Unit B, which is suspected of being prone to liquefaction is located along the water table surface and a level variation could have an important role. From the different methods applied the results are quite different along the sections and on the same sections as well, and this is connected with the significant variability of the soil profile. The results obtained from different methods on the same test location are anyway quite consistent and the slight difference given by each method is acceptable and reasonable, since the methods used are affected by a degree of uncertainty. In general, Unit A shows a factor of safety against liquefaction almost everywhere below 1 and usually around 0.6-0.7. Unit Ar and B show instead a more variable behaviour, and in some locations the factor of safety is always higher than 1 and in other locations it assumes the value around 0.7-0.8. It is relevant to note that the thickness of liquefiable layers in Unit B is quite variable and usually there is an alternation of small sublayers with factor of safety below 1 and sublayers with factor of safety above 1.

For what concerns the estimation of vertical settlements and horizontal movements, the empirical methods used provide estimations that are not realistic and not comparable with what has been observed after the earthquake.

---

The sensitivity analysis to the variation of  $p_{ga}$  has shown that for what has been considered a lower value of  $p_{ga}$  equal to 0.23 g the factor of safety against liquefaction is below 1 mainly for Unit A while it is usually above 1 in Unit B. On the other side, for the higher value of  $p_{ga}$  equal to 0.35 both Unit A and B show a factor of safety significantly below 1.

The sensitivity analysis to the variation of water table level has shown that only for some CPTU this has affected the thickness of liquefiable layers. This is due to the variability of the composition of the embankment body. In general almost half of the tests have shown a difference in the liquefaction susceptibility with an increase of the water table level of 1 m, but in all these cases the liquefiable layers the the first meter below water table are extremely thin and probably do not particularly affect the overall behaviour of the embankment body.

No more information can be obtained by the preliminary analysis carried out in chapter 7. The fact that there are two soil Units (A and B) that show some susceptibility to liquefaction is consistent with the effects experienced by the embankment during the seismic event. It is also remarkable that the factor of safety is not dramatically below the unit confirms that the liquefaction phenomenon was not massive, as it appears by the surficial manifestation.

Understanding if only one or both Units liquefied is a relevant aspect in the analysis, and an essential element to arrange a mitigation project; though, it is not possible to clarify this issue with the simplified analysis performed and, on the other hand, no sand boils, or at least no samples of ejected material have been collected and consequently it is not even possible to have a field confirmation about this aspect.

A numerical analysis with the use of an advanced soil constitutive model is required for improving the understanding of the embankment behaviour.

The numerical analysis is performed with the use of the computational finite element platform Opensees, introduced in chapter 4. Opensees has the capability to use advanced soil constitutive models able to study the stress-strain behaviour of soils under undrained cyclic loading and consequently to evaluate deformations and excess pore water pressure. The constitutive model adopted for the Units A and B which are the most critical for what concerns liquefaction aspect is the Stress-Density model developed by Cubrinovsky. The final purpose of this study is to perform a 2-D analysis of the embankment body in order to replicate the real event occurred the 20<sup>th</sup> of May and try to simulate the deformations on the embankment and understand which layers are responsible for the damage pattern.

Opensees is able to perform a 2D analysis and with the use of a graphic pre-processor it is possible to consider the real shape of the area as obtained by the topographic survey.

---



The choice of the model size and the boundary conditions has been carefully chosen in order to prevent alterations on the results due to the boundaries on the area of interest. The area of interest is the entire embankment body for a specific section (section C) and the model boundaries extend laterally for an identified space. The choice of the model depth is related to the site response analysis. The numerical analysis provides a site response analysis through the layers included in the model once a velocity time history is given as input at the base of the model. Theoretically the model should reach the bedrock depth, but in the case study it would mean to reach the depth of around 120 m with heavy computational load. It is assumed consequently and equivalent bedrock located at a depth of 60 m from ground surface, where the  $V_s$  reaches the values of 400 m/s which is assumed a reasonable value.

The velocity time history is obtained from the ground motion records from Mirandola station, through a signal deconvolution. Peak ground acceleration recorded at Mirandola during the main event of the 20<sup>th</sup> of May has been filtered with a low pass procedure with Seismosignal and with the use of Strata software is deconvolved down to the depth of around 60 m where the equivalent bedrock is located. The signal obtained is then transferred to the Scortichino location considering the distance from Mirandola, the epicentre and Scortichino through transfer function. Velocity time history is then derived from acceleration values.

Once the geometrical aspect of the model and the ground motion input are defined, the last key element to perform the numerical analysis is the definition of the soil profile and the calibration of soil constitutive models. The stratigraphy used in the model is based on the results from the in-situ tests, with a definition of 4 soil layers for the area of main interest (Unit A, B, C, Ar) as explained in chapter 6 and 7. For the deeper layers until the lower boundary (-60m) a more rough stratigraphy is used, with the main function of transferring the ground motion signal to the surficial layers, and with no interest in the evaluation of stress-strain behaviour of the layers.

The layers of more interest for the development of liquefaction are unit A and unit B and they must be calibrated carefully. The process of calibration is not complete yet in this study and is a necessary step in order to run the numerical analysis obtaining reliable results. The stress-density model requires the definition of a number of parameters that can be done using the laboratory tests performed on undisturbed samples. In particular double sample direct shear test and cyclic simple shear test provide the most reliable values for the model calibration. Fitting parameters must then be evaluated in order to replicate the reference resistance curve. A first use of 1-D basic layer with only one kind of soil should be used to calibrate the constitutive model and after calibrating all the main layers the complete model can be run to perform a good quality analysis.

---

Results are not available yet; when they will, deformations will be provided and a first comparison with the observed damage pattern will be possible. In addition other analysis can be performed for example on different sections. It is also possible, as a further development of the research, modifying the ground motion input to take into account aftershocks occurred in a short time after the event and evaluating the possible cumulative excess pore pressure. Finally it is also possible to study the effectiveness of remediation technologies, including them in the model, and comparing pre and post-intervention scenarios.

---

---

## LIST OF REFERENCES

- Andrus, R.D. and Stokoe, K.H., II. (2000). Liquefaction resistance of soils from shear-wave velocity. *Jnl GGE, ASCE*, 126(11), 1015-1025.
  - Bathe, K. –J. (1996) *Finite Element Procedures*, Prentice-Hall, Inc., NJ, 1037 pp.
  - Boulanger, R. W., and Idriss, I. M. 2014. *CPT and SPT based liquefaction triggering procedures*. Report No.UCD/CGM-14/01, University of California, Davis, CA, 134 pp.
  - Boulanger, R. W. and Idriss, I. M. (2004) “Evaluating the potential for liquefaction or cyclic failure of silts and clays”, Report No. UCD/CGM-04/01, December.
  - Bray, J. D. and Sancio, R. B. (2006) *Assessment of the liquefaction susceptibility of fine-grained soils*, *Journal of Geotechnical and Geoenvironmental Engineering, ASCE*, Vol. 132, No. 9, pp. 1165-1177.
  - Crespellani, T., J. Facciorusso , A. Ghinelli, C. Madiai, S. Renzi and G. Vannucchi [2012]. *Rapporto preliminare sui diffusi fenomeni di liquefazione verificatisi durante il terremoto in pianura padana emiliana del maggio 2012. 31 maggio 2012*, (Università degli Studi di Firenze, Dipartimento di Ingegneria Civile e Ambientale – sezione geotecnica), Technical report.
  - Cubrinovski, M. and Ishihara, K. (1998a). Modelling of sand behaviour based on state concept. *Soils and Foundations*, Vol. 38, No. 3, pp. 115-127
  - Cubrinovski, M. and Ishihara, K. (1998b). “State concept and modified elastoplasticity for sand modelling. *Soils and Foundations*; Vol. 38, No. 4, pp. 213-225.
  - Cubrinovski M. (2011). *Seismic effective stress analysis: Modelling and application*. In Verdugo, R., editor, 5th International Conference on Earthquake Geotechnical Engineering, pages 335–358, Santiago, Chile.
  - Cubrinovski, M., Henderson, D., Bradley, B.A. (2012). *Liquefaction impacts in residential areas in the 2010-2011 Christchurch earthquakes*. Tokyo, Japan: One Year after 2011 Great East Japan Earthquake: International Symposium on Engineering Lessons Learned from the Giant Earthquake, 3-4 Mar 2012.
  - Darendeli, M. B. (2001). *Development of a new family of normalized modulus reduction and material damping curves*. Austin, Texas: The University of Texas.
-

- 
- Green, R.A., Cubrinovski, M., Wotherspoon, L., Allen, J., Bradley, B.A., Bradshaw, A., Bray, J., DePascale, G., Orense, R., O'Rourke, T., Pender, M., Rix, G., Wells, D., Wood, C., Henderson, D., Hogan, L., Kailey, P., Robinson, K., Taylor, M., Winkley, A. (2012). *Geotechnical aspects of the Mw6.2 2011 Christchurch, New Zealand Earthquake*. Oakland, CA, USA: 2012 Annual Congress of the Geo-institute of ASCE, 25-29 Mar 2012.
  - Gruppo Lavoro Liquefazione [2012]. *Primo rapporto sugli effetti della liquefazione osservati a S. Carlo, frazione di S. Agostino (Provincia di Ferrara)*. A cura del gruppo di lavoro per la valutazione degli effetti di liquefazione a seguito dei terremoti del 20 e 29 maggio 2012 (Regione Emilia-Romagna, PG.2012.0134978 del 31/5/2012).
  - Idriss, I. M., and Boulanger, R. W. (2008). *Soil liquefaction during earthquakes*. Monograph MNO-12, Earthquake Engineering Research Institute, Oakland, CA, 261 pp.
  - Jitno, H. (2009). *Earthquake-induced deformations of Earth Dams*, Seminar on Seismology and Earthquake Engineering, Australian Geomechanics Society, South Australian Chapter, 24 September 2009, North Adelaide.
  - Kottke, A. R., Wang, X., Rathje, E. M. 2013. *Technical manual for Strata*. Geotechnical Engineering Center, Department of Civil, Architectural and Environmental Engineering, University of Texas.
  - Kramer, S. L. (1996). *Geotechnical Earthquake Engineering*. Upper Saddle River, New Jersey: Prentice Hall
  - Oka, F., Tsai, P., Kimoto, S., Kato, R. (2012). *Damage patterns of river embankments due to the 2011 off the Pacific Coast of Tohoku Earthquake and a numerical modeling of the deformation of river embankments with a clayey subsoil layer*, Soils and Foundations, 2012;52(5):890-909.
  - Robertson, P. K., and Wride, C. E. (1997). "Cyclic liquefaction and its evaluation based on SPT and CPT." in Proceedings, NCEER Workshop on Evaluation of Liquefaction Resistance of Soils
  - Robertson, P. K., and Wride, C. E. (1998). "Evaluating cyclic liquefaction potential using the cone penetration test." Canadian Geotechnical J. 35(3), 442–59.
  - Sasaki, Y., Kano, S., Tsuji, T. (2004). *Embankment reinforcement by geogrids to reduce its settlement during earthquakes*, 13° World Conference on Earthquake Engineering, Cancouver, B.C., Canada, August 1-6 2004, Paper n° 642.
  - Sasaki, Y. (2009). *River dikes failures during the 1993 Kushiro-oki earthquake and the 2003 Tokachi-oki earthquake*, Earthquake geotechnical case histories for performance-based design, Kokusho Ed., 2009, Taylor and Francis Group, London.
-

- 
- Sasaki, Y., Towhata, I., Miyamoto, K., Shirato, M., Narita, A., Sasaki, T., Sako, S. (2012). *Reconnaissance report on damage in and around river levees caused by the 2011 off the Pacific coast of Tohoku earthquake*, Soils and Foundations, 2012;52(5):1016-1032.
  - Seed H.B. and Idriss I.M. (1971). *Simplified procedure for evaluating soil liquefaction potential*. Journal of the Soil Mechanics and Foundations Division, ASCE, **107**(SM9):1249–1274
  - Seed, R.B., Cetin, K.O., Moss, R.E.S., Kammerer, A.M., Wu, J., Pestana, J.M., Riemer, M.F., Sancio, R.B., Bray, J.D., Kayen, R.E. & Faris, A. 2003. *Recent advances in soil liquefaction engineering: a unified and consistent framework*. Keynote Presentation 26<sup>th</sup> Annual ASCE Los Angeles Geotechnical Spring Seminar, Long Beach. Report No. EERC 2003-06.
  - Tsukamoto, Y., Kawabe, S., Kokusho, T. (2012). *Soil liquefaction observed at the lower stream of Tonegawa river during the 2011 off the Pacific Coast of Tohoku Earthquake*, Soils and Foundations, 2012;52(5):987-999.
  - Yamaguchi, A., Mori, T., Kazama, M., Yoshida, N. (2012) (a). *Liquefaction in Tohoku district during the 2011 off the Pacific Coast of Tohoku Earthquake*, Soils and Foundations, 2012;52(5):811-829.
  - Yamaguchi, Y., Kondo, M., Kobori, T. (2012) (b). *Safety inspections and seismic behavior of embankment dams during the 2011 off the Pacific Coast of Tohoku Earthquake*, Soils and Foundations, 2012;52(5):945-955.
  - Yasuda, S., Harada, K., Ishikawa, K., Kanemaru, Y. (2012). *Characteristics of liquefaction in Tokyo Bay area by the 2011 Great East Japan Earthquake*, Soils and Foundations, 2012;52(5):793-810.
  - Youd, T. L., Idriss, I. M., Andrus, R. D., Arango, I., Castro, G., Christian, J. T., Dobry, R., Finn, W. D., Harder, Jr., L. F., Hynes, M. E., Ishihara, K., Koester, J. P., Liao, S. S. C., Marcuson, III, W. F., Martin, G. R., Mitchell, J. K., Moriwaki, Y., Power, M. S., Robertson, P. K., Seed, R. B., and Stokoe, II, K. H. (2001) *Liquefaction Resistance of Soils: Summary Report from the 1996 NCEER and 1998 NCEER/NSF Workshops on Evaluation of Liquefaction Resistance of Soils*, Journal of Geotechnical and Geoenvironmental Engineering, ASCE, Vol. 127, No. 4, pp. 297-313.
-